Multifunctional Systems in Synthetic Biology: Single-Stranded DNA Signals Controls Precise Gene Activation



Sheung Hei Ng

St Edmund Hall

University of Oxford

A thesis submitted for the degree of

Doctor of Philosophy

Abstract

Signalling in synthetic biology provides the foundation for engineering responsive complex systems with precise control and functionality. Currently, signalling in synthetic biology commonly relied on a small set of small molecule transcription factors. Those systems often required high concentrations of signal molecules and had leaky expressions in the absence of the signal. Here we developed a single-stranded DNA (ssDNA) signalling system for selective gene activation. Our system works by ssDNA complementing defective constitutive promoters that control production of RNA, proteins, and enzymes. Selective gene activation was achieved by using different promoters or by using inhibitors to remove undesired signals by the DNA strand displacement reaction. Moreover, DNA signals were divided in half to construct complex logic gates (AND-OR-AND-OR-AND gates) that controlled gene activation. Using our robust ssDNA system, we investigated signalling in synthetic tissues comprised of networked nL-aqueous droplets connected to one another by droplet-hydrogel bilayers (DHBs) and droplet-interface bilayers (DIBs). In this system, lipid bilayers physically separated the signal from the genes with defective promoters. We demonstrated the ability to control entry of the signal into specific compartments containing the defective promoters by selectively disrupting the bilayers or by using a membrane potential to transport the signals across channel proteins in the bilayer. Looking forward, our work lays the groundwork engineering multifunctional systems for use in biotechnology and medicine, where different set of genes would be activated in response to different environmental triggers.

Acknowledgements

I extend my deepest gratitude to my supervisor, Prof. Hagan Bayley, a visionary thinker, for giving me the opportunity to work in his lab, develop the skills needed to manage complex research projects, and pursue my own original research. I also thank Prof. Yujia Qing for her guidance in both research and presentation skills. I am grateful to the Croucher Foundation and the University of Oxford for their generous financial support, along with additional funding from the COVID-19 Scholarship Extension Fund (CSEF).

Working alongside talented colleagues with diverse mindsets and values has been a truly stimulating experience. Most notably, Dr. Ravinash Krishna Kumar was instrumental in connecting the dots and shaping my research into a coherent story. Dr. Michael Booth taught me the importance of thoroughness and careful experimental design, always considering multiple possibilities. Yuying Ding collaborated with me on some of the most challenging aspects of the project. Matthew Cornall and Jorin Riexinger contributed key techniques essential to this work. It was also a pleasure to collaborate with Dr. Juan Liu, Dr. Fernando Valenzuela Gomez, Hansa Shree, Dr. Jiang Liu, Dr. Sejeong Lee, Dr. Denis Hartmann, and Shan Zhang on various projects. I also appreciate the support from other colleagues throughout my DPhil, particularly Dr. Linna Zhou, Dr. Razia Chowdhry and Dr. Assala Al Samad. My thanks also go my examiners for proofreading my thesis. I wish all my colleagues a bright future ahead and hope they find peace in life.

I also extend my gratitude to my college advisors, Prof. Stuart Ferguson and Prof. David Manolopoulos, for their support. My appreciation goes to the chemistry department staff, especially Takvor Takvorian, for his unwavering assistance.

As I approach the conclusion of my DPhil, I am grateful for the opportunity

to learn from exceptional scientists, including Prof. Lorenzo Di Michele, Prof. Masahiro Takinoue, and their remarkable teams. Working with such incredible people, I have come to understand the true importance of trust and mutual support in navigating the challenges of research. Prof. Di Michele emphasized the necessity of objectivity in scientific inquiry, cautioning against the influence of biases and wishful thinking. This principle has been a guiding force, reminding me to respect the fundamental laws of physics and seek to understand biological phenomena as they truly are.

Beyond my academic environment, I am fortunate to have friends who have stayed in touch despite being scattered across the world. Dr. Carina Mouritsen Luxhøj, Dr. Jonathan Lam, Dr. Mumina Akthar, YK Cheung, Matthew Kemp, Daniel Leung, Dr. Jonathan Leung, Hayton Au, Dr. Pauline Chow, Shirley Tse, Elena Tso, Rachel Cheng, Dr. Jackson Kwok, Dr. Jeremy Wong, Dr. Andrea Han, Dr. Marcus Cheung, and Dr. Minnie Cheung made my DPhil journey a truly enjoyable one, creating fond memories that will last a lifetime.

Most importantly, I dedicate this thesis to my family—my parents, Draco Ng and Estella Mok, and my brother, Chris Ng. Their unconditional belief in me and unwavering support, despite not always knowing the details of my research, have meant everything. My aunt, Celine Mok, has also taken great care of me throughout my time in Oxford. This thesis is dedicated to them.

Abbreviations

αHL α-hemolysin 39, 48, 49, 54, 60–62, 65, 68, 73, 81–83, 90, 91, 96, 102, 107, 114, 133–135

β-me 2-mercaptoethanol 110

ATP adenosine triphosphate 36, 111

BFP blue fluorescent protein 130

CCD charge-coupled device v

CTP cytadine triphosphate 111

DFHBI (5Z)-5-[(4-hydroxyphenyl)methylene]-3,5-dihydro-2-methyl-3-(2,2,2-trifluoroethyl)-4H-imidazol-4-one 9

DFHBI-1T (5Z)-5-[(3,5-difluoro-4-hydroxyphenyl)methylene]-3,5-dihydro-2-methyl-3-(2,2,2-trifluoroethyl)-4H-imidazol-4-one 9, 10, 19

DFHO 4-(3,5-difluoro-4-hydroxybenzylidene)-1-methyl-5-oxo-4,5-dihydro-1H-imidazole-2-carbaldehyde oxime 9, 10

DIB droplet interface bilayer 3, 11, 127, 128

DIR2s-Apt5 anti-dimethylindole red aptamer 45

DNA deoxyribose nucleic acid iv–vi, 4, 9, 17, 38, 48, 109–112

dsDNA double-stranded DNA 3, 8, 9, 38, 39

DTT 1,4-dithiothreitol 9, 110, 111, 115

E. Coli Escherichia coli 111

EDTA ethylenediaminetetraacetic acid vi, 110, 112

EM-CCD electron multiplying CCD 129

GE general electric 115

GFP green fluorescent protein 9, 10, 113, 130

GTP guanosine triphosphate 111

HEPES 4-(2-hydroxyethyl)-1-piperazineethanesulfonic acid 110, 111

IDT Integrated DNA Technologies 109

IPTG isopropyl β-d-1thiogalactopyranoside 114

IVT *in vitro* transcription 9, 112

IVTT *in vitro* transcription & translation 10, 11, 48, 112

LATE-PCR Linear-After-The-Exponential PCR 38

LB lysogeny broth 114

LED light-emitting diode 129

NBDG 2-Deoxy-2-[(7-nitro-2,1,3-benzoxadiazol-4-yl)amino]-D-glucose 54

NEB New England Biolabs Ltd. 45, 110

Ni^{2+}-NTA Ni^{2+}-nitrilotriacetic acid 115

NIH National Institutes of Health 113

nt nucleotides 16

OTB-SO3 oxazole thiazole blue - SO_3 45

PAGE polyacrylamide gel electrophoresis vi, 9

PCR polymerase chain reaction v, 38, 39, 112

PEG poly(ethylene glycol) vi

PEN DNA polymerase/exonuclease/nickase dynamic network assembly 7, 8

PMMA poly(methyl methacrylate) 127

PURE Protein Synthesis Using Recombinant Elements 11

RBS ribosome binding site 45

RNA ribonucleic acid vi, 2, 9, 15–17, 19, 36

RNAP RNA Polymerase 9, 22, 36, 110, 111

SDS sodium dodecyl sulfate vi, 112

SDS-PAGE SDS - PAGE 115

ssDNA single-stranded DNA 3, 8, 15, 16, 21, 37–39, 47, 109

TAE Tris-acetate-EDTA (40 mM Tris base, 20 mM acetic acid, 1 mM EDTA, pH 8.3 112

TAMRA tetramethylrhodamine 113, 130

TGX Tris-glycine-SDS (25 mM Tris, 192 mM glycine, 0.1 % SDS, pH 8.3 115

TO thiazole orange vi

TO1B TO1-3PEG-biotin 10, 19, 57

TO3B TO3-3PEG-biotin 10, 19

Tris tris(hydroxymethyl)aminomethane vi, 112, 115

tRNA transfer RNA 111

TXR texas red 113, 130

UTP uridine triphosphate 111

UTR untranslated region 44

UV ultraviolet 4

Contents

1 Introduction **1**

1.1 Signalling in synthetic biology 1

1.2 Gene activation control 3

1.3 Gene expression control using ssDNA 7

1.4 RNA transcription 9

1.5 RNA aptamers 9

1.6 In vitro transcription and translation 10

1.7 Synthetic cells as droplet networks in oil 11

1.8 Thesis outline 13

2 DNA signal selectively activated transcription **15**

2.1 Summary 15

2.2 Defective genes produced RNA aptamers 16

2.2.1 Summary 16

2.2.2 DNA signal activated transcription of defective genes 16

2.3 Selective gene activation by ssDNA signal using different promoters . 18

2.3.1 RNA aptamers specificity to fluorophore dyes 18

2.3.2 Selective gene activation by ssDNA signal using different promoters 20

2.4 Selective gene activation by ssDNA signals using signal inhibitors . . 23

2.4.1 Design rationale 23

2.4.2 Selective gene activation by ssDNA signals using signal inhibitors 24

2.4.3 Three defective genes 26

2.5 Combined use of DNA ligase and RNA polymerase 32

2.5.1 Splitting DNA signal to create AND gates . . . 32
2.6 Inverse defective genes . . . 36
2.7 Long defective gene synthesis . . . 37
2.8 ssDNA signal activated protein production . . . 41
2.9 DNA signal as a transcription factor mimic . . . 42
2.10 Chapter summary and outlook . . . 44
2.10.1 Future use of the DNA signal as a transcription factor mimic . 46
2.10.2 Production of eukaryotic proteins with IVTT mix . . . 48

3 ssDNA controlled communication in droplet networks 50
3.1 Introduction . . . 50
3.2 RNA and protein expression in water-in-oil emulsions . . . 51
3.2.1 RNA aptamer production in water-in-oil emulsions . . . 51
3.2.2 Protein production in water-in-oil emulsions . . . 52
3.3 DNA signal activated droplet network communication . . . 54
3.4 Hydrogel networks with residual compartmentalization . . . 55
3.4.1 Residual compartments in hydrogel structures . . . 56
3.5 Selective biopolymer signalling across droplet interface bilayers . . . 60
3.5.1 Introduction . . . 60
3.5.2 ssDNA translocation across protein pores . . . 60
3.5.3 Translocated DNA signal activated protein production . . . 61
3.5.4 Technical considerations . . . 63
3.5.5 Summary . . . 68
3.6 Chapter summary and outlook . . . 69

4 Further studies and applications 70
4.1 Introduction . . . 70
4.2 Thermoresponsive activation of defective genes . . . 70
4.3 Interfacing DNA signalling with cells . . . 72
4.4 One pot signalling . . . 73
4.4.1 Membrane potential control across multiple bilayers . . . 75

4.4.2 Osmolarity of IVT(T) solution . . . 77
4.4.3 Stability of droplet interface bilayers . . . 79
4.4.4 DNA signal capture at different lipid compositions . . . 81
4.4.5 Spermdidine deformed the signal droplets . . . 84
4.4.6 T7 RNAP degraded on Ag/AgCl wire . . . 85
4.5 Selective signalling by covalent chemistry . . . 89
4.5.1 Increasing the number of pores on the membrane . . . 96

5 Conclusions and future directions **102**
5.1 Perspectives . . . 102
5.2 Future directions . . . 105
5.3 Kinetics and thermodynamics characterization of the system . . . 106

6 Methods and materials **109**
6.1 Chemical and reagents . . . 109
6.1.1 Suppliers . . . 109
6.1.2 Conditions of enzymes . . . 110
6.1.3 Activity of enzyme and enzyme inhibitors . . . 110
6.1.4 Components of the PURE system . . . 111
6.2 General Methods . . . 112
6.2.1 Agarose gel electrophoresis . . . 112
6.2.2 Nanodrop spectrophotometers . . . 112
6.2.3 Calculation of DNA melting temperature . . . 112
6.2.4 Fluorescence measurements . . . 112
6.2.5 Molecular Biology . . . 114
6.3 Nucleic acid and protein sequences . . . 115
6.3.1 RNA Aptamer sequences . . . 115
6.3.2 DNA sequences . . . 116
6.3.3 Protein sequences . . . 121
6.4 Defective gene synthesis . . . 121
6.5 RNA production from defective genes . . . 122

6.5.1 Defective gene activation by DNA signal 122
6.5.2 Selective gene activation using multiple polymerases 123
6.5.3 Selective gene activation using inhibitors 123
6.5.4 Activation of inverse defective genes 124
6.5.5 Complex logic gates by splitting the DNA signal 125
6.5.6 Signal length effect on defective genes 125
6.6 Protein production from defective genes 125
6.6.1 DNA signal activates defective genes 125
6.6.2 DNA signal as a transcription factor mimic 125
6.7 Aqueous droplet networks in lipid-in-oil solution 126
6.7.1 Preparation of lipid films 126
6.7.2 Preparation of oil solution 127
6.7.3 Preparation of lipid-in-oil solution 127
6.7.4 Formation of droplet interface bilayers - without electrodes . . 127
6.7.5 Formation of droplet interface bilayers - with electrodes 127
6.7.6 IVT expression in lipid-in-oil solution compared to expression in bulk 130
6.7.7 IVTT expression in lipid-in-oil solution compared to expression in bulk 131
6.7.8 DNA signal activated hemolysin production in droplet networks 131
6.7.9 Droplet networks with droplet-hydrogel bilayers 132
6.7.10 Membrane potential controlled entry across protein pores . . . 133
6.7.11 Rectification factor of bilayer formed from different lipids . . . 133
6.7.12 Spermidine in signalling droplet 134
6.7.13 T7 RNAP degradation on electrodes 134
6.8 Single-channel electrical Recording 135
6.8.1 Recording chamber preparation 135
6.8.2 Electrical recording 136
6.8.3 Lipid bilayer formation 136
6.8.4 Single channel recording 136

6.8.5 Translocation rate of ssDNA across different mutant pores . . 137
6.8.6 Synthesis of signal precursor 137
6.8.7 Signal processing rate of catalytic cycle 138

Chapter 1

Introduction

This chapter begins by a review of signalling and communication in synthetic biology, with a focus on signalling and communication in synthetic cells, and the use of ssDNA to activate different biological processes. The chapter continues with a review on relevant literature on RNA transcription, RNA aptamers, and protein translation relevant to this thesis. The chapter concludes by providing a summary of this thesis, and outlining the structure of the remainder of this thesis.

1.1 Signalling in synthetic biology

In synthetic biology, signalling refers to the the transmission of information between biological elements to activate specific processes, including gene activation. Signalling plays an important role in synthetic biology, enabling engineered biological systems to communicate and respond to their environment (*1*, *2*).

Signalling is especially important in synthetic cells, intricately designed compartmentalized structures, as they have distinct intracellular environment compared to their surroundings (*3*, *4*).

Synthetic cells are generally aqueous systems enclosed by membranes, such as aqueous-in-oil droplets, liposomes, and proteasomes (*4*). The Elani group demonstrated through microfluidics that additional lipid-enclosed compartments can be formed within larger lipid-enclosed compartments, resulting in layered, compartmentalized structures reminiscent of organelles in living cells (*5*, *6*).

Synthetic cells can also refer to membraneless aqueous compartments formed through liquid-liquid phase separation. For instance, the Di Michele group investigated creating membraneless synthetic cells using cholesterol-anchored DNA strands that self-assemble and phase-separate from the bulk aqueous phase (*7*). Similar phase separation has also been achieved in the Di Michele group with RNA and DNA strands that self-assemble through base-pairing interactions (*8*, *9*).

Inspired by the ability of biological cells to send and receive signals across membranes (*10–13*), there is great interest in engineering synthetic cells to communicate with each other and with their surrounding environment. Advances were made engineering the synthetic systems to communicate both amongst themselves and with their surrounding environment, where communication predominantly relied on a small set of small molecules. (*14–25*). Such systems often had leaky off-state in the absence of the molecules, and relied on simple diffusion of the small molecules across membranes; hydrophobic molecules diffused across membranes directly, while hydrophilic molecules diffused across channel proteins on the membrane (reviewed in (*2*)). It is possible to control the diffusion of entrapped membrane-impermeable molecules within bilayers by controlling the channel proteins. For instance, the opening and closing of channels could be controlled by the binding of specific metal ions to the channel proteins, where ion binding would deactivate the channel (*26*). Alternatively, mechanical pressure could be applied to the bilayer to activate force-sensitive channel proteins, allowing the diffusion of small molecules across the membrane (*27*). Additionally, thermoresponsive lipids have also been used to construct bilayers that become porous above at higher temperatures, thereby allowing diffusion of hydrophilic molecules across the membrane above the critical temperature (*6*). Concurrently, synthetic cells were engineered to demonstrate versatile responses after entry of the small molecules. For example, the molecules could be processed by enzymes in the synthetic cells to generate fluorescent output (*26*, *28*). Fluorescence of the small molecules could also be activated after binding to RNA aptamer in the synthetic cells (*19*).

Recent progress in synthetic biology explored alternative methods for controlling

communication in engineered biological systems, each with different advantages and challenges. Cladyn group designed membrane-bound synthetic receptors that could bind to ligands on one side of the membrane, the resulting conformation change of the receptor propagated across the bilayer, and activated a fluorophore moiety on the other end of the receptor. The change in conformation was measured by circular dichroism and the fluorescence spectra of their receptors (*29*). Langton and colleagues synthesized supramolecular signal transducers that converted pH or copper signal outside of synthetic cells to esterase activity inside the synthetic cells (*30–32*). Yasuga and colleagues used applied potential across droplet interface bilayer (DIB) to drive ssDNA translocation across channel proteins. They showed that their translocated ssDNA could hybridize to form dsDNA that blocked pores due to their larger size compared to ssDNA (*33*).

Light was also used to control communication in synthetic cells. Schroeder group used light to activate optogenetic proteins in synthetic cells to communicate with natural cells (*34*). Wegner group designed artificial cells that emit light to trigger adhesion of synthetic cells (*35*). Moore group mimicked the photoinduced electron transfer reaction in photosynthesis, by attaching an electron donor and an electron acceptor to a photosensitive porphyrin group in a membrane, to generate a proton gradient for ATP synthesis (*36*). Similarly, Matile group demonstrated that p-octiphenyl rods bearing fluorescent naphthalene-diimides self-assembled in lipid bilayers to form helical structures. In the presence of an electron donor and acceptor system, irradiation of the transmembrane structure resulted in long-lived charge separation across the membrane (*22*). Notably, our lab contributed to this field by demonstrating the use of light to induce electric current generation in synthetic tissues (*37*, *38*).

1.2 Gene activation control

The synthetic biology field is particularly interested in using different inputs to control gene expression, as that could potentially allow on-demand production of proteins (*15*). However, despite numerable gene regulatory networks observed in

nature, gene expression in synthetic biology was often controlled using a few well-defined small molecule gene inducers. Those systems often had leaky expression in the absence of the inducers (reviewed in (*2*)).

To address those limitations, alternative approaches were investigated that use other inputs to regulate gene expression in engineered biological systems, each offering unique advantages and challenges.

For example, translational toehold switches are innovate approaches in which mRNA forms secondary structures that blocks ribosome binding until trigger RNA exposes the ribosome binding site. However, the short shelf life of input RNA remains a key limitation (*39*). Similarly, gene silencing using siRNA is another common strategy, though again the instability of siRNAs limits their long-term effectiveness (*40*).

Alternatively, light-based systems have shown promised in regulating transcription, but they are still limited by challenges including phototoxicity and limited penetration of light. For example, T7 RNA polymerase has been photocaged and transcription was activated by removing the cage with UV light (*41*). Our group previously developed UV light activatable DNA expression, by attaching bulky streptavidin proteins to the gene promoter region via a photocleavable linker, which blocked transcription. The gene products were only synthesized when the photocleavable linker was cleaved by UV light.of DNA using photocleavable groups (Fig. 1.1) (*2*, *42*–*44*). While UV light could be used as an effective trigger for tight transcription control, it poses a risk of DNA damage due to its toxicity. Other alternatives to UV light, such as split T7-RNAP, where the complementation of T7 RNAP fragments was controlled by a blue light-switchable VVD domain, has been constructed (*45*). Nevertheless, this method still required continuous blue-light illumination which was impractical in many settings. It is also possible to synthesize polymerases or fragments of a split-polymerase in situ to control gene activation (*19*, *21*, *46*, *47*). Nevertheless, once the polymerases were activated or synthesized, all genes containing the promoter of the polymerases were transcribed.

Temperature has also been used to control protein production. For example,

recent work from the Elani group introduced synthetic cells (liposomes) with heat-responsive mRNA to control protein production. At low temperatures, the mRNA formed secondary structures that blocked ribosome binding and subsequent protein synthesis. However, heating the sample melted the secondary structure. and allowed translation to occur (*48*). By integrating RNA thermometers with cell-free systems, researchers enabled precise temperature-dependent synthesis of both soluble and membrane proteins. This innovation also facilitated temperature-triggered cargo release, demonstrating potential applications in biotechnology and biomedicine. The work highlights a novel approach to creating programmable, thermally regulated synthetic cells.

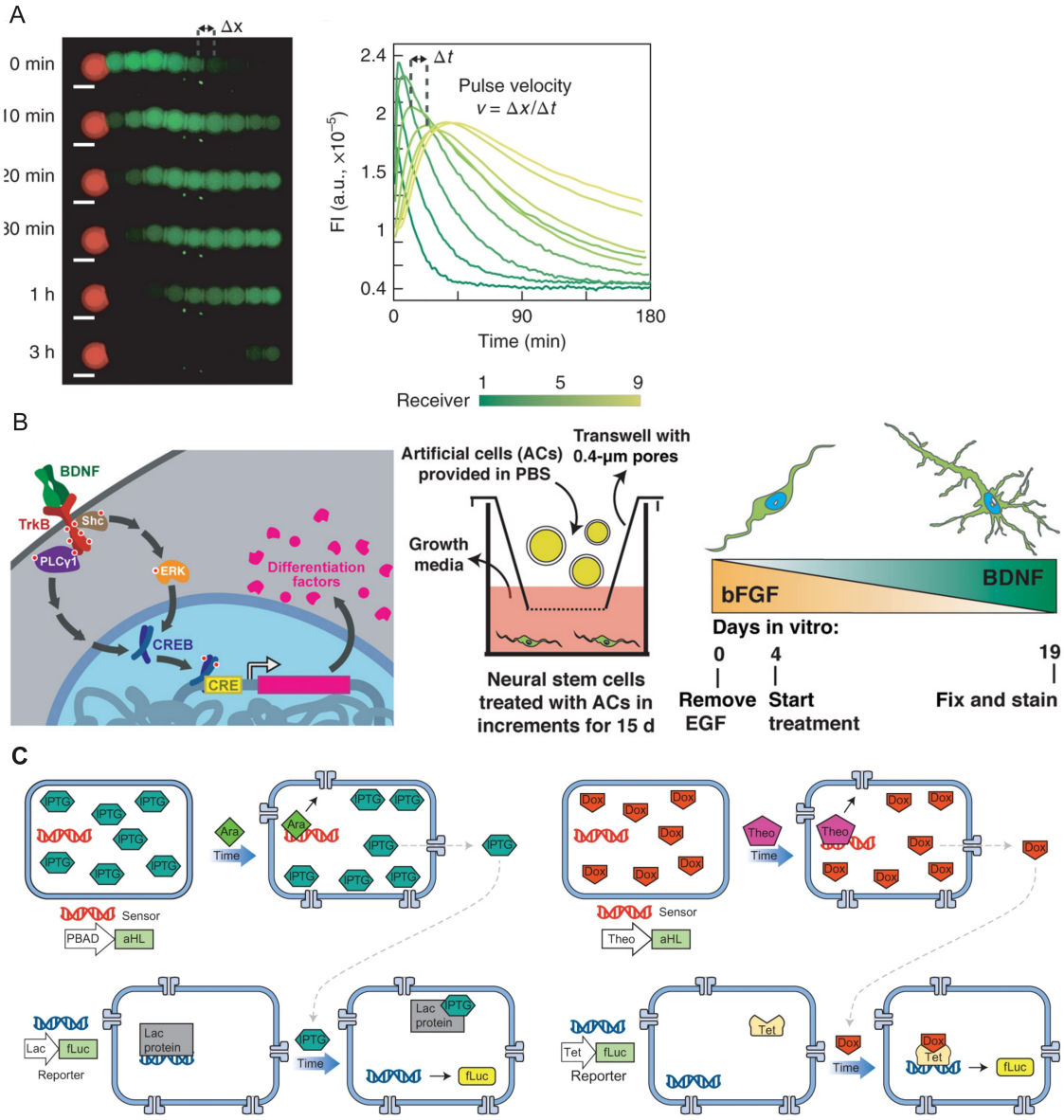


Figure 1.1: A highlight of recent literature on communication in synthetic biology using diffusion of small molecules or light. (A) A small molecule diffused across droplet networks, and the fluorescence of the molecule was activated by binding to RNA aptamers. The figure was adapted from (*19*). (B) A schematic of liposomes as artificial cells producing growth factors that diffused out of the liposomes to trigger growth of neurons. The figure was adapted from (*15*). (C) A schematic of two populations of liposomes that communicated with each other through soluble small molecule signals. The figure was adapted from (*49*). (D) A schematic of gene activation control using blue light and UV light. The figure was adapted from (*44*).

1.3 Gene expression control using ssDNA

Single-stranded DNA (ssDNA) is an another attractive candidate for gene expression control in synthetic biology due to stability of the DNA molecules and high sequence specificity of DNA base pairing (*50*). DNA molecules are also stable and highly non-toxic (*51*). As a result, ssDNA have been used to trigger various processes, including strand displacement reactions that remove DNAs strand attached to a fluorophores from other DNAs strand attached to fluorescence quenchers (*52*, *53*). ssDNA inputs were also used in isothermal amplification reactions (PEN DNA) that allowed its detection by non-sequence specific DNA binding dyes (*54*). ssDNA could also be used to control the dissociation of DNA nanostructures assembled by complementary base pairings, via a strand-displacement reaction that broke the links between the DNA nanostructures (*7*, *55*). In addition, ssDNA strands covalently attached to lipid bilayers were used to control the fusion of liposomes, and were recently used to fuse liposomes containing cell-free extracts (*21*, *56*, *57*). An intriguing yet underexplored application involved using ssDNA to regulate gene activation, which would enable the production of diverse functional RNA and protein products, such as therapuetic RNA or proteins. ssDNA could activate genes with a single-stranded promoter that cannot produce transcripts on their own. While such designs were instrumental in fundamental RNA polymerase studies (*58–60*), they were also used to construct models of negative feedback circuits that mimicked neural networks (*57*, *61*). The use of DNA complementation for gene activation were used in synthetic cells to produce RNA and proteins. ssDNA could activate gene production through either non-selective diffusion into polymersomes (*62*) or by co-localizing with the genes with single-stranded promoters in the same compartment (*19*) (Fig. 1.2). Nevertheless, selective gene activation, where different single-stranded DNAs activate distinct genes with single-stranded promoters, remains largely unexplored. Moreover, the selective transport of ssDNA across lipid bilayers and the use of transported DNA for gene activation still remains to be demonstrated.

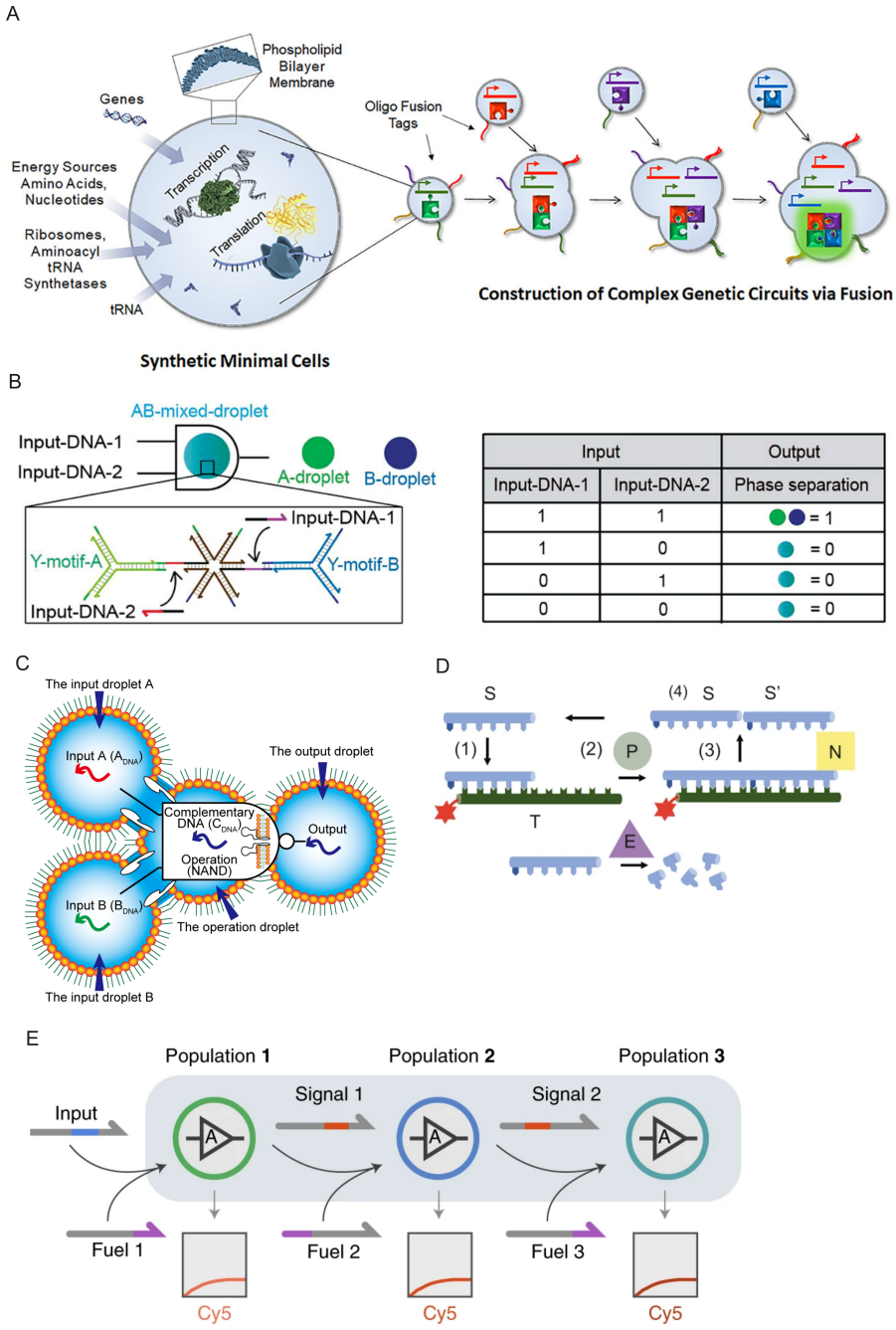


Figure 1.2: A highlight of recent literature using ssDNA to control different processes in synthetic biology. (A) A schematic of ssDNA covalently attached to lipid bilayers to control fusion of liposomes containing cell-free extracts. Figure adapted from (*21*). (B) A schematic of ssDNA controlling dissociation of DNA nanostructures assembled by complementary base pairings, via a strand-displacement reaction that broke the links between the DNA nanostructures. Figure adapted from (*55*). (C) A schematic of the use of applied potential to drive ssDNA translocation across channel proteins. The translocated ssDNA can hybridize to form dsDNA that would block pores due to their larger size compared to ssDNA. Figure adapted from (*33*). (D) A schematic of ssDNA inputs used in isothermal amplification reactions (PEN DNA) that allowed its detection by non-sequence specific DNA binding dyes. Figure adapted from (*54*). (E) ssDNAs were used in strand displacement reactions to remove quenchers from fluorophores. Figure adapted from (*52*).

1.4 RNA transcription

In transcription, a DNA-dependent RNA Polymerase (RNAP) synthesizes RNA from a double-stranded DNA (dsDNA) gene sequence. RNAP recognizes and binds to specific promoter sequence on the gene. The polymerase subsequently unwinds the dsDNA and uses the template DNA strand to synthesize the RNA from the gene (*63*). The transcription of RNA outside biological cells is known as *in vitro* transcription (IVT). This reaction requires the gene of interest, ribonucleotide triphosphates, RNAP, and a buffer system with 1,4-dithiothreitol (DTT) and magnesium ions (*64*). The reducing reagent DTT is also needed to prevent oxidation of thioredoxin sulfhydryl groups in RNAP, as oxidation inhibits transcription (*65*). The commonly used high yield RNAP were T7 RNAP, T3 RNAP and SP6 RNAP. Each polymerase is specific to their own promoter sequences, by recognizing bases in the promoter region from -12 to -8 of the transcription start site (*66*). Martin group showed that RNA transcripts from T7 RNAP were no longer detected by denaturing PAGE when the non-template strand was missing from -8 to +5 nucleotides of the transcription start site (*58*). Therefore, genes with single-stranded promoters were not expected to produce transcripts in the IVT reaction.

1.5 RNA aptamers

In this thesis, transcription activation was assessed by the production of RNA aptamers, which could bind and activate the fluorescence of small molecule dyes (*67*). Broccoli aptamer could bind and activate the green fluorescence of DFHBI-1T, a GFP chromophore mimic. As Broccoli aptamer had high sequence homology with Spinach aptamer, which was known to bind DFHBI with a G-quadruplex structure, it was likely that Broccoli also binds DFHBI-1T with a G-quadruplex structure. 37 nt out of 49 nt of the Broccoli sequence overlapped with the Spinach sequence. Meanwhile, the dyes DFHBI-1T and DFHBI shared the same core fluorophore structure (*68*, *69*). Developed after the Broccoli aptamer, Corn aptamer could bind and activate fluorescence of DFHO. DFHO mimicked the fluorophore of red fluorescent

protein. DFHO was red-shifted compared to DFHBI-1T (*70*). Mango aptamer could bind and activate the green fluorescence of TO1B and the red fluorescence of TO3B, both dyes were based on thiazole-orange. Multiple Mango aptamers were developed, among which Mango-III (A10U) was used in this thesis as it had the highest fluorescent enhancement. Mango-III (A10U) aptamer would be referred to as Mango aptamer in the rest of this thesis. Mango aptamers could also bind to their targets with a G-quadruplex structure (*71*, *72*). Developed after the Mango aptamer, Peach aptamer could also activate the green fluorescence of TO1B and the red fluorescence of TO3B. Peach 1 was the brightest among the Peach aptamers. Mango aptamer had a higher affinity for TO1B than TO3B, whereas Peach aptamer had a higher affinity for TO3B than TO1B (*73*). Pepper could bind and activate the green fluorescence of HBC530 and the red fluorescence of HBC620. Both dyes were designed based on the GFP fluorophore (*74*). The dimeric form of the Pepper aptamer was used in this thesis. Crystal structures suggested that Pepper could bind to its target with a base-quadruple-base-triple stack structure (*75*).

1.6 In vitro transcription and translation

The RNA produced from the transcription reaction could be further translated into proteins. The RNA needed to contain a ribosome binding site (Shine-Dalgano sequence), which could recruit ribosomes to initiate translation at the start codon (AUG) downstream of the binding site. Translation terminated at the stop codon at the end of the coding sequence. The process required tRNAs, ribosomes, amino acids, accessory proteins, and other small molecules (*76*).

The process of producing proteins from genes outside biological cells was known as *in vitro* transcription & translation (IVTT). While this process could be achieved using cell-free extracts made from cell lysates, the contents of the cell-free extracts were not fully defined and cell-free extracts often contained DNA nucleases. It was expected that the overhang in the defective genes would be particularly vulnerable to degradation. While phosphate backbone modifications could potentially be used to protect the defective genes from nuclease digestion (*77*), this thesis used the

Protein Synthesis Using Recombinant Elements (PURE) system to express proteins from DNA. PURE system was developed by Ueda and colleagues (*76*). Instead of using cell-free extracts for IVTT, the components required for IVTT were separately purified. This prevented any unwanted bacterial components from interfering with the IVTT reaction. The PURE system was also commercially available (*78*). The list of the PURE components and their concentration in PURE system is provided in the methods section.

1.7 Synthetic cells as droplet networks in oil

While membrane-bound synthetic cells could be formed as emulsion droplets, liposomes, polymerosomes and proteinosomes (*2*, *4*), synthetic cells formed from aqueous-in-oil emulsion droplets were used in this thesis. Emulsion droplets were formed by adding aqueous droplets to a lipid-in-oil solution, where a lipid monolayer would form spontaneously around the droplets. The droplets were then brought together to form a droplet interface bilayer (DIB) between them (Fig. 1.3).

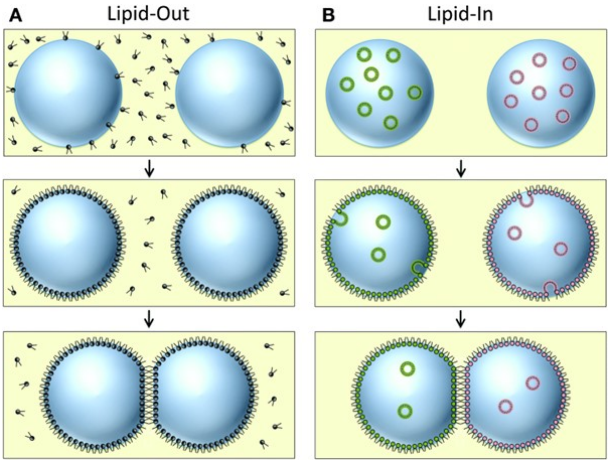


Figure 1.3: Droplet networks were formed with aqueous droplets in an oil solution. Two methods could be used to form droplet networks. (A) In the first method (lipid-out), the lipid was present in the oil solution, therefore a lipid monolayer spontaneously assembled around the droplet when it was added to the oil. The two monolayers assembled into a bilayer when two droplets were brought to contact. (B) In the second method (lipid-in), the lipid was present as liposomes in the aqueous droplets. When the droplets were added to the oil solution, the liposomes would deposit on the droplet surface to form a lipid monolayer. A lipid bilayer was formed when two monolayers were brought into contact. Figure adapted from (*79*).

Emulsion droplets in oil had two distinct characteristics compared to other types

of synthetic cells. Firstly, multiple droplets could be interconnected through the lipid bilayers to form droplet networks, also known as synthetic tissues. Thousands of connected droplets could be conveniently created by using a droplet printer (*79*, *80*). Secondly, as the oil solution was electrically insulating, electrodes could be inserted into the droplets to control the membrane potential across the bilayer, as well as to monitor the bilayer conductance (Fig. 1.4) (*80–82*).

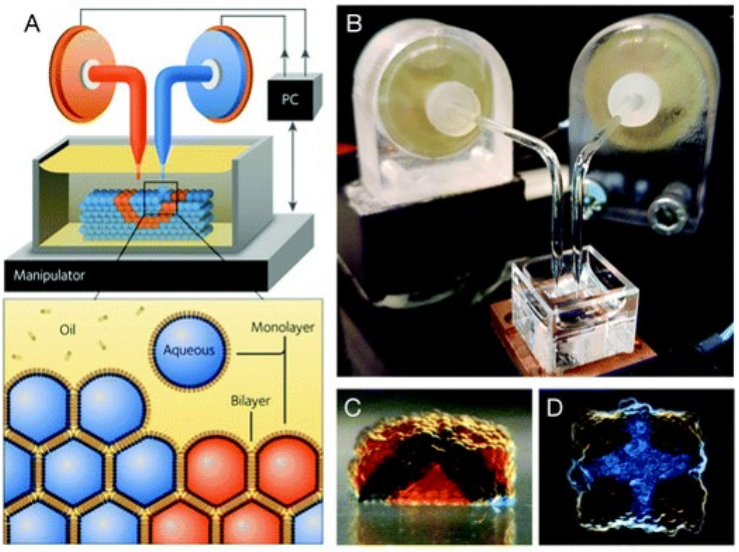


Figure 1.4: Using droplet printer to create 3D droplet network with multiple droplets. (A) A schematic showing two printing nozzles, each printing a different droplet solution into a 3D-patterned droplet network. A micromanipulator moved the recipient oil chamber to allow precise placement of the droplets, while a piezo transducers (PC) controlled the droplet size. (B) Photo of the 3D droplet printer. (C and D) Two different droplet networks with different solution in the droplets. Figure adapted from (*79*).

Droplets could also contain molten hydrogel, which could solidify with the bilayer intact (*83*). The synthetic droplet networks could also be transferred to an aqueous environment, which would enable direct chemical communication between the droplet networks and the aqueous surrounding (Fig. 1.5) (*84*).

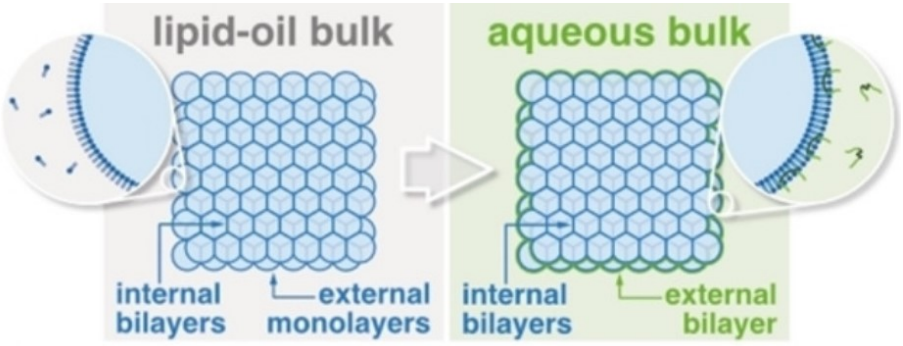


Figure 1.5: Phase transfer of droplet networks in a lipid-in-oil solution to an aqueous solution. The phase transfer was carried out by adding the aqueous solution around the droplet network structure, followed by the removal of the oil phase using a surfactant block copolymer Pluronic F68. Figure adapted from (*85*).

1.8 Thesis outline

This thesis introduces novel strategies utilizing ssDNA to regulate selective gene activation through base-pairing complementation of genes with single-stranded defective promoters, which for simplicity are referred to as defective genes in this thesis. (Fig. 1.6). Selective gene activation was achieved by using different promoters or by using inhibitors to remove undesired ssDNA inputs. The ssDNA was further split in half to construct complex logic gates (AND-OR-AND-OR-AND gates) controlling gene activation. ssDNA activated production of multiple RNA, proteins, and functional enzymes. Furthermore, we demonstrate the ability to control movement of the ssDNA across droplet networks by selectively disrupting the bilayer or using a membrane potential to deliver the ssDNA across protein pores ion the bilayer.

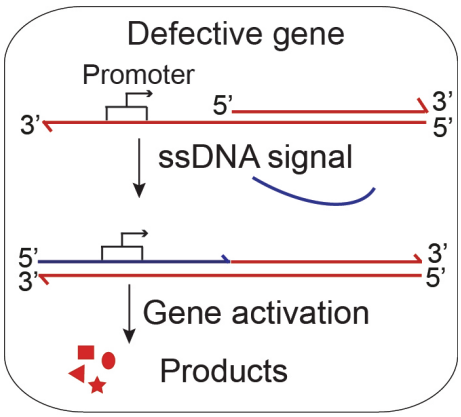


Figure 1.6: Schematic view of the gene activation process. ssDNA signal complemented defective genes with a single-stranded promoter to produce products.

In chapter 2, two distinct approaches are demonstrated for selective gene activation. Firstly, defective genes with unique promoters were exclusively activated by ssDNA inputs carrying matching promoter sequences. Secondly, we utilized DNA strand displacement reactions to eliminate unwanted ssDNA from the defective genes. The ssDNA would have an exposed toehold after binding to the defective genes, allowing the inhibitors to remove the undesired ssDNA through strand displacement reactions. Additionally, by splitting the ssDNA into two fragments, we demonstrated the combined use of RNA polymerase with DNA ligase to construct complex logic gates (AND-OR-AND-OR-AND gates).

In chapter 3, we described the synthesis of long defective genes coding for proteins, and demonstrated that the ssDNA input complementing to the defective genes could produce functional proteins and enzymes, acting as a transcription factor mimic to activate multiple genes simultaneously.

In chapter 4, to use ssDNA to control gene activation in synthetic tissues, we separated the ssDNA and the defective gene in distinct compartments separated by bilayers, such that gene activation occurred only upon bilayer rupture or membrane potential. This facilitated on-demand gene production where gene activation only occurred in the presence of suitable environmental triggers.

Chapter 2

DNA signal selectively activated transcription

2.1 Summary

This chapter discusses the use of the ssDNA signals to selectively produce RNA transcripts and proteins. By complementing defective genes that had single-stranded promoters and were inactive on their own, ssDNA signals activated gene expression (Section 2.2). Two different strategies were used for selective gene activation. Firstly, the defective genes had different promoters and were only activated by signals carrying the same promoter sequence (Section 2.3). Second, the signals were engineered to have an exposed toehold after binding to the defective genes. Signal inhibitors could selectively remove the undesired signals from the defective genes by stand displacement reaction (Section 2.4). We further demonstrate that RNA polymerase and DNA ligase could be used in combination with the DNA signal. This allowed the construction of complex logic gates (AND or AND or AND gate) to regulate gene expression (Section 2.5). We then explored the use of ssDNA signals to produce functional proteins and enzymes. After optimizing production of long defective genes with single-stranded promoters (Section 2.7), we demonstrate that DNA signal activated protein production by complementing defective genes (Section 2.8). We finally discuss the use of DNA signal as a transcription factor mimic to simultaneously activate production of multiple proteins (Section 2.9).

2.2 Defective genes produced RNA aptamers

2.2.1 Summary

This section describes the use of the ssDNA signals to activate the defective genes, producing RNA aptamers that could bind and activate the fluorescence of small molecule dyes.

2.2.2 DNA signal activated transcription of defective genes

To use the ssDNA signals to activate transcription, we designed genes that were single-stranded from approximately -20 to +20 nucleotides of the transcription start site, with the non-template strand missing. The single-stranded region included the promoter (∼20 nt) and the beginning (5' end) of the transcribed region (∼20 nt). We referred to those constructs as defective genes in this thesis. The defective genes coding for RNA aptamers were made by annealing two ssDNA strands of different lengths. Briefly, the strands were heated to 98 °C for 10 s and cooled at a rate of 0.1 °C s^{-1} to 20 °C. The ssDNA strands (<200 nt) were obtained commercially (Fig. 2.1).

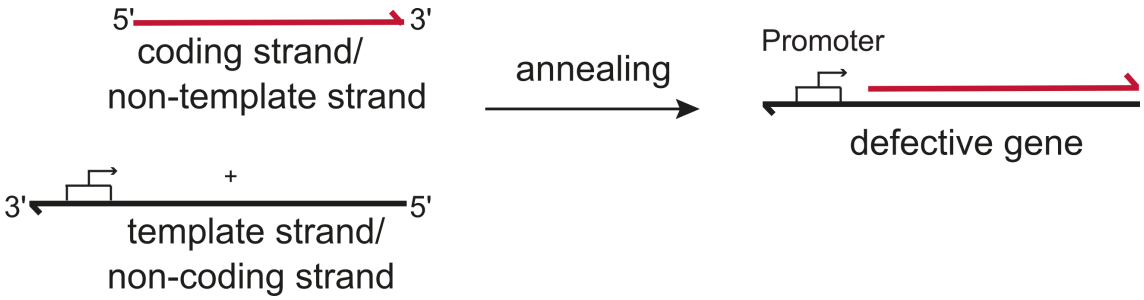


Figure 2.1: A schematic of the defective gene fabrication process. Defective genes were made by annealing two single-stranded DNA of different lengths. The coding strand, also called the non-template strand or sense strand, shares the same sequence as the RNA transcript produced, with thymine instead of uracil. The template strand, also known as the anti-sense strand, serves as the template for RNA synthesis through base-pairing interactions.

The ssDNA signals were complementary to the single-stranded region on the defective genes, such that transcription activation occurred only when the ssDNA signals complemented the promoter region (Fig. 2.2A). As the signals annealed to the defective genes, even if the signals complemented the defective genes perfectly,

there would be a nick (strand-break) between the 3' end of the signals and the defective genes. The nick was on the non-template strand at approximately +20 nucleotides of the transcription start site. Since the full-length transcripts could still be made from DNA when the non-template strand was entirely missing after the promoter (*58*), the nick was not expected to significantly affect RNA transcription.

To assess the production of RNA, we designed defective genes to code for RNA aptamers that could bind and activate the fluorescence of small molecule dyes. Transcription activation was studied at different concentrations of the defective gene and the signal from 0 to 1000 nM, using defective genes coding for Broccoli RNA aptamer, which could activate the fluorescence of DFHBI-1T. After 3 h incubation, we found that a 35 fold increase in Broccoli fluorescence was observed with as little as 10 nM of the defective gene coding for Broccoli (with sequence B1, note that DNA sequences are in the Methods chapter) and 10 nM of the single-stranded DNA signal (with sequence s1) complementary to the defective Broccoli (Fig. 2.2B). Furthermore, the fluorescence without the defective gene or the signal remained within 2 fold of the fluorescence of a transcription mixture without any DNA. This demonstrated precise on-off control of our gene activation system. It was especially important to verify the low background fluorescence in our system, as it was reported that nonspecific transcription could occur when a high concentration of T7 RNAP was used (8.6 units/μL) (*86*), which was just less than two times higher than the NEB recommended concentration (5 units/μL) used in this thesis.

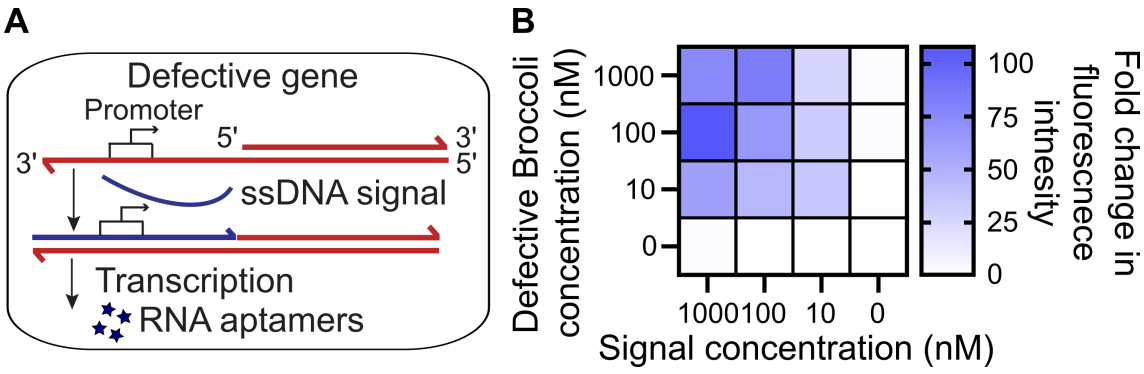


Figure 2.2: (A) A schematic of the gene activation process. ssDNA signals complemented defective genes with a single-stranded promoter (with a shorter coding strand) to produce RNA transcripts. (B) A heat map of the fold change in fluorescence intensity from the produced RNA when different concentrations of the defective Broccoli (B1) and the Broccoli signal (s1) were mixed in bulk after 3 h, compared to the control with no signal and no defective gene. Values in the heatmap are the mean of $n = 4$ technical repeats.

2.3 Selective gene activation by ssDNA signal using different promoters

An advantage using ssDNA for gene activation was that the high sequence specificity required for DNA complementation (*87*) allowed selective gene activation by different ssDNA signals, where different DNA signals activated specific defective genes. This was similar to small-molecule gene activators where different molecules could activate different genes (*2*). We explored two different strategies for selective gene activation. This section describes the first strategy for selective gene activation - the defective genes had different promoters and were only activated by the signals carrying the same promoter sequence. We defined successful gene activation when the aptamer fluorescence had increased by at least 3 fold in the presence of the DNA signal, compared to samples without any DNA signal.

2.3.1 RNA aptamers specificity to fluorophore dyes

To illustrate the differentiation between activation of distinct defective genes, the genes were designed to code for different RNA aptamers upon activation, each aptamer binding to a different fluorophore. This design required orthogonal pairs of RNA aptamers and fluorophores, where each aptamer only activated its corre-

sponding fluorophore without affecting others, as well as non-overlapping fluorescence spectra of the fluorophores. Consequentially, the fluorescence of IVT mixture would inform us as to which gene was activated. While many RNA aptamer and fluorophore pairs were developed (*67*), Broccoli-DFHBI and Malachite green aptamer - Malachite green remained the only widely used orthogonal RNA aptamer-fluorophore pairs (*88*, *89*). Unfortunately, malachite green was highly toxic to cells (*90*). As we envisioned potential use of the ssDNA signal, the defective genes, and RNA aptamers in synthetic systems interfaced with living cells (more will be discussed in section 4.3), orthogonal aptamer-fluorophore pairs with non-toxic fluorphores would be preferred. The Unrau group reported Mango-TO1B and Peach-TO3B as orthogonal aptamers. According to the Unrau group, Mango aptamer had a higher affinity for TO1B (K_d = 1.7 ± 1.0 nM) than TO3B (K_d = 160 ± 20 nM), while Peach aptamer had a higher affinity for TO3B (K_d = 20 ± 1 nM) than TO1B (K_d = 43 ± 4 nM). Both aptamers therefore could bind considerably to both fluorophores (*73*). SRB-2 - TMR-DN pair was reported to be orthogonal to both Spinach - DFHBI and Malachite green aptamer - Malachite green pairs. TMR-DN was not commercially available and it was therefore difficult to be adapted for use (*91*).

To achieve these requirements, we investigated the ability of the RNA aptamers Broccoli, Mango and Pepper to activate the fluorescence of DFHBI-1T, TO1B and HBC620. All three fluorophores were commercially available and non-toxic. By performing these experiments for 3 h, we found two sets of orthogonal RNA aptamer-fluorophore pairs: Broccoli/DFHBI-1T and Pepper/HBC620, as well as Mango/TO1B and Pepper/HBC620. DFHBI-1T fluorescence was activated by Broccoli aptamer but not by Pepper and Mango aptamer (Fig. 2.3A). TO1B fluorescence was activated by both Broccoli and Mango aptamer, but not by Pepper aptamer (Fig. 2.3B). HBC620 fluorescence was activated by Pepper aptamer, but not by Broccoli or Mango aptamer (Fig. 2.3C).This investigation revealed two sets of orthogonal RNA aptamer-dye pairs: Broccoli/DFHBI-1T and Pepper/HBC620, as well as Mango/TO1B and Pepper/HBC620. TO1B fluorescence was activated by

both Broccoli and Mango aptamer, and therefore could not be used orthogonally in this combination. It is important to note that the fold change in fluorescence strongly depended on the fluorophore used, as different fluorophores had different brightness (summarised in (*67*)).

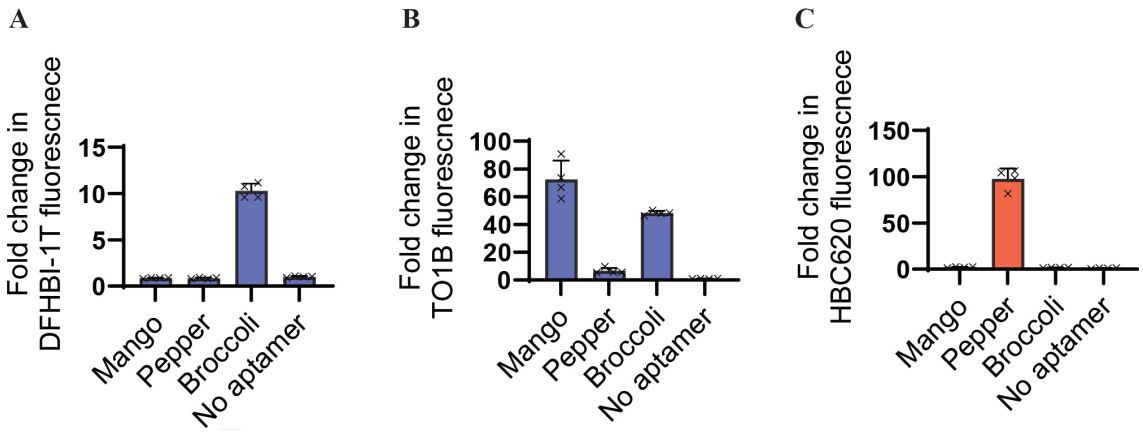


Figure 2.3: (A to C) Bar graphs of fold change in fluorescence intensities of (A) DFHBI-1T, (B) TO1B, and (C) HBC620, with DNA transcribing different RNA aptamers in bulk after 3 hours, compared to the control with no aptamer. Technical replicates are displayed by crosses and the heights of the bars are the mean. The error bars show the standard deviation.

While this was not a focus of this thesis, the discovery of commercially available non-toxic orthogonal fluorophore-aptamer pairs might be useful for RNA imaging in cells, where co-localization and trafficking of multiple RNA targets could be studied using orthogonal fluorophore-aptamer pairs (*74*). This may be especially useful in the study of anaerobic bacteria, where the use of fluorescent proteins labels were limited. Maturation of fluorescent proteins required oxygen, which was toxic to many species of anaerobic bacteria (*92*).

2.3.2 Selective gene activation by ssDNA signal using different promoters

In the first strategy for selective gene activation using the ssDNA signals, distinct defective genes with different promoters were selectively activated by the signals carrying matching promoter sequences. This strategy was expected to work despite the fact that T3, T7 and SP6 polymerases were structurally similar, as there were

only 7 identical bases in the T3, T7 and SP6 consensus promoters sequences (CACTAXAG, -7 to +1 nucleotides from the transcription start site) (*66*). This sequence had a calculated T_m 8 °C (*93*). At the transcription temperature of 37 °C, the ssDNA signal (∼40 nt) containing sequences of one of the promoters would bind strongly to the defective genes with the same promoter, but not bind significantly to the defective genes with sequences of the other promoters. For example, ssDNA containing sequences of T7 promoter would only bind significantly to defective genes with the T7 promoter by base-pairing interaction, but not to defective genes with the SP6 promoter, as there are only 7 bases between the two that can form Watson-Crick base-pairs. Therefore, we used a mixture of the defective Broccoli with a single-stranded T7 promoter (B1) and the defective Pepper with a single-stranded SP6 promoter (P1) (Fig. 2.4A). After 3 h incubation, the presence of the Broccoli signal with the T7 promoter sequence (s2) only produced the Broccoli aptamer, while the presence of the Pepper signal with the SP6 promoter sequence (s3) only produced the Pepper aptamer. In the presence of both the Broccoli and the Pepper signals, both aptamers were produced, whereas without the signals no aptamers were produced (Fig. 2.4B,C). When more than two fluorophores were used, fluorescence intensity was normalized for each aptamer to account for differences in brightness and facilitate result visualization. The mean fluorescence of the brightest condition was set to 100, while the mean fluorescence of the no-signal control was set to 0. Data showing the fold change in fluorescence before normalization is also provided alongside the normalized data.

We also showed the flexibility of this different promoter strategy, which worked for a defective Mango with T7 promoter (M1) and a defective Pepper with SP6 promoter (P1) (Fig. 2.5A). After 3 h incubation, the presence of a Mango signal with the T7 promoter sequence (s4) only produced the Mango aptamer, while the presence of a Pepper signal with the SP6 promoter sequence (s3) only produced the Pepper aptamer. In the presence of both the Mango and Pepper signals, both aptamers were produced, whereas without the signal no aptamers were produced (Fig. 2.5B,C).

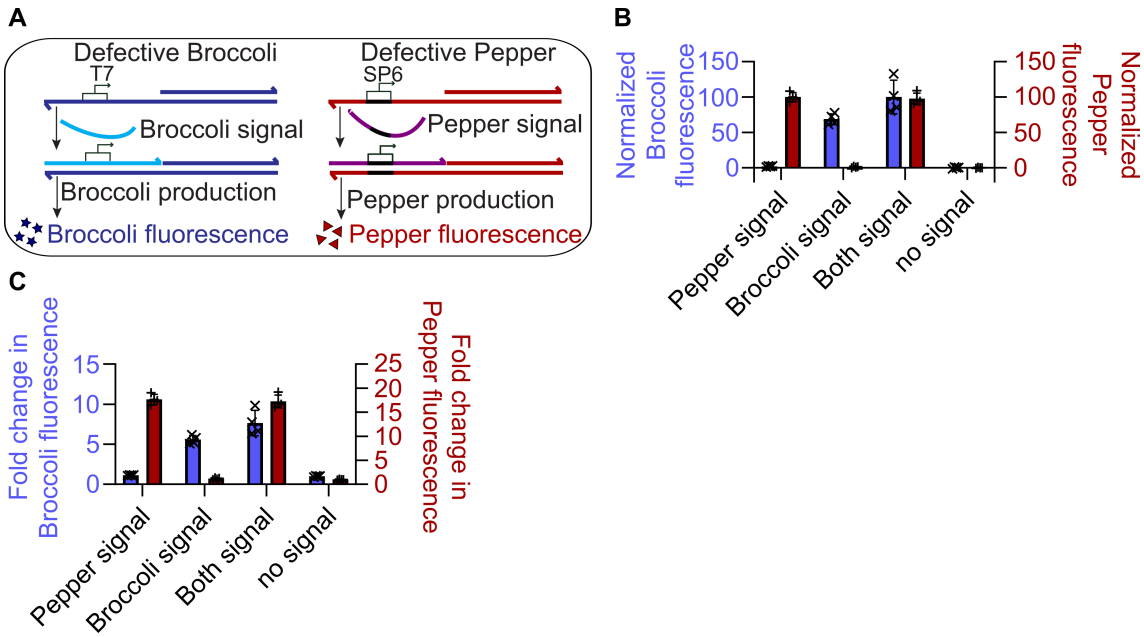


Figure 2.4: (A) A schematic of selective gene activation using the defective Broccoli with the T7 promoter and the defective Pepper with the SP6 promoter. The defective genes were only activated by the signals carrying the same promoter sequences. (B) A bar graph of the normalized fluorescence intensity of the defective Pepper (P1) and the defective Broccoli (B1) mixture in bulk after 3 h when the Pepper (s3) and/or the Broccoli (s2) signal were added. The mean fluorescence intensity of the no signal control and the brightest sample were normalized to 0 and 100 respectively. (C) A bar graph of the fold change in fluorescence intensity of the defective Pepper and the defective Broccoli mixture in bulk after 3 h when the Pepper and/or the Broccoli signal were added. In the bar graphs, technical replicates are displayed by crosses and the heights of the bars are the mean. The error bars show the standard deviation.

In this orthogonal signalling design, as the DNA signal specificity was achieved using different promoters, the number of RNAP with distinct promoter sequences placed a limit on the number of orthogonal signal and defective gene pairs. The next section describes an alternate approach to achieve signal specificity using only T7 RNAP.

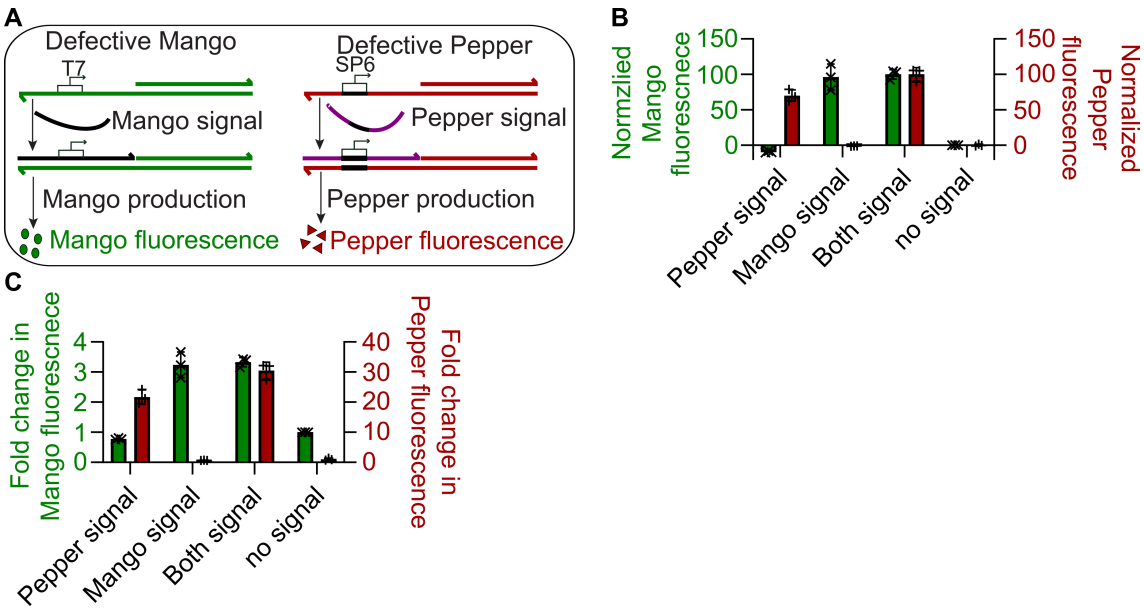


Figure 2.5: (A) A schematic of selective gene activation using the defective Mango with T7 promoter and the defective Pepper with SP6 promoter. The defective genes were only activated by the signals carrying the same promoter sequences. (B) A bar graph of normalized fluorescence intensity of defective Mango (M1) and Pepper (P1) mixture in bulk after 3 hours when Pepper (s3) and/or Mango signal (s4) were added. The mean fluorescence intensity of the no signal control and the brightest sample were normalized to 0 and 100 respectively. (C) A bar graph of fold change in fluorescence intensity of defective Mango (M1) and Pepper (P1) mixture in bulk after 3 h when Pepper (s3) and/or Mango signal (s4) were added.In the bar graphs, technical replicates are displayed by crosses and the heights of the bars are the mean. The error bars show the standard deviation.

2.4 Selective gene activation by ssDNA signals using signal inhibitors

2.4.1 Design rationale

Our second strategy for selective gene activation involved using the same T7 RNA polymerase but with different adjacent sequences to the promoter for complementation of different signals. It was more challenging to achieve signal specificity when only one polymerase was used, as the T_m of the full-length T7 promoter consensus sequence was 57 °C (TAATACGACTCACTATAG, -17 to +1 nucleotides from the transcription start site) (*94*). The Uberla group reported alternate high activity T7 promoter variants, but all of them still shared the same sequence -17 to -5 nucleotides from the transcription start site (TAATACGACTCAC) (*94*). This sequence still had a calculated T_M of 47 °C (*93*). Therefore, any signals bound to the

wrong defective gene would only detach above 47 °C. At the transcription temperature of 37 °C, all the signals carrying the T7 promoter sequence would activate all the defective genes with the defective T7 promoter, regardless of whether the sequences adjacent to the promoters could form Watson-Crick base-pairs or not. To achieve selective gene activation using T7 RNA polymerase only, we constructed novel signals with exposed toeholds after binding to the defective genes, thus DNA strand displacement reaction could be used to remove undesired signals via complementary inhibitors (Fig. 2.6, A and B).

2.4.2 Selective gene activation by ssDNA signals using signal inhibitors

With this principle, we designed defective Broccoli (B1) and defective Pepper (P2) that had single-stranded T7 promoter sequences but were activated by different signals. The defective genes had different sequences flanking the promoter. Broccoli signal (s2) matched the single-stranded region on the defective Broccoli, with extra 20 nucleotides (nt) at the 3' end of the signal. Similarly, Pepper signal (s5) matched the single-stranded region on the defective Pepper, with an extra 20 nt at the 3' end. Broccoli signal inhibitor (I1) and Pepper signal inhibitor (I2) were reverse complementary to the Broccoli signal and the Pepper signal respectively. We also designed an Universal signal (s6) which only had the complementary T7 promoter sequence, lacking the flanking sequences required for strand displacement reactions by the inhibitors.

In mixtures that contained the defective Broccoli and the Pepper signal inhibitor, after 3 h incubation, the Broccoli signal or the Universal signal produced Broccoli aptamer, while the Pepper signal did not (Fig. 2.7A). Similarly, in a mixture that contained the defective Pepper and the Broccoli signal inhibitor, the Pepper signal or the Universal signal produced Pepper aptamer, while the Broccoli signal did not (Fig. 2.7B). In contrast, when the inhibitors were not used, high activation of the defective genes by the wrong signals were observed (Fig. 2.7C), demonstrating that the signal inhibitors were necessary to prevent defective gene activation by the wrong

signal. The fold change in fluorescence data are in (Fig. 2.7D-F)

To confirm that selective gene activation was achieved because of the strand displacement reactions, we verified that the Pepper signal could be removed from the defective Broccoli by the Pepper signal inhibitor, by analysing the size of the constructs with agarose gel electrophoresis. The coding strand of the defective Broccoli (lane 1) and the template strand of the defective Broccoli (lane 2) annealed to form the defective Broccoli (lane 3). The Pepper signal (lane 4) could bind to the defective Broccoli (lane 5), and the Pepper signal inhibitor (lane 6) removed the Pepper signal from the defective Broccoli (lane 7) (Fig. 2.8).

To provide perspective on the lengths of the complementary regions on the signals and the defective genes used in this design, the sequences of the Broccoli signal, the Pepper signal, the defective Broccoli, and the defective Pepper were illustrated here (Fig. 2.9).

We showed the flexibility of this inhibitor strategy which also worked for a defective Mango (M1) and a defective Pepper (P2). This system had different sequences flanking the promoter and therefore different sequences involved in the strand-displacement reactions, but selective gene activation was also observed after 3 h incubation. Both the defective Mango and the defective Pepper contained the single-stranded T7 promoter. Mango signal (s4) was reverse complementary to Mango signal inhibitor (I3), and Pepper signal (s5) was reverse complementary to Pepper signal inhibitor (I2).

Previously, the Universal signal (s6) included only the T7 promoter sequence, lacking flanking sequences that would enable removal by inhibitors during strand displacement reactions once bound to a defective gene. Here, we designed a new Universal signal (s7) that incorporated flanking sequences around the T7 promoter. These sequences were unique and did not match the flanking sequences of any inhibitors, ensuring that inhibitors could not displace the new Universal signal (s7) in strand displacement reactions. This design aimed to demonstrate that the flanking sequences of the Universal signal do not interfere with its function. Additionally, we introduced a PolyA signal containing 40 adenine nucleotides as a control, which

was not expected to activate transcription.

In a mixture of the defective Pepper and the Mango signal inhibitor, after 3 h incubation, presence of the Pepper signal or the Universal signal activated Pepper aptamer production, while presence of the Mango signal or the polyA signal did not (Fig. 2.10A). In a mixture of the defective Mango (M1) and the Pepper signal inhibitor (I2), presence of the Mango signal or the Universal signal activated Mango aptamer production, while presence of the Pepper signal or the polyA signal did not (Fig. 2.10B). In contrast, presence of the Mango signal without the Mango signal inhibitor led to high activation of the defective Pepper (Fig. 2.10C), demonstrating that the Mango signal inhibitor was necessary to prevent defective Pepper activation by the Mango signal.

2.4.3 Three defective genes

We then expanded the system to include three defective genes: defective Pepper (P2), defective Mango (M1), and defective Broccoli (B2). The Pepper signal (s5), the Mango signal (s4), and the Broccoli signal (s9) were reverse complementary to the Pepper signal inhibitor (I2), the Mango signal inhibitor (I3), and the Broccoli signal inhibitor (I4) respectively. After 3 h incubation, in a mixture of the defective Pepper, the Mango signal inhibitor and the Broccoli signal inhibitor, the defective Pepper was activated by the Pepper signal or the Universal signal, but not by the Broccoli signal or the Mango signal. This was also observed when using the correct combinations of the inhibitors for the Broccoli and the Mango signal/ defective gene pairs (Fig. 2.11, A to B). Overall, our findings demonstrate that ssDNA signals could selectively activate genes by using 1) multiple promoters or, 2) by using strand displacement reactions to remove undesired signals when one promoter was used. In our system, each signal activated a different defective gene, while the universal signals activated multiple defective genes.

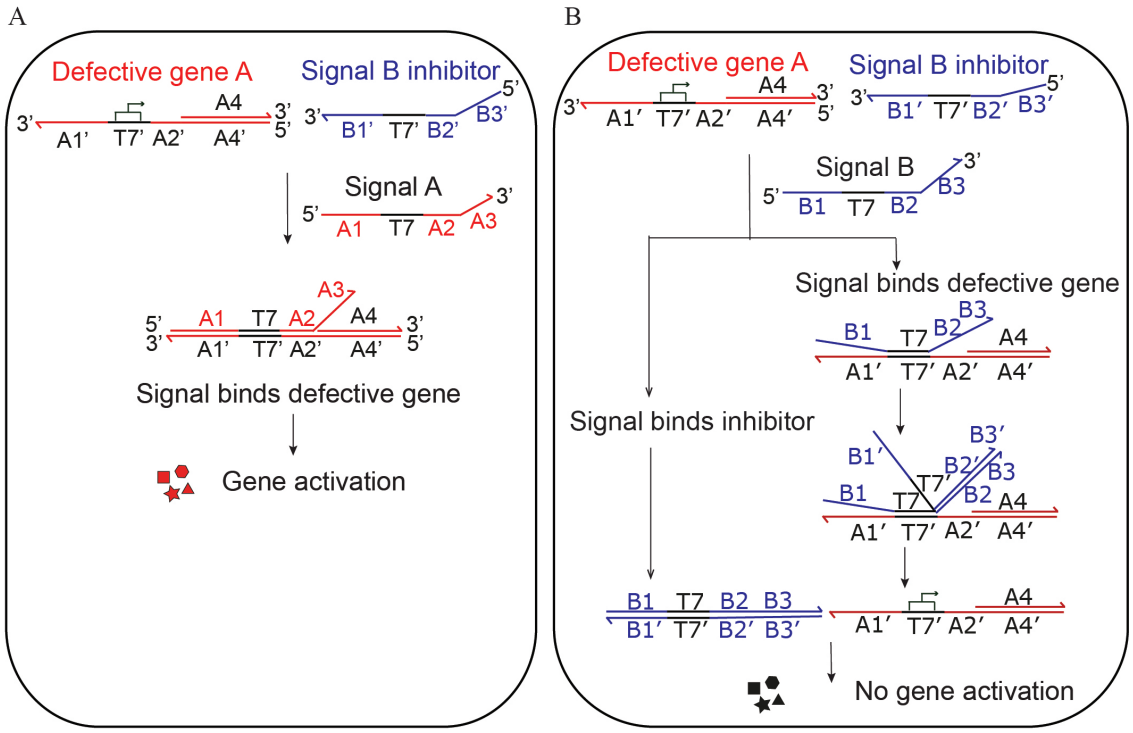


Figure 2.6: (A) A schematic of successful gene activation using an uninhibited signal. The coding strand and the template strand sequences of the T7 promoter were labelled T7 and T7' respectively. Other than the promoter sequences, DNA sequences on the coding strand of defective gene A were labelled A1, A2, A3 etc. DNA sequences on the template strand of defective gene A were numbered A1', A2', A3' etc. Sequences with labels differ by ' (e.g. A1 and A1') were reverse complementary to each other. In a mixture of defective gene A and signal B inhibitor, signal A was not inhibited by signal B inhibitor and could activate defective gene A. Signal A matched the single-stranded region on defective gene A, with 20 extra nucleotides (nt) on the 3' end of the signal. As signal A was longer than the single-stranded region on defective gene A, a toehold (A3) was exposed after signal binding. Defective gene A was activated as the presence of the toehold did not inhibit transcription. (B) A schematic of signal removal using signal inhibitors. In a mixture of defective gene A and signal B inhibitor, signal B could bind directly to signal B inhibitor as they were complementary to each other, or it could also bind to defective gene A due to the T7 promoter sequence. In the latter case, the exposed toehold (B3) was recognized by signal B inhibitor, and signal B inhibitor removed signal B from defective gene A. In either case, defective gene A was not activated by signal B.

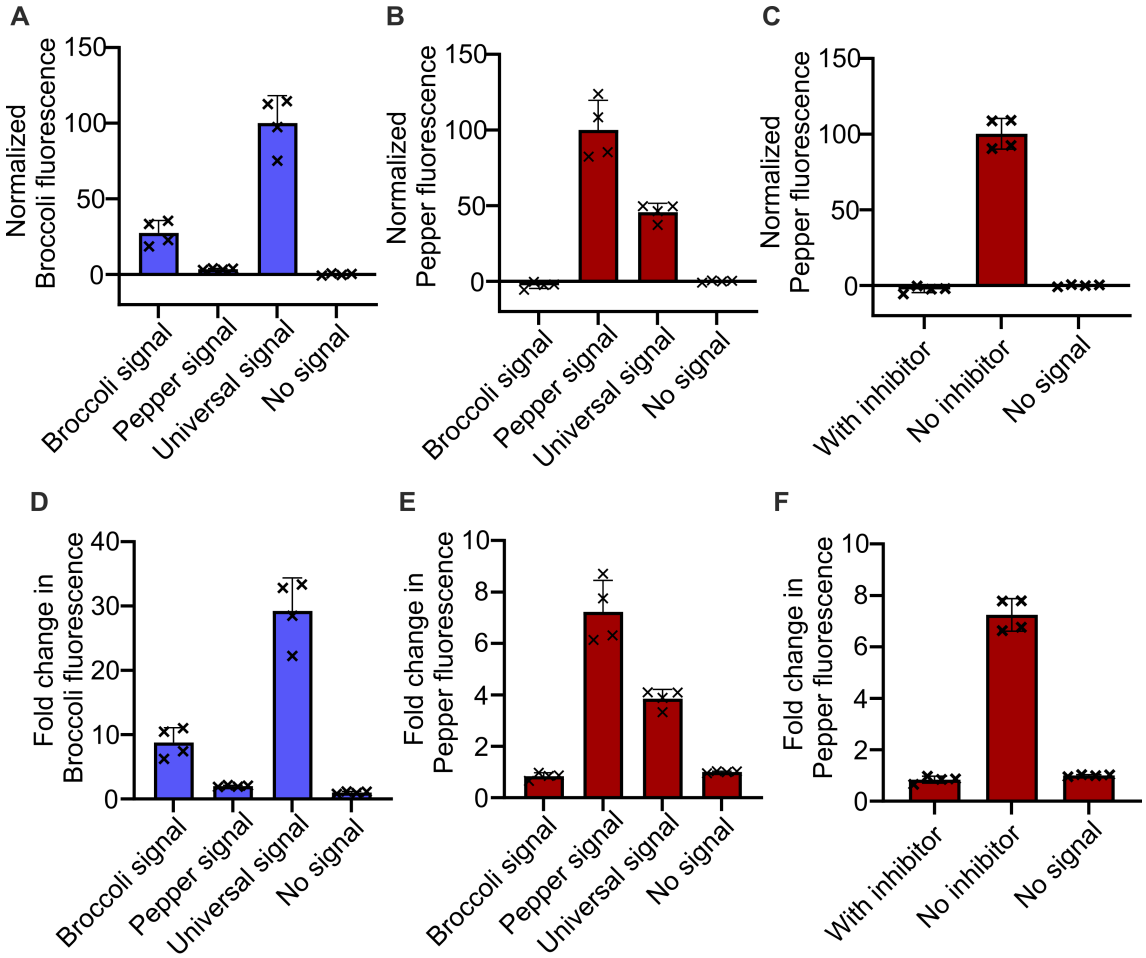


Figure 2.7: (A) A bar graph of normalized fluorescence intensity of the Broccoli aptamer in a bulk mixture of the defective Broccoli (B1) and the Pepper signal inhibitor (I2) after 3 h of addition of the signal. (B) A bar graph of normalized fluorescence intensity of the Pepper aptamer in a bulk mixture of the defective Pepper (P2) and Broccoli signal inhibitor (I1) after 3 h of signal addition. (C) A bar graph of normalized fluorescence intensity of the Pepper aptamer in a bulk mixture of the defective Pepper (P2) and the Broccoli signal (s2) after 3 h, with or without the Broccoli signal inhibitor (I1). (D) A bar graph of fold change in fluorescence intensity of the Broccoli aptamer in a bulk mixture of the defective Broccoli and the Pepper signal inhibitor after 3 h of addition of the signal, compared to the control with no signal. (E) A bar graph of normalized fluorescence intensity of the Pepper aptamer in a bulk mixture of the defective Pepper and Broccoli signal inhibitor after 3 h of signal addition, compared to the control with no signal. (F) A bar graph of normalized fluorescence intensity of the Pepper aptamer in a bulk mixture of the defective Pepper and the Broccoli signal after 3 h, with or without the Broccoli signal inhibitor, compared to the control with no signal. In the bar graphs, technical replicates are displayed by crosses and the heights of the bars are the mean. The error bars show the standard deviation. In A to C, the mean fluorescence intensity of the no signal control and the brightest sample were normalized to 0 and 100 respectively.

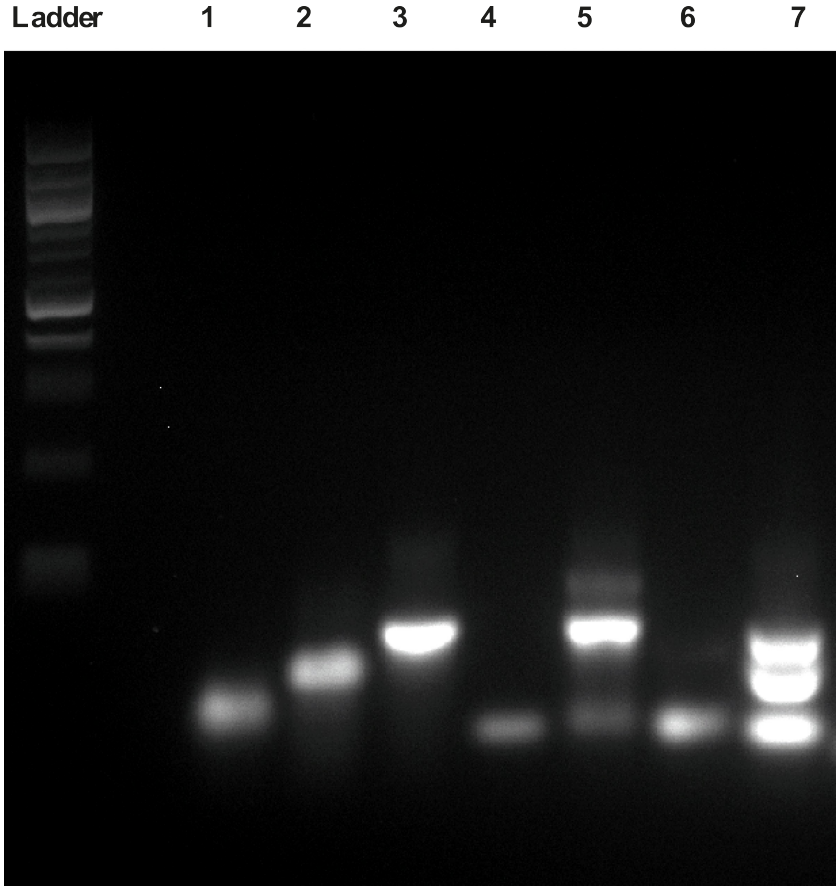


Figure 2.8: Agarose gel electrophoresis of DNA constructs (3% Agarose). Ladder: 100 bp DNA ladder (NEB). Lane 1: The coding strand of the defective Broccoli (B1) (49 nt). Lane 2: The template strand of the defective Broccoli (B1) (74 nt). Lane 3: The defective broccoli (B1, 49 bp and 25 nt overhang), formed by annealing the coding strand and the template strand. Lane 4: The Pepper Signal (s5, 44 nt). Lane 5: The Pepper signal (s5, 44 nt) bound to the defective Broccoli (B1, 49 bp with 25 nt overhang). Lane 6: The Pepper signal inhibitor (I2, 44 nt). Lane 7: The Pepper signal inhibitor (I2) removed the Pepper signal (s5) from the defective Broccoli (B1). nt: nucleotides, bp: base pairs.

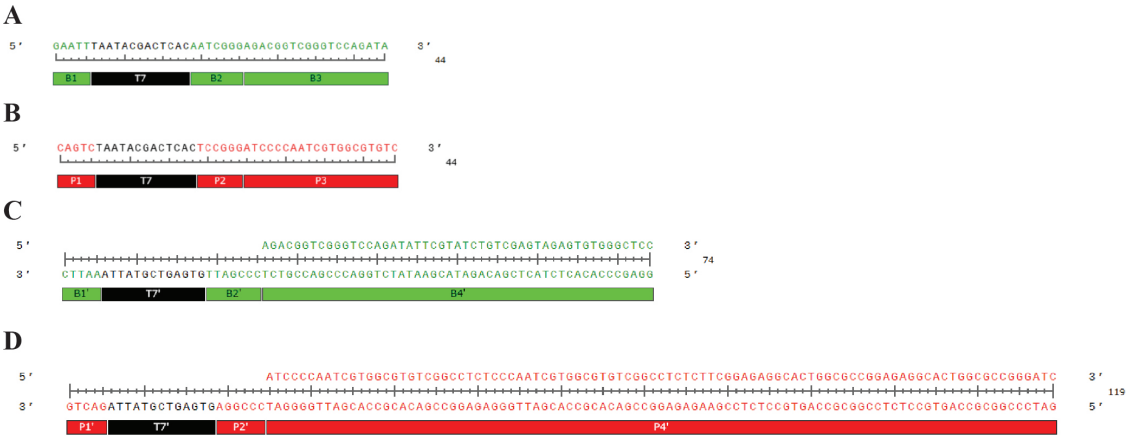


Figure 2.9: Diagrams showing the sequences and lengths of (A) the Broccoli signal, (B) the Pepper signal, (C) the defective Broccoli, (D) the defective Pepper. Sequences differ by ’ (e.g. T7 and T7’) were reverse complementary to each other.

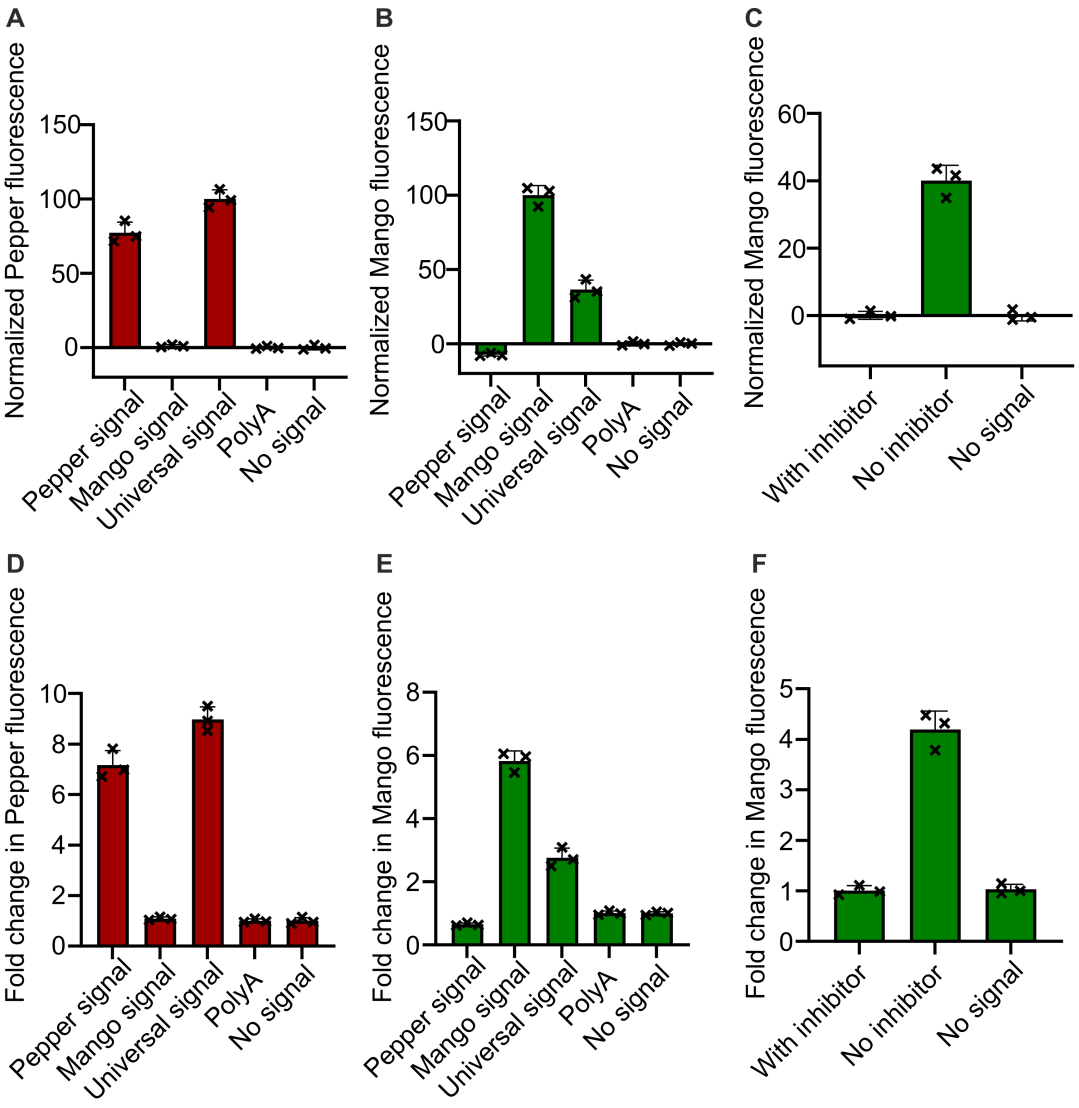


Figure 2.10: (A) A bar graph of fluorescence intensity of the Pepper aptamer in a bulk mixture of the defective Pepper (P2) and the Mango signal inhibitor (I3) after 3 h of signal addition. (B) A bar graph of fluorescence intensity of the Mango aptamer in a bulk mixture of the defective Mango (M1) and the Pepper signal inhibitor (I2) after 3 h of signal addition. (C) A bar graph of fluorescence intensity of the Mango aptamer in a bulk mixture of the defective Mango (M1) and the Pepper signal (s4) after 3 h of signal addition, with or without the Pepper signal inhibitor (I2). For each aptamer, the mean fluorescence intensity of the no signal control and the brightest sample were normalized to 0 and 100 respectively. (D) A bar graph of fold change in fluorescence intensity of the Pepper aptamer in a bulk mixture of the defective Pepper (P2) and the Mango signal inhibitor (I3) after 3 h of signal addition, compared to th control with no signal. (B) A bar graph of fold change in fluorescence intensity of the Mango aptamer in a bulk mixture of the defective Mango (M1) and the Pepper signal inhibitor (I2) after 3 h of signal addition, compared to the control with no signal. (C) A bar graph of fluorescence intensity of the Mango aptamer in a bulk mixture of the defective Mango (M1) and the Pepper signal (s4) after 3 h of signal addition, with or without the Pepper signal inhibitor (I2), compared to the control with no signal. In the bar graphs, technical replicates are displayed by crosses and the heights of the bars are the mean. The error bars show the standard deviation.

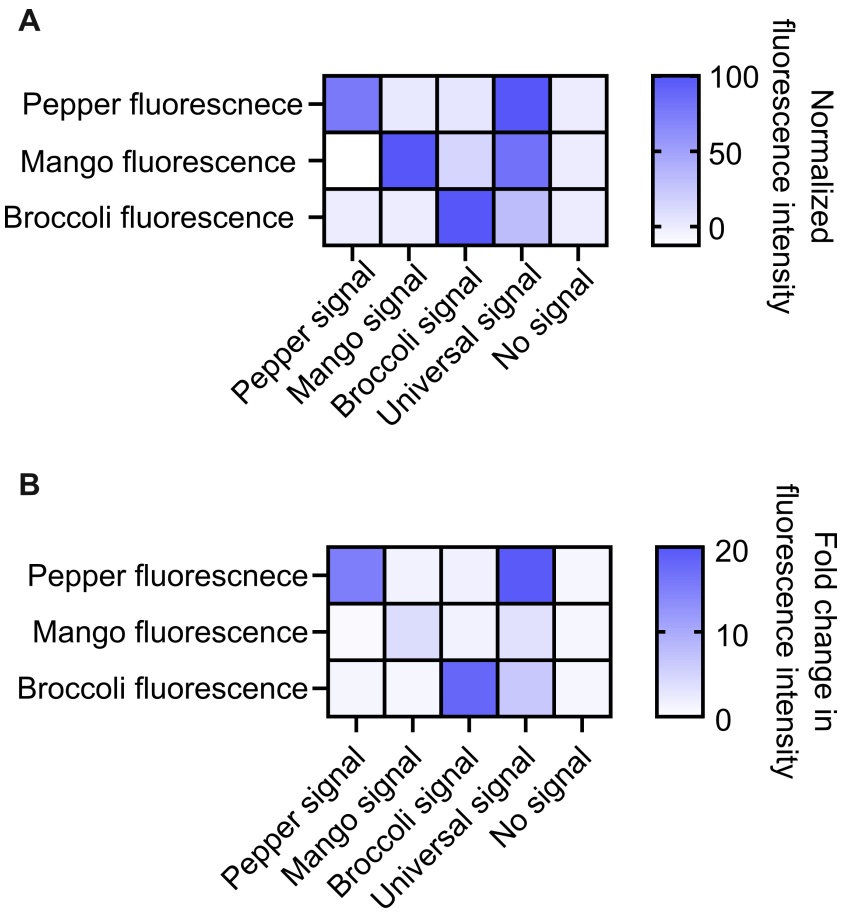


Figure 2.11: (A) A heat map of normalized fluorescence intensity of RNA aptamers after 3 h when different signals were added. The first row showed normalized fluorescence intensity of the Pepper aptamer in a bulk mixture of the defective Pepper (P2), the Mango signal inhibitor (I3), and the Broccoli signal inhibitor (I4). The second and third rows showed the normalized fluorescence intensity of the Mango aptamer and the Broccoli aptamer respectively, in a bulk mixture of the correct combination of the defective genes and the signal inhibitors. For each aptamer, the mean fluorescence intensity of the no signal control and the brightest sample were normalized to 0 and 100 respectively. (B) A heat map of fold change in fluorescence intensity of the RNA aptamers after 3 hours when different signals were added. (B) A heat map of fold change in fluorescence intensity of RNA aptamers 3 h after different signals were added, compared to the no signal control, in the same conditions as (A).

2.5 Combined use of DNA ligase and RNA polymerase

This section demonstrates that RNA polymerase and DNA ligase could be used in combination with the DNA signal. This allowed construction of complex logic gates (AND or AND or AND gate) to regulate gene expression.

2.5.1 Splitting DNA signal to create AND gates

We next investigated whether by using a combination of DNA ligases and RNA polymerases we could construct complex logic gates, a prerequisite for building computational devices. The Broccoli signal (s2) was split into two shorter ssDNA fragments, each carrying part of the promoter sequence. The signal fragments were numbered by the position where the signal was split. The upstream signal fragments were denoted by U and the downstream signal fragments were denoted by D. The downstream signal was 5'phosphorylated, which allowed the fragments to be ligated by DNA ligase. After 3 h incubation, transcription activation only occurred when both signal fragments were present, equivalent to an AND gate in logic operations (Fig. 2.12A). For instance, AND gate was formed by splitting the signal after -12 nucleotides from transcription start site. The upstream signal (-12U) and the downstream signal (-12D) must both be present to activate the defective Broccoli. This created an AND gate for gene activation, where gene activation was triggered by (-12U and -12D). This was mathematically equivalent to (-12D $\wedge$ -12U), where $\wedge$ denoted 'AND'. We created four AND gates by splitting the signal after position -12, -11, -10 and -9 nucleotides from the transcription start site. The gates were: (-12D $\wedge$ -12U), (-11D $\wedge$ -11U), (-10D $\wedge$ -10U), and (-9D $\wedge$ -9U). Transcription activation was observed only when both the upstream signal fragment and the downstream signal fragment were present (Fig. 2.12B).

Transcription activation did not occur when the downstream signal fragment was not 5' phosphorylated, showing the necessity of ligation for gene activation (Fig. 2.13.

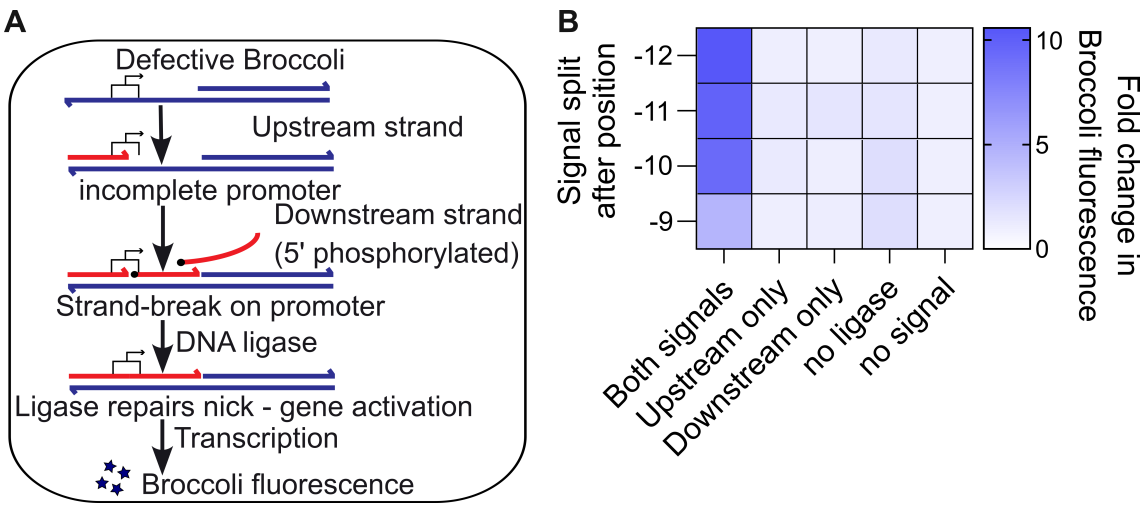


Figure 2.12: Combined use of DNA ligase and RNA polymerase to construct complex logic gates. (A) Schematic representation of AND gate construction. The DNA signal was split into two shorter ssDNA, each carrying part of the promoter sequence. Transcription activation occurred only when both fragments annealed to the defective gene and the two strands were ligated. (B) A heat map of fold change in fluorescence intensity of the Broccoli aptamer in a bulk mixture of the defective Broccoli and the signal fragments after 3 h, when the signal was split after -12, -11, and -10 nucleotides from the transcription start site, compared to the control with no signal fragments. Values in the heatmap are the mean of n = 3 technical repeats.

To provide perspective on the lengths of the signal fragments and the defective gene used in this design, the sequences of the signal fragments -10U and -10D, as well as the sequence of the defective Broccoli were illustrated here (Fig. 2.14).

We found that the AND gates formed by splitting the signal -12, -11, and -10 nucleotides from transcription start site were orthogonal to each other, such that correctly matching pairs of upstream and downstream signal fragments were required for gene activation (Fig. 2.15A-B). The signal fragment -10U and the downstream signal -12D contained the entire promoter sequence. However, the pair had overlapping sequences (-12 to -11) and could not be ligated. Subsequently, gene activation was not observed. The three signal pairs in combination created an AND-OR-AND-OR-AND gate, where gene activation was triggered by (-12U and -12D) or (-11U and -11D) or (-10U and -10D). In mathematical notation, (-12D $\wedge$ -12U) $\vee$ (-11D $\wedge$ -11U) $\vee$ (-10D $\wedge$ -10U), where $\wedge$ denoted 'AND' and $\vee$ denoted 'OR' (Fig. 2.15B). We constructed the truth table of the logic gate using a total of 26 possible combinations of the 6 signal fragments (Fig. 2.15C). The combinations included: no fragments (input 1), a single fragment (input 2-7), a pair of non-matching fragments (input

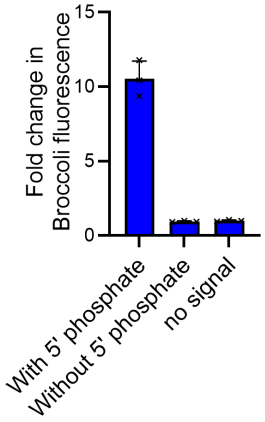


Figure 2.13: A bar graph of fold change in the fluorescence intensity of the Broccoli aptamer in a bulk mixture of the defective Broccoli, -10U signal fragment, and -10D signal fragment after 3 h of signal addition, with or without 5' phosphate on -10D, compared to the control with no signal. -10U and -10D were the upstream and downstream signal fragments from splitting the Broccoli signal after position -10. Technical replicates are displayed by crosses and the heights of the bars are the mean. The error bars show the standard deviation.

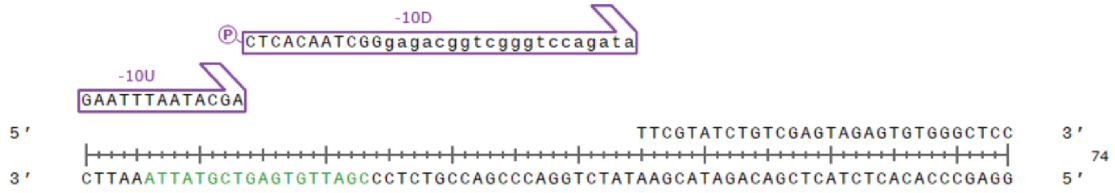


Figure 2.14: A diagram showing the sequences of the signal fragments -10U and -10D, as well as the defective Broccoli. The T7 promoter sequence was labelled green on the defective gene

8-13), a pair of matching fragments (input 14-16), a pair of matching fragments with an additional non-matching fragment (input 17-18), a pair of matching fragments with two additional non-matching fragments (input 19-21), two pairs of matching fragments (input 22-23), two pairs of matching fragment with one additional non-matching fragment (input 24-25), and all three pairs of fragments (input 26). When more than two fragments were simultaneously present, as in the case of -10D, -11U, and -11D (condition 18), the non-matching fragment -10D could compete with the matching fragments -11U and -11D for binding the defective gene. Although this competition led to a slight reduction in the final fluorescence intensity (approximately 20 %), the results remained clearly distinguishable from reactions lacking any matching pairs of DNA signal fragments.

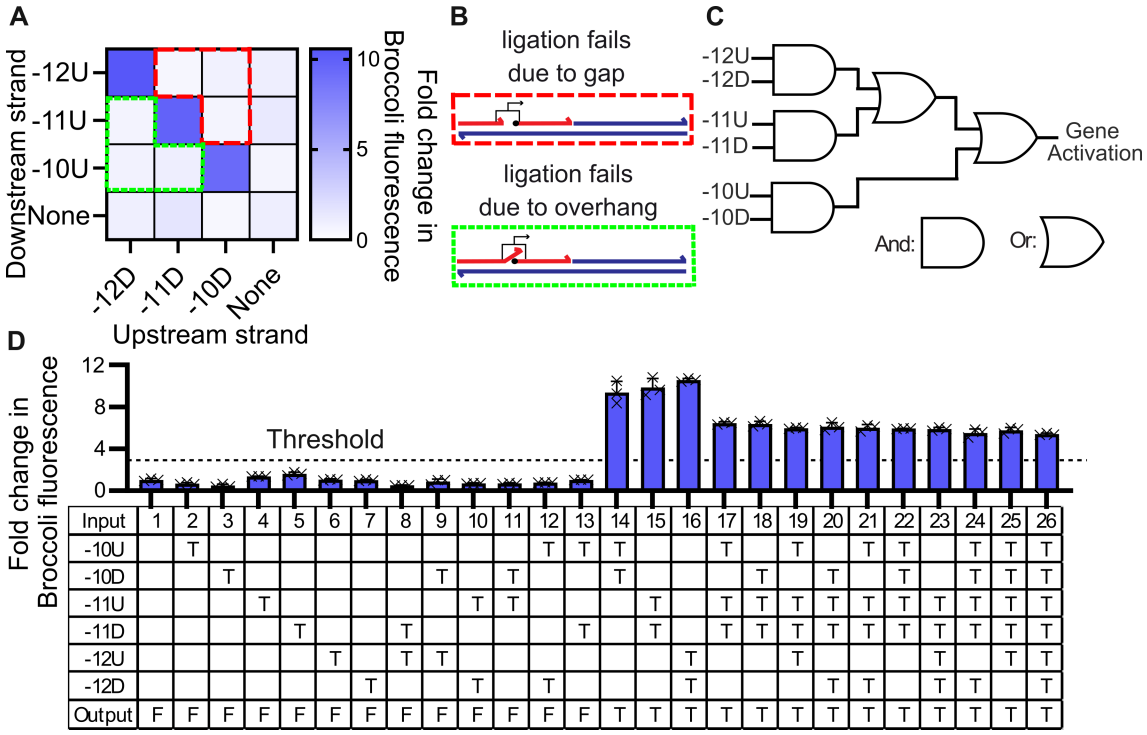


Figure 2.15: (A) A heat map of fold change in fluorescence intensity of the Broccoli aptamer when the defective Broccoli, the signal fragments, and DNA ligase were mixed after 3 h, compared to the control with no signal fragments. Values in the heatmap are the mean of n = 3 technical repeats. The upstream signal was denoted by U and the downstream signal is denoted by D. (B) Schematic representation of ligation failure with non-matching signal fragments. Top: when the two signal fragments together did not contain the entire promoter sequence, they were not ligated due to a gap. Bottom: when the two signal fragments together contained the entire promoter sequence, but there were overlapping sequences between the fragments, an overhang would be present when the two fragments were bound to the defective gene. This overhang would prevent ligation of the two fragments (C) Equivalent logic gate circuit diagram of an AND-OR-AND-OR-AND gate constructed by combining the AND gates. (D) The truth table of AND-OR-AND-OR-AND gates, with a bar graph of fold change in fluorescence intensity of the Broccoli aptamer in a bulk mixture of the defective Broccoli and different combinations of signal fragments after 3 h in the presence of DNA ligase, compared to the control with no signal fragments. T: presence of signal fragment. F: absence of signal fragment. The threshold (dotted line) was set at 3 fold increase in fluorescence intensity. Conditions with mean fluorescence intensity above the threshold had output = T, while conditions with mean fluorescence intensity below the threshold had output = F. In the bar graph, technical replicates are displayed by crosses and the heights of the bars are the mean. The error bars show the standard deviation.

2.6 Inverse defective genes

Most of the defective genes used this work (B1-2, B4, P1-2, M1, C1, G1, A1) had a single-stranded promoter with the coding/ non-template strand missing. As the signal bound to the defective gene, even if the signal complemented the defective gene perfectly, a nick was present between the 3' end of the signal and the 5' end of the coding/ non-template strand of the defective gene. To understand if the constructs could be designed with the template/ non-coding strand missing in the promoter region instead, we designed genes with a single-stranded promoter where the template/non-coding strand was missing. Those constructs would be referred to as inverse defective genes. Those inverse defective genes produced low level of transcripts even in the presence of the complementary DNA signal, as the DNA signal binding resulted a nick (strand-break) on the template/non-coding strand. T7 RNAP was reported to terminate at lesion on the template strand 50% of the time (*95*). It was therefore expected that less full length RNA would be produced from the inverse defective genes. We hypothesized that DNA ligase could repair the nick between the signal and the inverse defective gene, using ATP and Mg^{2+} to form phosphodiester bond between the 5' phosphate and the 3' hydroxyl groups to repair the strand-break, leading to improved transcription activation.

We studied transcription activation of inverse defective Pepper (P3) with a defective SP6 promoter. After 3 h incubation, presence of a Pepper signal (s10) led to low level of transcription activation, and the activation was improved when the DNA ligase was also present in the reaction mixture. As a control, presence of the ligase without the DNA signal did not led to transcription activation (Fig. 2.16A-B).

Similarly, we also studied transcription activation of inverse defective Broccoli (B3) with a defective T7 promoter (Fig. 2.16C-D). Presence of a Broccoli signal (s11) led to low level of transcription activation, and the activation was improved with the DNA ligase (Fig. 2.16C-D).

Therefore, DNA ligase repaired the nick between the signal and the inverse defective gene, improving gene activation. Inverse defective genes could also be used for gene activation by ssDNA signal.

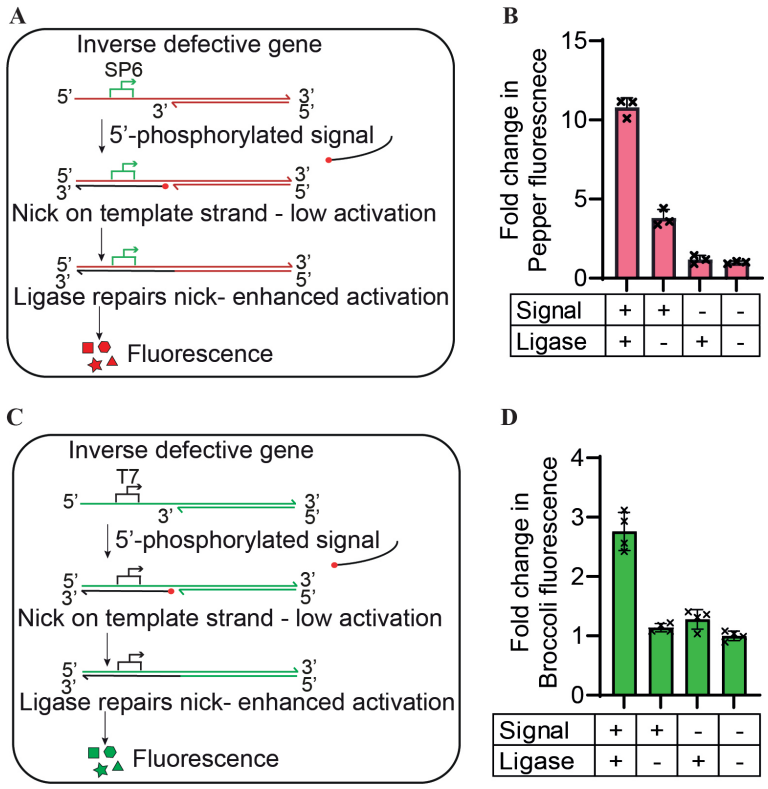


Figure 2.16: Inverse defective gene activation by DNA signal and DNA ligase. (A) A schematic of inverse defective Pepper activation. The inverse defective Pepper produced low level of transcripts even in the presence of the DNA signal, as DNA signal binding resulted in a nick (strand-break) on the template/non-coding strand. DNA ligase repaired the nick between the signal and the inverse defective gene and improved gene activation. (B) A bar graph of fold change in fluorescence intensity of the Pepper aptamer in a bulk mixture of the Pepper signal (P3) and the inverse defective Pepper (s10) after 3 hours, with or without DNA ligase, compared to the control with no signal. (C) A schematic of inverse defective Broccoli activation. The inverse defective Broccoli with T7 promoter produced low level of transcripts even in the presence of the DNA signal, as the DNA signal binding resulted in a nick (strand-break) on the template/ non-coding strand. (D) A bar graph of fold change in fluorescence intensity of the Broccoli aptamer in a bulk mixture of the Broccoli signal (s11) and the inverse defective Broccoli (B3) after 3 h, with or without T4 DNA ligase, compared to the control with no DNA signal. In the bar graphs, technical replicates are displayed by crosses and the heights of the bars are the mean. The error bars show the standard deviation.

2.7 Long defective gene synthesis

We then explored the use of ssDNA signals to produce functional proteins and enzymes. After optimizing production of long (>1000 bp) defective genes with single-stranded promoters, we demonstrate that DNA signal activated protein production by complementing defective genes (Section 2.8). We finally discuss the use of DNA signal as a transcription factor mimic to simultaneously activate production

of multiple proteins (Section 2.9).

We next investigated whether the ssDNA signals and the defective genes could be used to produce proteins. The defective genes coding for proteins such as mCherry and mNeonGreen (mNG) were also made by annealing two ssDNA strands of different lengths, but the required ssDNA strands were synthesized in our lab as long ssDNA (around 1000 nt) strands were not routinely synthesized commercially (*96*).

While different biochemical techniques for synthesizing long ssDNA were reported (*96*), we eventually chose a modification of Linear-After-The-Exponential PCR (LATE-PCR) for ssDNA synthesis. Linear-After-The-Exponential PCR (LATE-PCR) or asymmetric PCR was used to synthesize long ssDNA, using an excess of one primer compared to the other primer in PCR thermocycles. In the beginning cycles, as both primers were present, the double stranded DNA template was amplified exponentially. Once the limiting primer was consumed, subsequent thermocycles produced the acrshortssDNA using the primer in excess. 1:20 to 1:100 ratio of primers were commonly used.

This method was difficult to be adopted for use, as both the exponential phase and the linear phase of the reaction had to be successful to produce the correct ssDNA product. If the exponential phase ended early in the thermocycles, there would not be sufficient double-stranded template for the linear PCR reaction. If the exponential phase ended late in the thermocycles, there would not be enough thermocycles/dNTPs for the linear PCR reaction. The number of thermocycles and the dsDNA yield of the exponential phase depended on the primer melting temperature, primer concentration, and temperature used in the thermocycle. As a result, meticulous screening of primer melting temperature and primer concentrations were often required to ensure successful production of the correct ssDNA product (*96*–*99*).

To circumvent the challenge, we separated the asymmetric PCR into a two-step PCR reaction. A standard PCR was first used to generate a dsDNA template. A linear PCR reaction then made the ssDNA from the dsDNA template, using a single primer. A high concentration of dsDNA template (4-8 ng/µL) was used in the linear

PCR. The single-stranded product was separated from the double-stranded template by preparative gel-electrophoresis, recovered by crushing the ssDNA-containing gel in buffer, and concentrated by diafiltration. The two ssDNA strands of the defective gene were subsequently annealed in a 1:1 ratio (determined by gel densitometry) to form the defective gene. The annealed products were sequentially purified by a desalting column, followed by a silica column, and eluted in nuclease-free water. The purification steps ensured that the defective genes contain minimal amount of salt (260/280 >1.9 and 230/260 > 1.9 by spectrophotomter), since salt was reported to inhibit PURE reaction (Fig. 2.17, A to B) (*78*) .

The linear PCR reaction was optimized. Increasing the starting dsDNA template concentration and the number of thermocycles improved linear PCR yield, while increasing primer concentration did not have a significant effect on the ssDNA yield (Fig. 2.17, C to D).

Defective mCherry, defective mNeonGreen, defective αHL and defective β-galactosidase were produced with this method. Typically, a linear PCR reaction used 6-8 ng per µL of double-stranded DNA in the reaction, and produced 6-8 ng ssDNA per µL of PCR reaction. About 35-50 % of the ssDNA produced remained after annealing and purification.

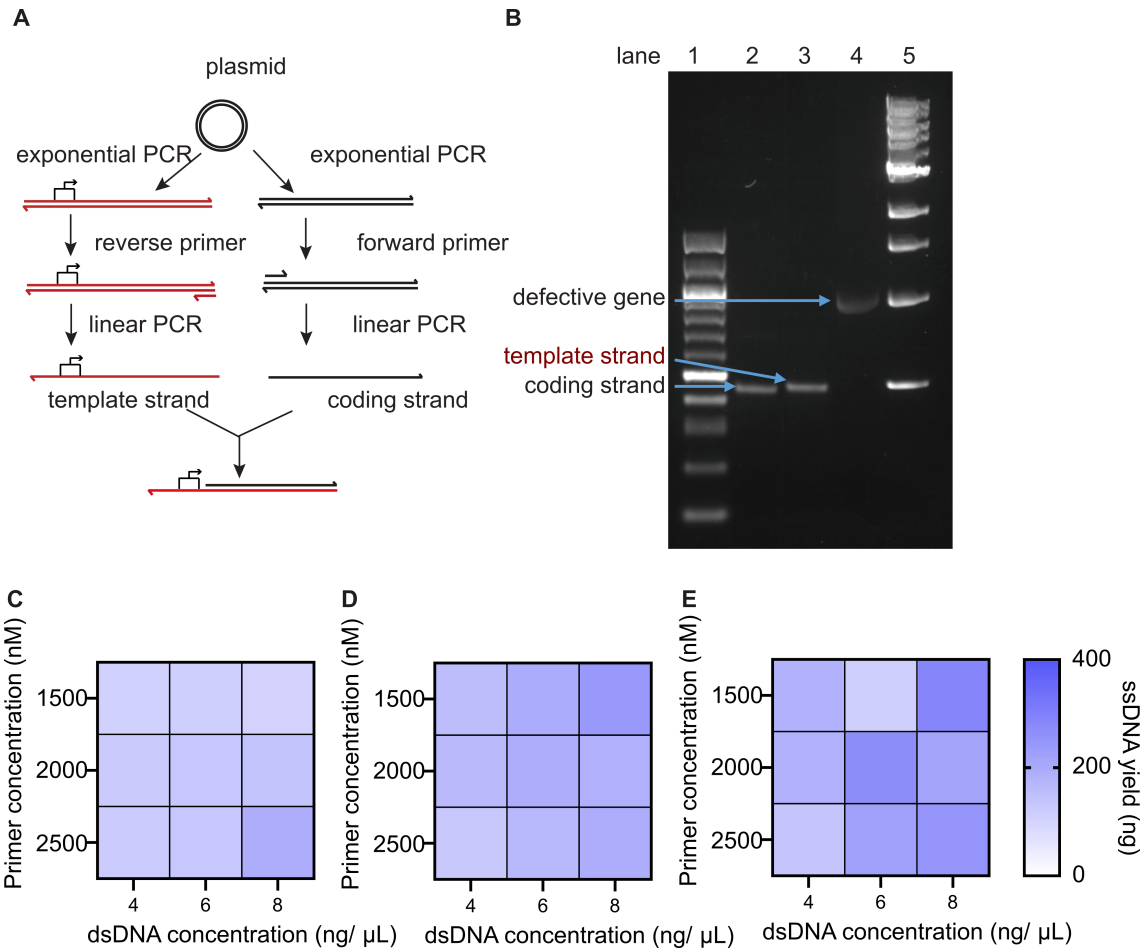


Figure 2.17: Long defective gene (>1000 bp) synthesis. (A) A schematic representation. Long ssDNA (>1000 nt) was made by 2-step PCR. The required sequences was first amplified by a standard exponential PCR with a pair of primers. The exponential PCR product was then used to produce the ssDNA in a linear PCR reaction with only one primer. The defective genes coding for protein sequences (>1000 bp) were the made by annealing two ssDNA of different lengths. (B) Agarose gel (1%) electrophoresis of the DNA constructs. Lane 1: DNA ladder 100 bp (NEB). Lane 2: The coding strand of defective mNG. Lane3: The template strand of defective mNG. Lane 4: The defective mng formed from annealing the two ssDNA. Lane 5: DNA ladder 1 kb (NEB). (C to E) Optimisation of the linear PCR reaction to produce the ssDNA used for defective gene synthesis. A heat map of mean ssDNA yield of the coding strand of the defective mNG per 40 µL PCR reaction mix at different primer concentrations, dsDNA concentrations and number of thermocycles. (C) 10 cycles, (D) 15 cycles, (E) 20 cycles. Values in the heatmap are the mean of n = 2 technical repeats.

2.8 ssDNA signal activated protein production

This section demonstrates the use of the DNA signals to produce protein. The defective genes coding for proteins had a single-stranded promoter and were inactive on their own. The DNA signal complemented the defective genes and allowed transcription and translation of the gene to produce proteins (Fig. 2.18A).

We investigated protein expression at different DNA signal and defective gene concentrations. Protein expression was observed with as little as 500 pM of the signal (s12) and 5 nM of the defective gene coding for mCherry (C1) (Fig. 2.18B), or 50 pM of the signal (s12) and 5 nM of the defective gene coding for mNG (G1) (Fig. 2.18C).

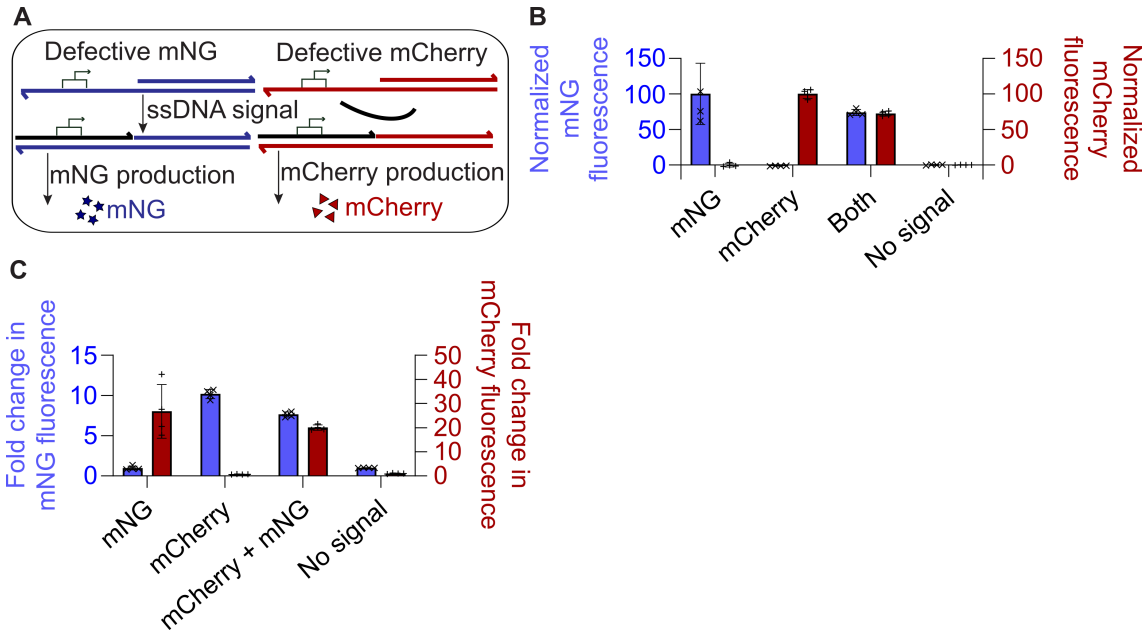


Figure 2.18: DNA signal activated functional protein production. (A) A schematic of the gene activation process. The ssDNA signal complemented the defective genes with a single-stranded promoter to produce RNA transcripts that were further translated into proteins. (B) A bar graph of fold change in mCherry fluorescence intensity when different concentrations of the DNA signals (s12) were mixed with the defective mCherry (C1) in bulk after 3 h, compared to the control with no DNA signals. (C) A bar graph of fold change in mNG fluorescence intensity when different concentrations of the DNA signals (s12) were mixed with the defective mNG (G1) after 3 h, compared to the control with no DNA signals. In the bar graphs, technical replicates are displayed by crosses and the heights of the bars are the mean. The error bars show the standard deviation.

2.9 DNA signal as a transcription factor mimic

In biological cells, intracellular signals such as transcription factors could often simultaneously activate multiple genes (*13*). Similarly, the DNA signals could also function as transcription factor mimics, simultaneously activating multiple genes. To illustrate this, we designed a DNA signal (s12) that could complement both the defective mCherry (C1) and the defective mNG (G1) (Fig. 2.19A). The DNA signal activated production of mCherry protein in the presence of the defective mCherry, activated production of mNG in the presence of the defective mNG, and activated production of both mCherry and mNG in the presence of both defective genes (Fig. 2.19B-C).

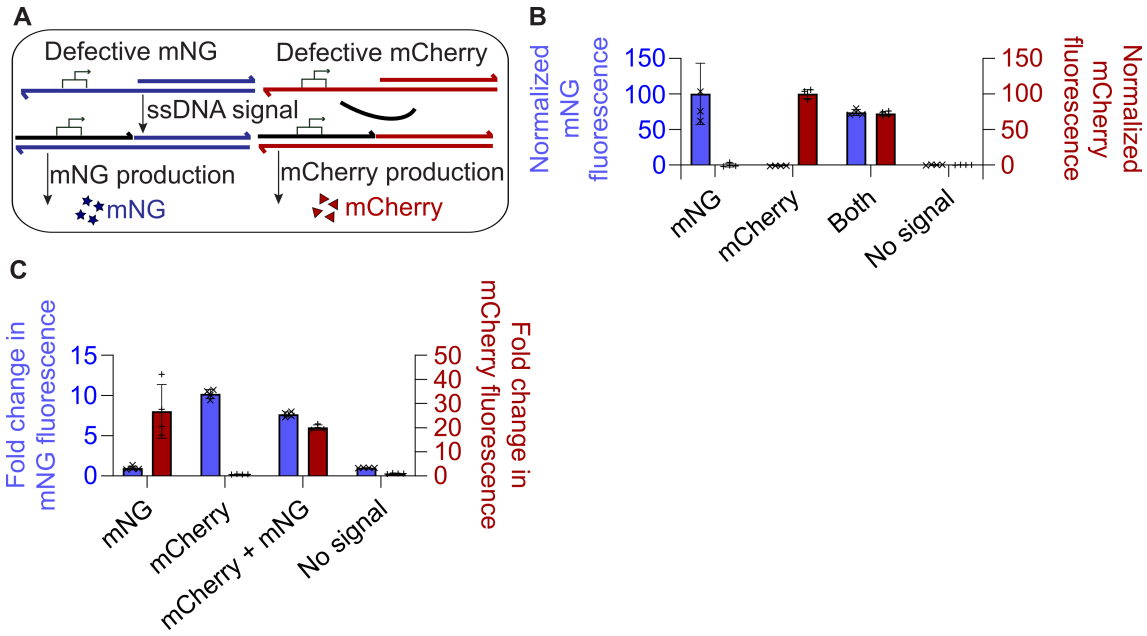


Figure 2.19: (A) A schematic of multiple protein production using a universal DNA signal and two different defective genes. The DNA signal was analogous to transcription factors that activated multiple defective genes sharing the same defective promoter. (B) A bar graph of normalized fluorescence intensity of IVTT mix in a bulk mixture of the DNA signal (s12) and different defective genes after 3 h of signal addition. In each fluorescence channel, the mean fluorescence intensity of the no signal control and the brightest sample were normalized to 0 and 100 respectively. (C) A bar graph of fold change in fluorescence intensity of IVTT mix in the conditions described in (B), compared to the no signal control. In the bar graphs, technical replicates are displayed by crosses and the heights of the bars are the mean. The error bars show the standard deviation.

We aimed to test whether ssDNA could activate defective genes in synthetic cells. As an initial step, we encapsulated the DNA signal, defective genes, and the

PURE system in aqueous droplets embedded within an organogel. Fluorescence of mCherry and/or mNG was observed only when the corresponding defective genes were present (Fig. 2.20, A to D). Specifically, the DNA signal activated mCherry production in the presence of defective mCherry, mNG production in the presence of defective mNG, and both mCherry and mNG production when both defective genes were present. No protein production was observed without defective genes. These encapsulation experiments were conducted in collaboration with Dr. Dennis Hartmann. Encouraged by the successful gene activation in well-separated aqueous-in-organogel droplets, the next chapter explores gene activation in aqueous-in-oil droplets, where the droplets are separated by lipid bilayers.

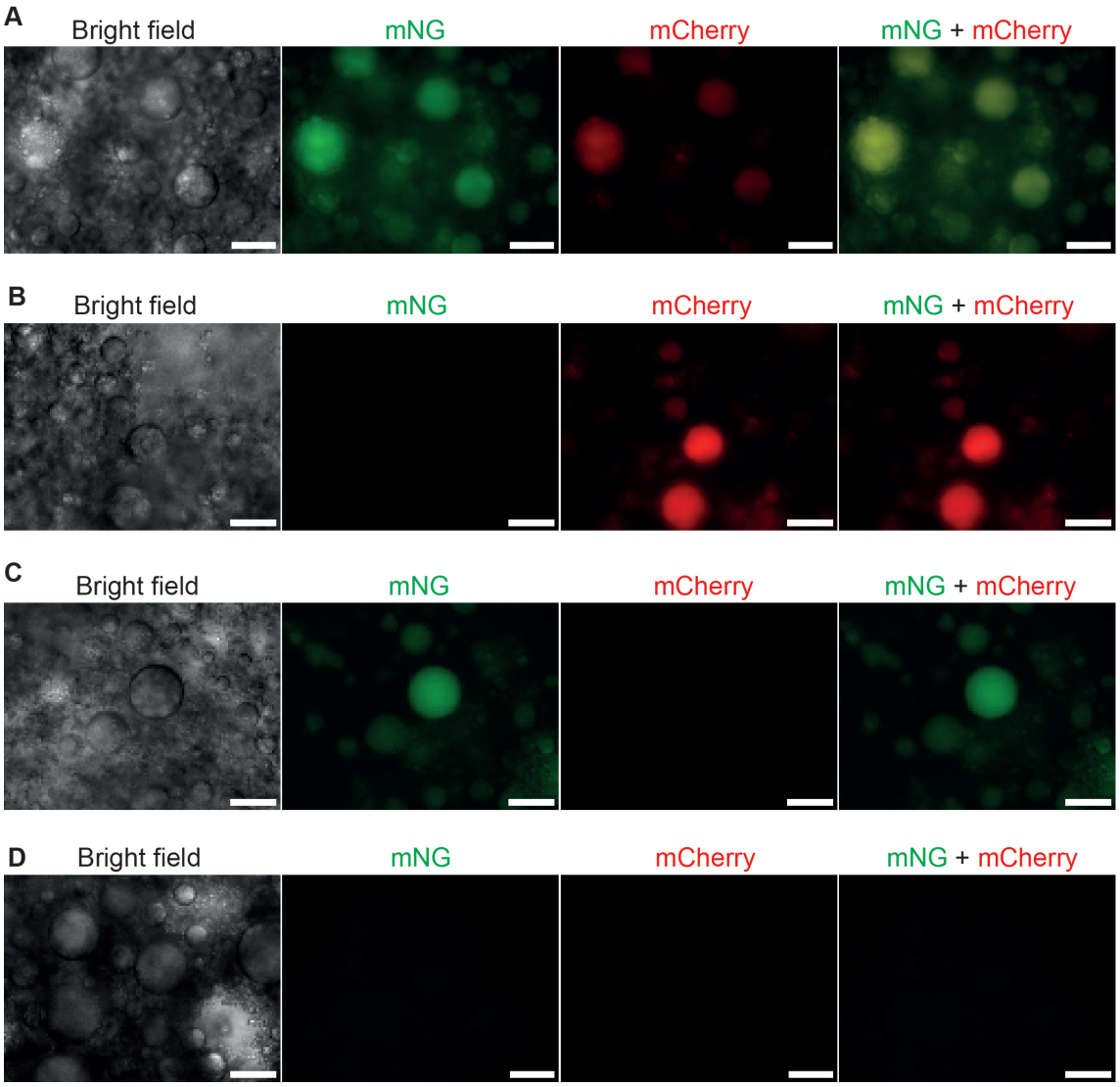


Figure 2.20: Bright field and fluorescence images of droplets in organogel with DNA signal and different combinations of defective genes (A) with defective mCherry and mNG gene. (B) with defective mCherry only (C) with defective mNG only (D) without defective gene. Images are representative of n = 2 technical replicates. Scale bars, 100 µm. Scale bars, 100 µm.

2.10 Chapter summary and outlook

Our work demonstrates the efficient use of ssDNA signals for transcription and translation activation by complementing genes with a defective promoter, resulting in the production of both RNA and proteins. A signal concentration as low as 50 pM was sufficient to activate defective genes for protein production. It was likely that optimization of defective gene sequences, particularly 5'UTR sequence, would further enhance protein expression in the presence of DNA signal. For example, DNA templates with T7 g10 leader sequence was been found to improve mCherry

expression by 7 fold compared to compared to RBS from NEB, which was also the RBS used in defective genes (*100*). Selective gene activation was achieved by using different promoters or by using inhibitors to remove undesired signals. The DNA signal was further split in half to construct complex logic gates (AND-OR-AND-OR-AND gates) controlling gene activation.

We introduced two pairs of commercially available, nontoxic, orthogonal aptamer-fluorophore pairs: Broccoli / DHFBI-1T and Pepper / HBC620, as well as Mango/ TO1B and Pepper/HBC620. Our findings offer new possibilities for RNA imaging in live cells.

The fluorescent small molecules used in this work would emite either green or red light. It was unfortunate that blue fluorescent dyes were not commercially available and could not be readily used, otherwise we might be able to find 3 sets of orthogonal aptamer-fluorophore pairs with nonoverlapping fluorescence. For example, DIR2s-Apt5 was reported to bind and activate the blue fluorescence of OTB-SO3 (*101*). The aptamer could bind to its dye with a helix and two parallel short stem-loops, resembling a tuning fork-like architecture (*102*). As the aptamer had a different fold compared to Broccoli, Mango, and Pepper, it is likely that DIR2s-Apt5/ OTB-SO3 aptamer-fluorophore pair would be orthogonal to the other pairs used in this thesis. While aptamer fluorescence was used for simplicity to study transcription activation, the brightness of the samples may not directly correlate with the RNA concentration produced during transcription due to factors such as RNA misfolding or self-quenching of the small-molecule dyes (discussed further in later chapters). More precise quantification of RNA production could be obtained through qPCR or quantitative gel electrophoresis.

Our work also expanded our understanding of T7 and related polymerases, and their applications in synthetic biology. For example, we revealed that T7 promoter cannot tolerate strand breaks on the coding strand from -12 to -9 nucleotides from the transcription start site. Although this observation aligned with the known importance of -17 to -4 nucleotides from the transcription start site in polymerase binding and transcription initiation (*66*), it remained unknown whether strand breaks

were tolerated at other locations on the promoter. We also demonstrated the combined use of RNA polymerase and DNA ligase in vitro, creating orthogonal AND gates by splitting the ssDNA signal at different positions. It was plausible that even more orthogonal AND gates could be constructed by splitting the signal at other positions. It might also be possible to split the signal into more than 2 fragments to increase the complexity of the logic gates, which could eventually be used to build complicated computational devices.

At the same time, new questions were raised regarding the properties of T7 RNA polymerase. For example, when DNA signals of different lengths were added to the defective Broccoli (B4), there was a significant variation in the final fluorescence intensity of the reaction mixture (Fig. 2.21. The signals added to the defective Broccoli were s2 (44 nt), s15 (27 nt), s16 (23 nt), s1 (17 nt) and s6 (13 nt). s2, s15, s16, and s1 began from -22 nucleotides from the transcription start site, while the shortest signal s6 began from -18 nucleotides from the transcription start site. After 3 h incubation, there was at least 7 fold increase in Broccoli fluorescence for all the signals tested, the fold change increase in Broccoli fluorescence compared to the no signal control ranged from 7 fold to almost 100 fold. This was very intriguing as the initial amount of nucleotides and polymerase in the reaction mix were equal in all the samples. If all the nucleotides in the IVT mix were converted into full-length RNA transcripts, the same final concentration of product RNA would be reached regardless of the signal concentration, the defective gene concentration, and the transcription rate. Our observations clearly was not consistent with this. Understanding this phenomenon might lead to new tools for transcription rate optimization, which could be applied to RNA synthesis in synthetic biology (*103*) and therapeutics (*104*).

2.10.1 Future use of the DNA signal as a transcription factor mimic

In our results, while mCherry and mNeonGreen could be produced together, they functioned separately and there were no synergy between the two protein products.

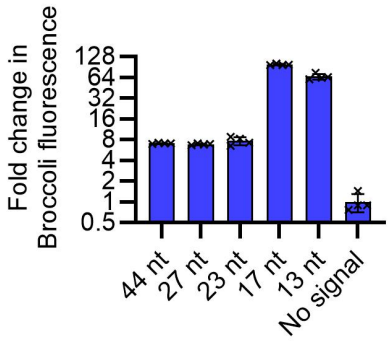


Figure 2.21: Bar graph of fold change of Broccoli fluorescence when different signals were mixed with the defective Broccoli after 3 hours in bulk, compared to the control with no signal. In the graph, technical replicates are displayed by crosses and the heights of the bars are the mean. The error bars show the standard deviation.

This was unlike most transcription factors in biology where the genes activated by the transcription factors often produced proteins that together achieve a desired biological output.

We had a few designs where the DNA signal could be used to produce multiple proteins that work cooperatively. For example, ssDNA signal could be used to activate two defective genes, each producing a different fragment of a split luciferase enzyme (*105*). We expected that both defective genes needed to be present to produce both fragments, resulting in bioluminescence, while the bioluminescence level would be very low when only one defective gene was present. Similarly, the defective genes could code for different fragments of the split GFP (*106*) or the split β-galactosidase (*107*).

Of course, in biological systems, transcription factors often activated production of very different types of proteins that synergistic achieve a desired biological function, rather than just fragments of the same protein. In another design, we attempted to recreate the E. coli *Lac* operon using defective genes. *Lac* operon was essential in metabolism of lactose in E. coli. In the presence of lactose and absence of glucose, the operon produced β-galactoside permease (encoded by *LacY* gene) and β-galactosidase (encoded by *LacZ* gene). β-galactoside permease was a proton and lactose symporter, while β-galactosidase initiated the breakdown of lactose. The two proteins had very different functions but they were activated by the same signal to produce a desired biological outcome - lactose metabolism (*107*).

To recreate this system using defective genes, we envisioned that the DNA signal could trigger production of both α-hemolysin and β-galactosidase. α-hemolysin was a channel protein which permitted transport of a lactose analogue (3-Carboxyumbelliferyl-β-D-galactopyranoside) into synthetic cells (*19*), which would then be subsequently hydrolysed by β-galactosidase to release fluorescence metabolites.

The feasibility of this design was tested using normal genes with double stranded promoter, in a droplet network in a lipid-in-oil solution. Two droplets were separated by a lipid bilayer, an IVTT mix droplet and a sugar storage droplet. The IVTT mix droplet contained a normal double-stranded DNA coding for lactase and another DNA coding for αHL, while the sugar storage droplet contained the lactose analogue CUG. When both gene products were produced, α-hemolysin allowed transportation of CUG from the sugar storage droplet to the IVTT mix droplet, CUG was then hydrolyzed by lactase to produce UCA with a blue fluorescence (Fig. 2.22A-B).

Motivated by the observations, it was highly likely that similar experimental outcome could be repeated using DNA signals and defective genes to create a lac operon mimic.

2.10.2 Production of eukaryotic proteins with IVTT mix

We noted that while cell free extracts have also been developed for IVTT reaction, they often contained nucleases that would digest non-circular DNA (*78*). We would not be able to use defective gene in those systems without protecting the DNA from degradation, such as using phosphothioate chemistry (*108*). This might be necessary if we would like to produce mammalian proteins with post-translational modification in the future, since analogues to the PURE system was still not available for mammalian expression system.

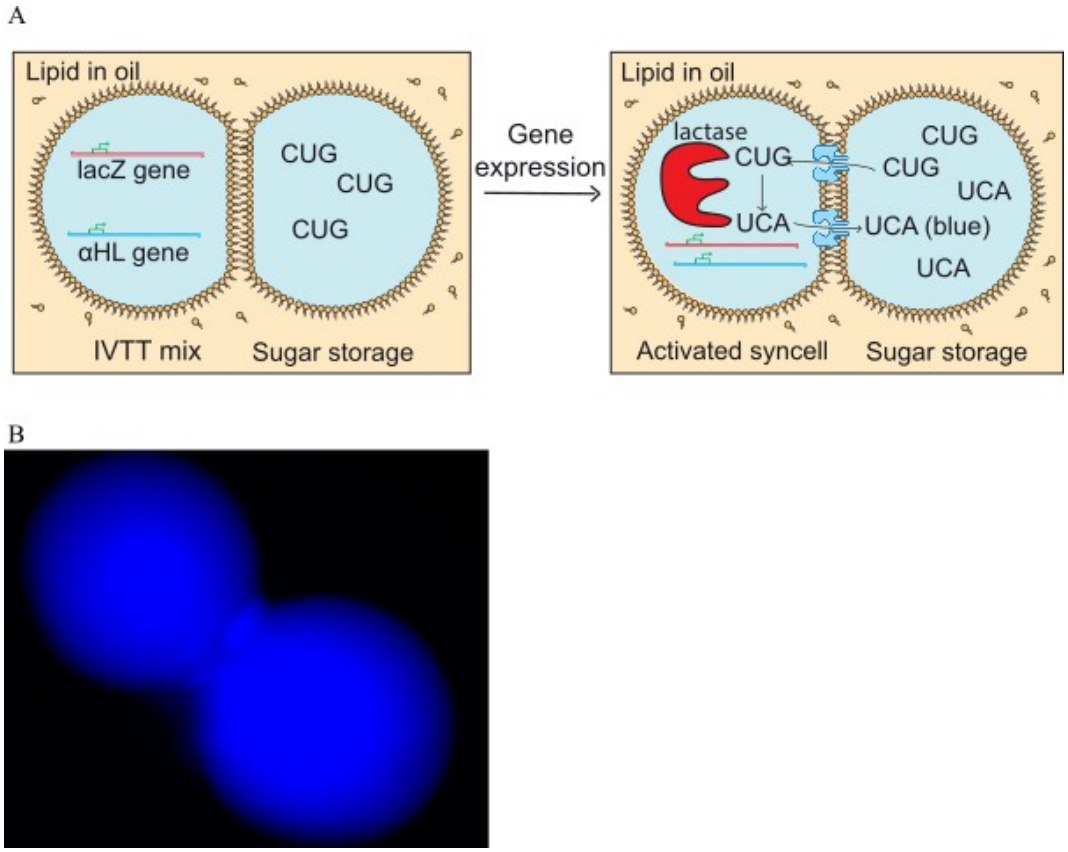


Figure 2.22: (A) A schematic of the lac operon mimic in a droplet network. The IVTT mix produced both channel protein αHL (lactose permease mimic) and lactase. The channel protein allowed entry of a lactose analogue CUG across the bilayer, which was broken down by lactase to produce UCA with blue fluorescence. The product could diffuse to the sugar storage droplet through the channel protein. (B) Fluorescnece microscopy image of the droplet pair after 3 hour incubation at 37 °C.

Chapter 3

ssDNA controlled communication in droplet networks

3.1 Introduction

In this chapter, we finally demonstrate the use of the ssDNA signalling system in droplet networks (*79*). Gene activation was investigated in synthetic tissues formed with droplet-hydrogel bilayers (DHBs) and droplet-interface bilayers (DIBs). We first investigated expression of RNA and proteins in droplet networks in lipid-in-oil solution (Section 3.2). Then, we showed that DNA signal and defective genes could be used to produce the protein pore α-hemolysin (αHL), which inserted into DIBs and allowed dye transfer between two compartments separated by the DIBs (Section 3.3).

Next, we introduce two mechanisms used to control the access of ssDNA signals to the gene expression machinery. Firstly, the bilayer could be disrupted by adjusting the oil content to decrease lipid solubility (Section 3.4). Secondly, membrane potential could be used to regulate the entry of ssDNA signal across channel protein pores embedded in the bilayers, thereby restricting DNA signal to selected cells (Section 3.5).

3.2 RNA and protein expression in water-in-oil emulsions

Together with Dr. Matthew Cornall, we investigated IVT and IVTT reactions in aqueous droplets in lipid-in-oil solution.

3.2.1 RNA aptamer production in water-in-oil emulsions

We found that Mango aptamer expression was a lot lower in aqueous droplets in a lipid-in-oil solution than in a bulk solution. The oil solution contained silicone oil and hexadecane, both were filtered with 0.22 µm membrane prior to use. We investigated different treatments of the silicone oil prior to expression of the Mango aptamer in the oil solution. We found that washing the silicone oil with water did not improve Mango expression compared to the unwashed control. However, washing the silicone oil with acid, followed by base, and then by buffer (5 mM MOPS pH 8.0, 50 mM $MgCl_2$, 2 mM spermidine, 100 mM KCl) (acid-base-buffer wash), improved Mango aptamer expression in the lipid-in-oil solution (Fig. 3.1A). The aqueous phase became cloudy after the base wash step (Fig. 3.1B), suggesting that the wash was changing the composition of the silicone oil, potentially by removing certain impurities or contaminants in the oil. If those components contained alcohol or carboxylic acid groups, washing in base would deprotonate those components, increasing their solubility in the aqueous phase, and potentially allowing them to be extracted in the aqueous solution.

Nevertheless, the mechanisms by which the silicon oil solution affected RNA expression, and the mechanisms by which the acid-base-buffer wash improved RNA expression, remained to be determined. This problem was complicated by the fact that silicon oil was a complex mixture of polymers, without a well-defined chemical structure. It was conceivable that a combination of mass spectrometry and NMR studies would provide more information on how silicone oil affected RNA expression.

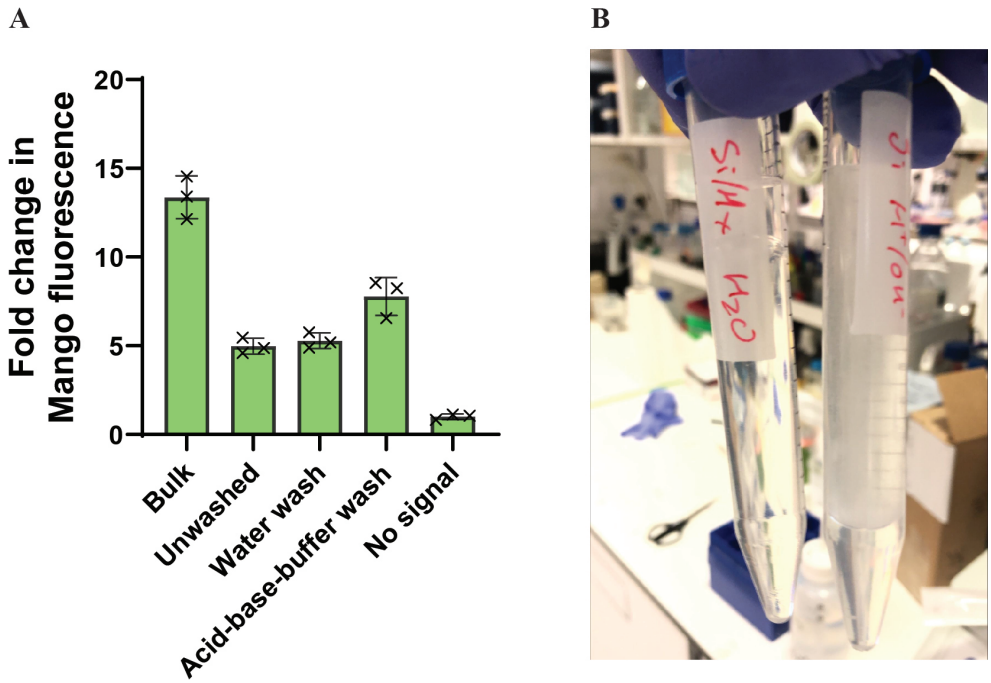


Figure 3.1: Washing silicone oil improved IVT expression in droplet-in-oil emulsions. (A) A bar graph of the fold change in Mango fluorescnece intensity compared to the control with no signal, after three hours of Mango aptamer expression in aqueous droplet in the lipid-in-oil solution, where the silicone oil was pretreated with different methods. (B) A photo of two falcon tubes after shaking 3 mL of silicone oil vigorously with 12 mL of water (left) or with 12 mL of 10 mM potassium hydroxide (right).

3.2.2 Protein production in water-in-oil emulsions

On the contrary, fluorescence intensity from the PurExpress IVTT reaction was not affected by expression in in lipid-in-oil solution compared to expression in bulk. We investigated expression of mVenus in PurExpress within aqueous droplets in 4 lipid compositions, 10 mg/mL DPhPC, 10 mg/mL 1:1 (w/w) DPhPC: POPC, 2 mg/mL DPhPC, and 2 mg/mL 1:1 (w:w) DPhPC: POPC, in 1:1 (v/v) silicone oil (AR20): hexadecane solution, as well as expression in bulk solution (PCR tube). The samples were imaged after 3 hours, 6 hours, and 19 hours, and there were no significant difference between the samples expressed in the lipid-in-oil solution versus those expressed in the bulk solution (Fig. 3.2). Therefore, expression in the lipid-in-oil solution was not expected to affect protein expression with PurExpress. It remained to be investigated why IVT reaction, but not IVTT reaction, was affected by expression in emulsion droplets in the lipid-in-oil solution. It was plausible that RNA production in IVT reaction, and protein production in IVTT reaction, had

different limiting factors, and therefore they were affected differently by the lipid-in-oil solution. It was also plausible that some components in the IVTT mix protected the reaction mixture from the lipid-in-oil solution.

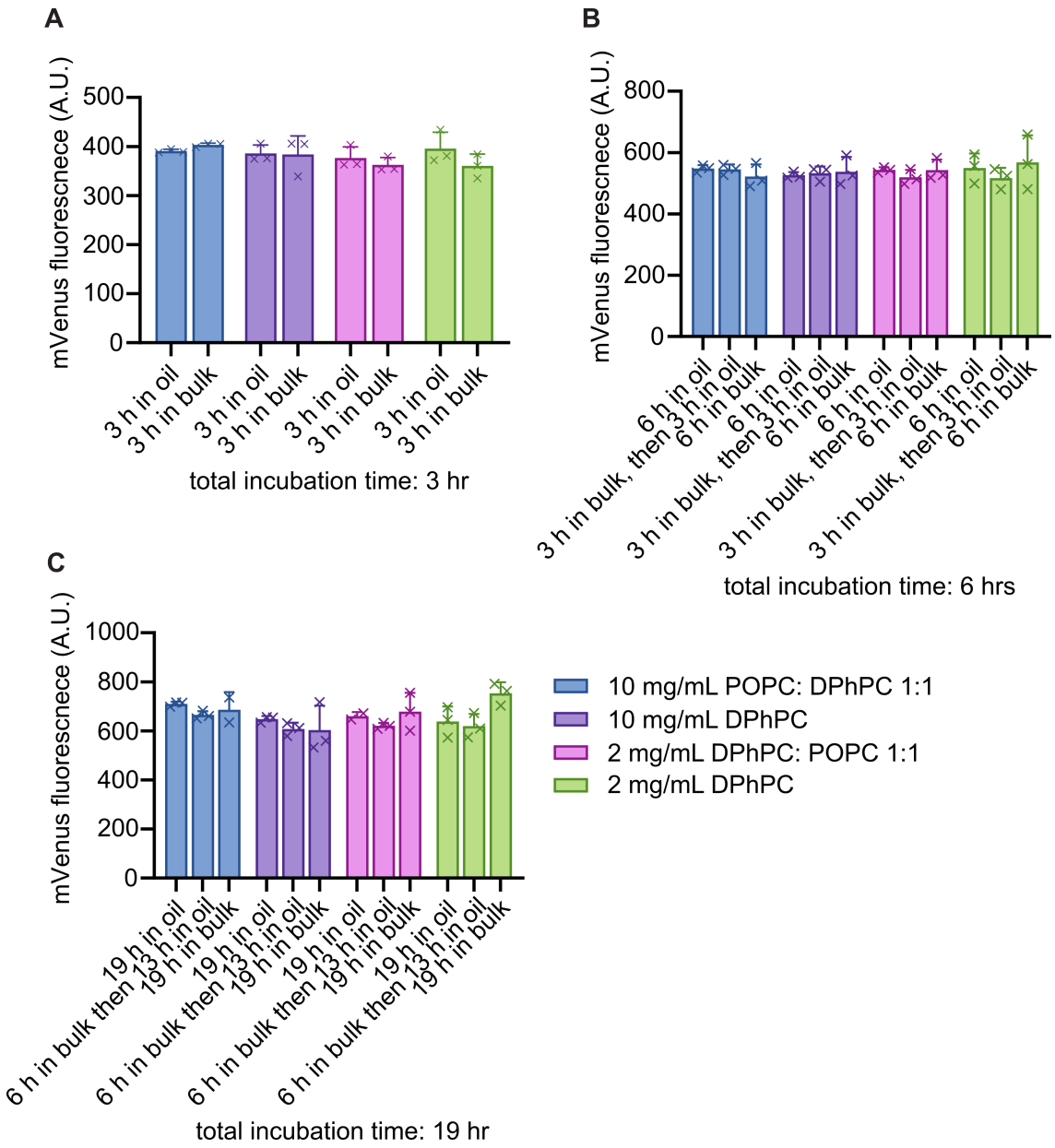


Figure 3.2: Bar graphs of change in mVenus fluorescence intensity in IVTT mix (A) 3 hours, (B) 6 hours, (C) 19 hours after DNA template coding for mVenus was added, and the IVTT mix was incubated in bulk or in aqueous droplets in lipid-in-oil solution. In the bar graphs, technical replicates are displayed by crosses and the heights of the bars are the mean. The error bars show the standard deviation.

3.3 DNA signal activated droplet network communication

This section describes the use of the DNA signal and the defective genes to activate communication in droplet networks. We designed defective genes coding for α-hemolysin (αHL), a toxic protein known to lyse cells by forming pores in cell membranes (*109*). The defective genes coding for αHL (A1) and the fluorescent dye 2-Deoxy-2-[(7-nitro-2,1,3-benzoxadiazol-4-yl)amino]-D-glucose (NBDG) were separated in two droplets by a droplet interface bilayer (Fig. 3.3A). The lipid bilayer was normally impermeable to NBDG (*26*). However, in the presence of the DNA signal, αHL was produced overtime and inserted into the lipid bilayer, and subsequently allowing NBDG to diffuse across protein pores in the membrane. Importantly, dye transfer across the membrane was not observed without the DNA signal (Fig. 3.3, B to D). Nevertheless, even in the presence of the signal and the defective gene, the rate of NBDG diffusion was slow, which could be attributed to the low signal (20 nM) and defective gene (6 nM) concentration used in this study.

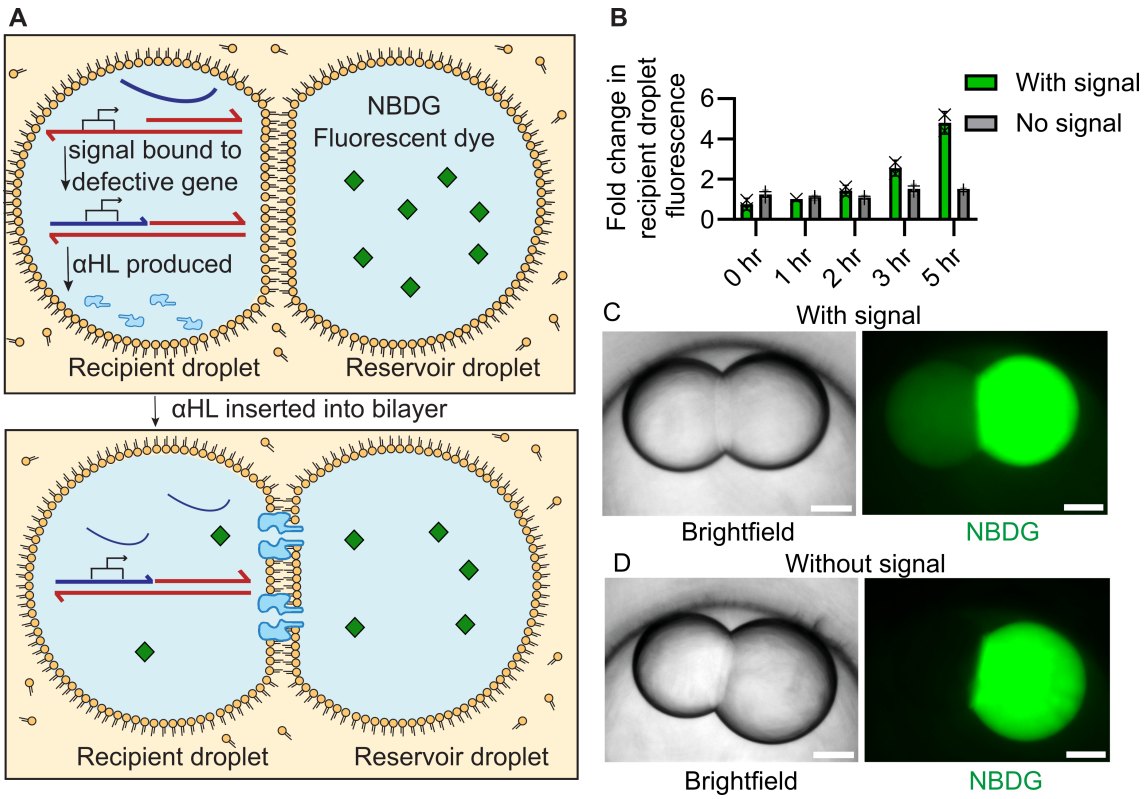


Figure 3.3: (A) A schematic of the DNA signal (s12) activating defective αHL (A1) in the signal droplet. αHL inserted into lipid-bilayer and allowed fluorescent dye to enter signal droplets from reservoir droplets. (B) A bar graph of fold change in fluorescence intensity of signal droplets overtime, compared to the mean fluorescence intensity at t = 0. Green Bar: signal cells with DNA signal. Grey bar: signal cells without DNA signal. (C to D) Brightfield and fluorescence microscopy images of signal droplets and reservoir droplets after 5 hours of incubation. (C) With signal (D) Without signal. Scale bars, 200 µm. In the bar graphs, technical replicates are displayed by crosses and the heights of the bars are the mean. The error bars show the standard deviation.

3.4 Hydrogel networks with residual compartmentalization

A major advantage in using DNA signals to control gene activation in droplet networks was that the lipid bilayers could physically separate the signal from the defective genes, allowing control over the ssDNA access to the defective genes by manipulating the droplet network environment. This section describes construction of multi-compartment hydrogel network that physically separated the signals from the defective genes until the network was activated.

Compartmentalized hydrogel droplet networks were made in the same fashion as droplet-interface bilayer networks, except that a gelling agent was present in the

aqueous phase that gelated the aqueous contents after formation of the network. The bilayers between the hydrogel compartments remained intact. The commonly used gelling agents included agarose, matrigel and silk hydrogel. The bilayers between the compartments could be subsequently broken and allow the hydrogel contents to mix (*83*).

In one example, two droplets comprised of a hydrogel (1.5% (w/v) ultra low gelling temperature agarose in a 1:1 (v/v) ratio of hexadecane to silicone oil AR20) – signal droplet and receiver droplet, were physically separated by a single lipid bilayer. The signal droplet contained the DNA signal (s4) and the receiver droplet contained the defective Mango (M1). By breaking the bilayer, such as by increasing the silicone oil ratio in the system to lower the lipid solubility (*83*), the signal reached the defective Mango, and activated Mango aptamer production (Fig. 3.4A). Critically, Mango aptamer production was not observed when the droplet networks were not activated by bilayer disruption (Fig. 3.4, B to D), therefore gene activation only occurred in response to specific stimuli that disrupted the bilayers.

Alternate methods of breaking lipid bilayers were extensively explored in the literature. Light, temperature, pressure, magnetism, acoustics, redox states, enzymes, electric field and small molecules were reported to control breaking of bilayers (reviewed in (*4*)).

We envisioned that those methods could be used for gene activation in soft biological implants comprised of hydrogel structures. The hydrogel structures would be either activated remotely on demand or they were activated automatically when the required conditions were reached in the client.

3.4.1 Residual compartments in hydrogel structures

In the previous example, once the hydrogel structures were activated, all components were allowed to mix by diffusion, and compartmentalisation was lost.

We explored whether limited compartmentalization could remain after hydrogel activation. For example, the fluorphore dye could be immobilize in sepharose beads, and the beads would also be immobile in the hydrogel solution. This would therfore

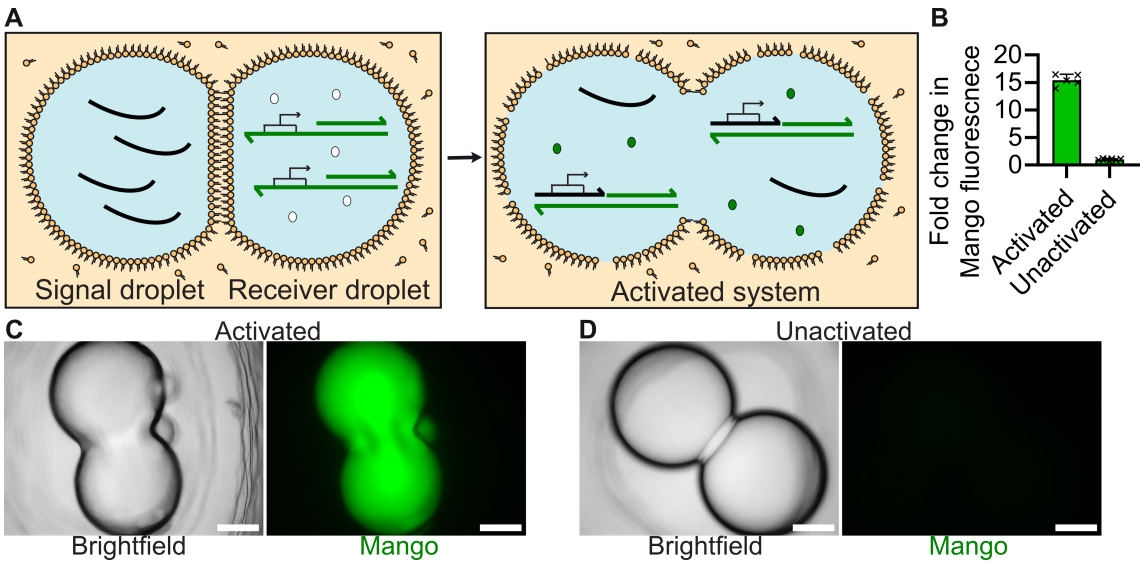


Figure 3.4: (A) A schematic of gene activation in droplet networks formed with droplet-hydrogel bilayers. Lipid bilayers physically separated the signal from the gene expression machinery. Activating the network by bilayer disruption triggered gene expression. (B) A bar graph of fold change in fluorescence intensity of the Mango aptamer in the hydrogel network after 3 hours, compared to the unactivated control. (C to D) Bright field and fluorescence microscopy images of hydrogel network consisting of the DNA signal and the defective Mango. (C) Microscopy images of an activated system after 3 hours. The system was activated and the bilayer was disrupted. (D) Microscopy images of an unactivated system after 3 hours. The system was not activated and the bilayer remained. Scale bars, 200 µm. In the bar graphs, technical replicates are displayed by crosses and the heights of the bars are the mean. The error bars show the standard deviation.

limit the fluorescence activation to specific compartments (Fig. 3.5A). Since the fluorescent dye activated by the Mango aptamer (TO1B) contained a biotin moiety, the dye was immobilized in straptavidin-coated sepharose beads (beads diameter 77 ± 5 µm as measured by microscopy from an average of 3 beads).

Here, three droplets comprised of a hydrogel (1.5% (w/v) ultra low gelling temperature agarose in a 1:1 (v/v) ratio of hexadecane to silicone oil AR20) – signal droplet, defective gene droplet, and fluorophore droplet, were physically connected to each other by lipid bilayers. The signal droplet contained the DNA signal (s4), the receiver droplet contained the defective Mango (M1), and the fluorophore droplet contained the sepharose beads with immobilized TO1B dye. By breaking the bilayer, also by increasing the silicone oil ratio in the system to lower lipid solubility, the signal annelaed to the defective gene, and produced Mango aptamer. The aptamer subsequently diffused into the sepharose beads and slightly increased the fluores-

cence in the beads (Fig. 3.5, B to D). A mean of 26 ± 4 beads (calculated from 8 droplets) were observed in each fluorophore droplet (300 nL), and there was no observable movement of sepharose beads in the hydrogel.

While we did not observe an increase in fluorescence outside of the beads in the activated droplet network, the fluorophore showed a high level of background fluorescence when immobilized on the sepharose beads, even in the absence of the Mango aptamer. Therefore, production of the Mango aptamer by activation of hydrogel structures only led to a weak increase in fluorescence intensity in the beads. Perhaps a more feasible approach would be to immobilize the RNA aptamer instead of the fluorophore on the beads. We could immobilize biotin-labelled ssDNA on straptavidin-coated beads. Then, we could extend the RNA sequence to include a binding domain complementary to the ssDNA already immobilized on the beads. This would allow the RNA to be captured by the beads through complementary base-pairing(*9*). It might also be possible to immobilize other components to the sepharose beads. For example, the DNA signal and the defective gene could be immobilized in the straptavidin-coated beads if the DNA contain 5' or 3' biotin.

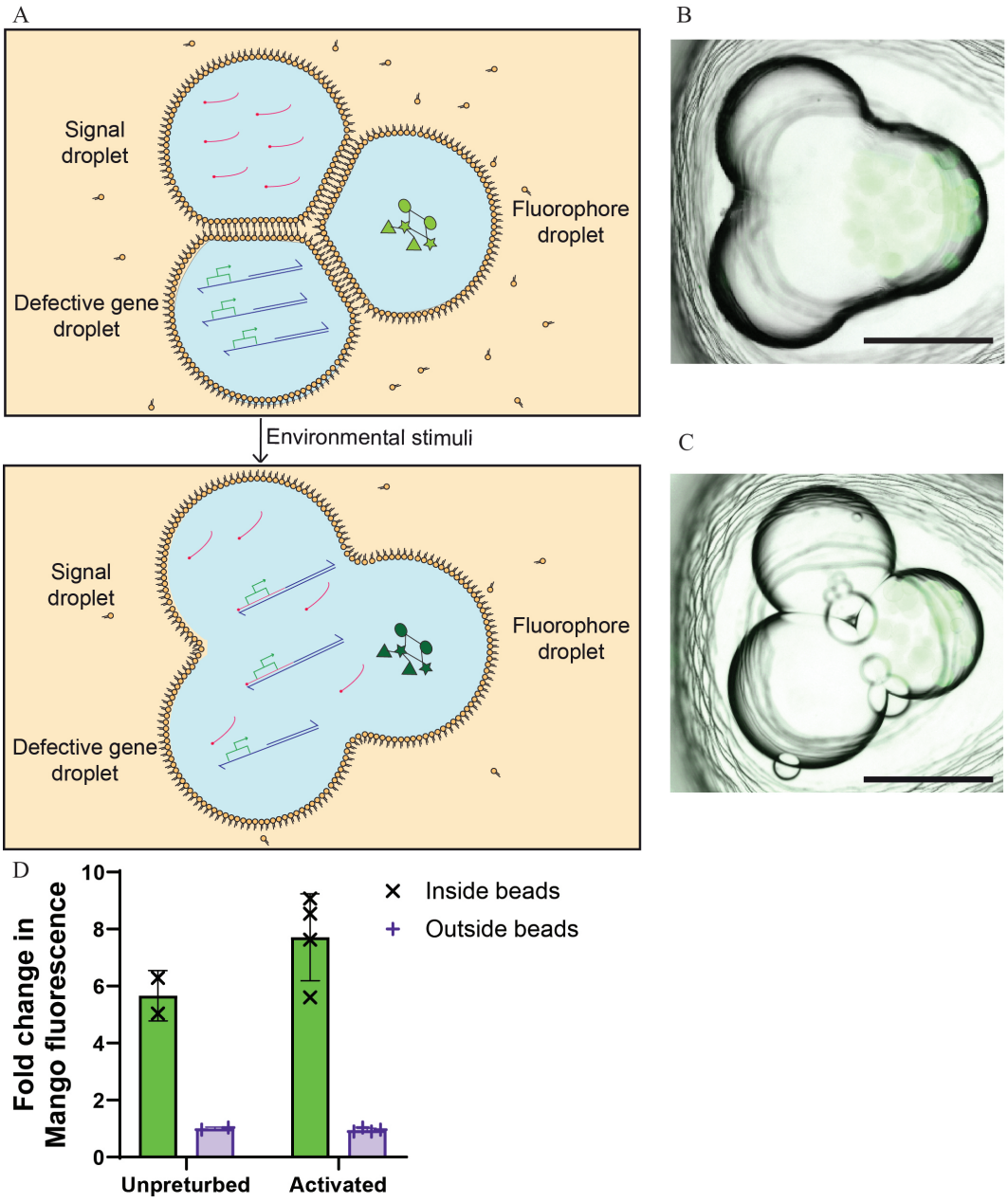


Figure 3.5: (A) A schematic view of gene activation in synthetic tissues formed with droplet-hydrogel bilayers. Lipid bilayers physically separated the signal from gene expression machinery. Activating the network by bilayer disruption activated gene expression. The fluorophore was immobilised within agarose beads in the fluorophore compartment. As a result, only the fluorophore compartment would become fluorescent. (B to C) Overlay of bright field and fluorescence microscopy images of (B) activated, (C) unperturbed hydrogel droplet-networks. Scale bars, 500 µm. (D) A bar graph of fold change in the fluorescence intensity of the Mango aptamer after 3 hours inside and outside the agarose beads, compared to the fluorescence intensity outside the beads of the unperturbed sample, when the droplet network was either unperturbed or activated. The green bars were the fluorescence intensity inside the beads, and the purple bars were the fluorescence intensity outside the beads in the droplets. In the bar graphs, technical replicates are displayed by crosses and the heights of the bars are the mean. The error bars show the standard deviation.

3.5 Selective biopolymer signalling across droplet interface bilayers

This section describes the use of membrane potential to regulate the entry of DNA signals across αHL channel protein pores in lipid bilayers, thus restricting the DNA signal to selected cells.

3.5.1 Introduction

ssDNA was known to translocate across αHL protein pores, and this translocation had been used for nucleic acid detection and even nucleic acid sequencing (*110*). Although the diameter of αHL constriction (1.4 nm) was wider than the ssDNA signal (*109*, *111*), the ssDNA signal could not spontaneously translocate across the αHL pores, as the translocation process was entropically unfavorable. Applied potential was commonly used to transport ssDNA across αHL pores in membranes (*110*). Rates of ssDNA translocation through single αHL channels were commonly obtained by monitoring the electrical current across the channel, as each translocation event transiently decreased the ionic current flowing through the pore (*111*).

To date, there had been limited applications of any nucleic acids translocating through channel protein pores. Of course, ssDNA translocated across the pores were detected by acrshortpcr (*112*). It was also shown that DNA translocated across the pores could hybridized to their complementary strands to form dsDNA that would cause large current blockades in αHL (*33*). Motivated by our work using the ssDNA signals to activate defective genes, we therefore envisioned that applied potential could be used to control ssDNA signal entry across αHL pores on lipid bilayers to activate defective genes.

3.5.2 ssDNA translocation across protein pores

αHL was chosen to translocate ssDNA signals because of three reasons. The first reason was that the αHL pores were commonly used to translocate dyes and small molecules across droplet interface bilayers and GUV membranes (*2*, *28*). While the

maximum density of channel proteins on the membrane had not been determined, the existing findings strongly suggested that it might be possible to reach sufficiently high density of αHL on the bilayer membrane without severely affecting the bilayer stability. The second reason was that the rate of ssDNA translocation across αHL pores had been systematically studied in our group, where DNA translocation rate was measured across different αHL mutants (*111*). In the study, it was found that the E111N αHL mutant and the N113R αHL mutant increased the rate of DNA translocation across αHL pores by 30 fold per pore. The study also reported that the threshold voltage, which was the minimal voltage required for translocation events to be observed, was 40 mV for the E111N mutant and the N113R mutant. This was considerably lower than the threshold voltage of the wild type αHL mutant at 80 mV. The importance of threshold voltage in signalling will be discussed in more detail in sections describing the voltage-dependent stability of droplets interface bilayers.

To further improve the rate of ssDNA translocation across αHL pores, we hypothesized that the construction of a new αHL mutant (E111N/N113R) by combination the two known mutations could further enhance the rate of DNA signal translocation per pore and lower the threshold voltage. As αHL formed heptameric pores, the two mutation removed 7 negative charges (glutamic acid) and introduced 7 positive charges (arginine) into the pore lumen. By measuring the rate of DNA translocation across single pores, at + 80 mV, the new mutant increased the rate of DNA translocation by 80 times per pore compared to the wild type αHL (wild type data reported in (*111*)) (Fig. 3.6). Translocation was observed even at +40 mV.

3.5.3 Translocated DNA signal activated protein production

This subsection highlights the main experimental finding in this section, that the DNA signal could translocate across protein pores on a bilayer when a membrane potential was applied, and the DNA signal could subsequently activate defective genes to produce proteins. Please refer to the next subsection for a more detailed technical discussion of the experimental techniques, methods, and characterisations of the system.

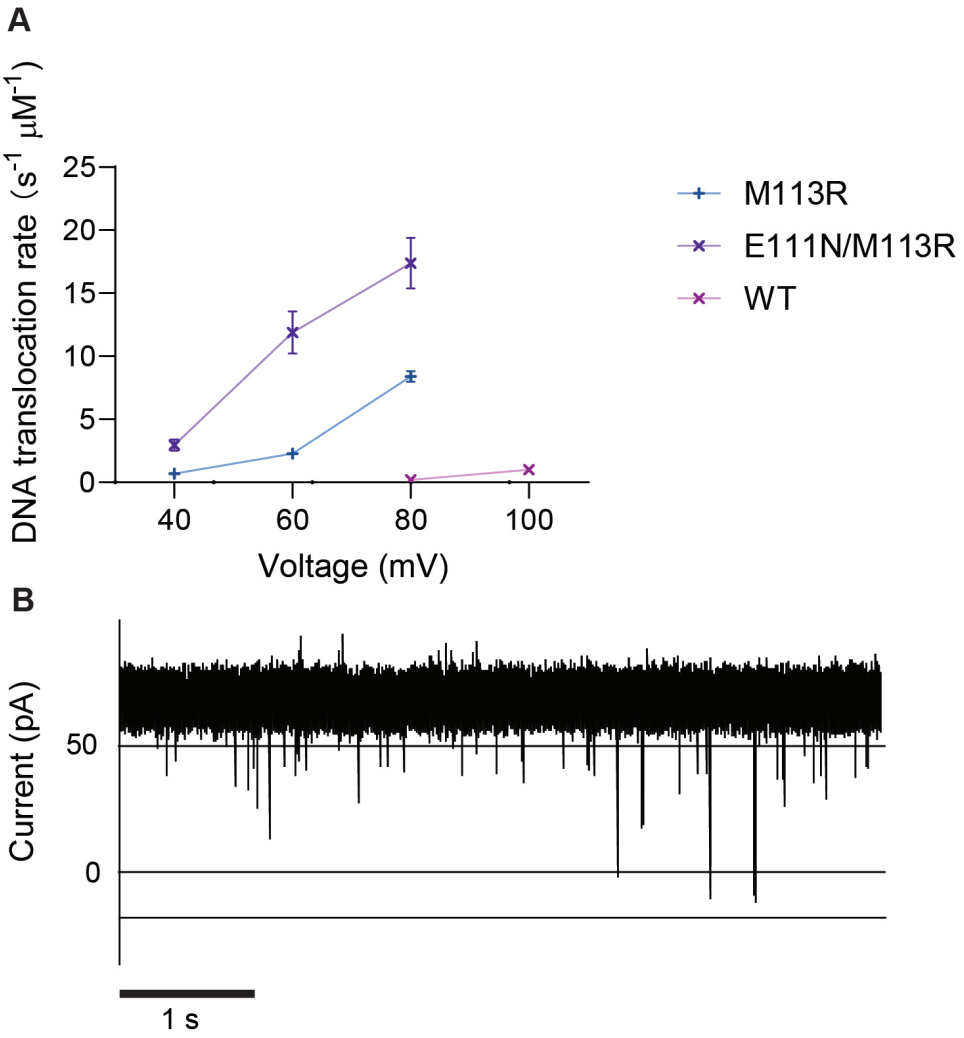


Figure 3.6: (A) DNA translocation rate (s14) across different αHL pores. The crosses are the mean translocation rates from more than 30 translocation events, the error bars are the standard error of the mean. Data for wild type αHL was published in (*111*). (B) Representative current trace of the DNA translocation through a single E111N/M113R pore at +60 mV.

Two aqueous compartments, signal droplet and receiver droplet, were physically separated by a lipid bilayer (Fig. 3.7, A to B). The signal droplet contained a fluorescently labelled DNA signal (s13) and αHL. As the bilayer was formed, αHL inserted into the bilayer and formed pores on the membrane. Therefore, we generated a membrane potential through Ag/AgCl electrodes inserted into the droplets (*113*), to stimulate signal entry into the receiver droplets.

Membrane potential was applied until 10 nM of the fluorescently-labelled DNA signal (s13) was transported across the bilayer, as determined from the fluorescence in the receiver droplet. DNA signal entry was not observed when there was no membrane potential for the equivalent duration of time (Fig. 3.7C). After signal

entry into the receiver droplet, the receiver droplet was supplemented with the defective mCherry (C1), along with cell-free expression components required for protein production. The receiver droplets with the DNA signals produced mCherry protein, which led to 7 times increase in fluorescence intensity, while mCherry protein production was not observed in the receiver droplets without the DNA signal (Fig. 3.7D).

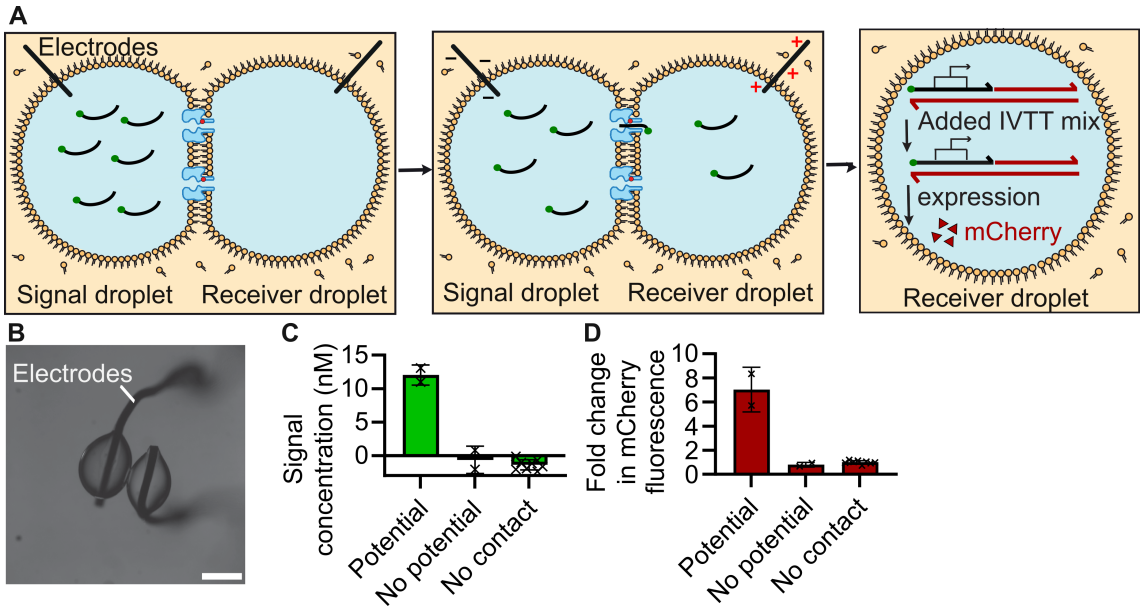


Figure 3.7: (A) A schematic of membrane potential controlling DNA signal entry across bilayers. Membrane potential was required for the DNA signal to enter channel protein pores embedded in bilayers separating synthetic cells. (B) Microscopy images of the signal droplet and the receiver droplet separated by droplet interface bilayers. Electrodes were inserted into the cells to provide the membrane potential. Scale bar, 500 µm. (C) A bar graph of the signal concentrations (s13) in receiver droplets with or without membrane potential between the signal droplet and the receiver droplet. (D) A bar graph of the fold change in fluorescence intensity of mCherry (C1) in receiver droplets after supplementing with IVTT mix for 3 hours, compared to the control with no signal. In the bar graphs, technical replicates are displayed by crosses and the heights of the bars are the mean. The error bars show the standard deviation.

3.5.4 Technical considerations

This subsection details some of the technical challenges encountered in the previous experiments. Those challenges were specifically highlighted in this thesis because membrane potential had not been applied to bilayers with multiple (>1000 pores) pores before to control DNA translocation.

When the membrane potential was applied across bilayers with multiple pores, it was not possible to observe each translocation event across the bilayer because of three reasons. Firstly, channel protein pores were usually the components causing most electric noise in the current recording, when the current flowing through a bilayer was recorded (*114*). Therefore, a large number of pores would multiply the amount of noise in the electrical recording. Secondly, each channel protein could be modelled as a resistor, and multiple channel proteins could be considered as multiple resistors in parallel (*115*). While this had not been experimentally verified for a large (>100) number of pores and may be inaccurate when the density of pores on the membrane was high, such that the current through each pore would affect current flowing through other pores, the total bilayer conductance was approximated as the number of channel protein pores multiplied by the conductance of each pore, and therefore the ionic current flowing through the bilayer was proportional to the number of pores on the bilayer. When the number of pores was high, a less sensitive amplifier - one with lower current resolution but with higher range of current recording had to be used instead, in order not to overload the amplifier with a high current. This decreased the current resolution and made it difficult to observe individual translocation events. Thirdly, the frequency of translocation events increased with the number of pores on the bilayer, and therefore the translocation events would overlap with each other and it would not be able to distinguish between signals from each event. The three factors combined resulted in the fact that it was not possible to directly observe and quantity the amount of DNA translocation across multiple (>1000) channel protein pores on the bilayer by electrical recording of the bilayer.

It was however possible to estimate the translocation rate through other means. If we assumed that each protein channel was independent (events occurring at one channel did not affect events occurring at other channels), we could approximate the rate of ssDNA translocation through bilayer (R) with the following equation:

$$R = n\,f$$

where R was the total signal translocation rate across the bilayer (per unit time), n

was the number of channels on the bilayer, and f was the rate of DNA translocation per channel (per unit time).

f increased with signal concentration in the signal droplet, and increased with the membrane potential, with the negatively charged DNA translocating to the side with more positive potential, and it was also dependent on the αHL mutant as discussed previously. Typically, 100-300 µM signal was present in the signal droplet, and the receiver droplet had a final signal concentration of around 10 nM. Given that no noticeable evaporation of the droplets occurred during the experiments, the signal concentration in the signal droplet remained approximately constant throughout the experiment, and therefore the rate of ssDNA translocation across each pore (f) was not expected to change throughout an experiment. However, the number of protein pores on the bilayer was observed to vary across experiments as well as throughout an experiment, even when the same protein concentration was used. In each experiment, the number of channel proteins on a bilayer increased with time as more of the channel protein monomers would heptamerize and insert onto the bilayer. It was however not well understood why the number of channel proteins inserted onto the bialyer varied a lot across experiments that had the same protein concentration and droplet size (around 5 fold difference). As a result, the rate of ssDNA translocation across the bilayer (R) would vary across and throughout experiments due to the variation in the number of channels on the bilayer.

Therefore, in order to account for the variation in the number of channel proteins inserted onto the bilayer, so that different experiments could be compared, we defined channel time as the integral of the number of channel proteins on the bilayer with time. Mathematically,

$$channel\,time = \int_0^t f\,n(t)\,dt$$

The channel time of a bilayer was defined in a way such that the same amount of DNA would be translocated across the bilayers in different droplet pairs, if the bilayers had the same channel time, and the same potential was applied to the bilayer.

The signal concentration in the receiver droplet (C) at time t was therefore given by:

$$C = \int_0^t R(t)\,dt = \int_0^t f\,n(t)\,dt = f\int_0^t n(t)\,dt$$

or

$$C = f\,channel\,time$$

As explained, the number of channel proteins at a given time was determined from the bilayer conductance, and the number of channel proteins on the bilayer was determined by dividing the bilayer conductance by the conductance of a single channel protein (*116*).

However, if we wanted to continuously monitor the number of channel proteins over time, the conductance measurement would interrupt the application of the membrane potential for signal translocation.

Therefore, to approximate channel time of a bilayer, the number of channel proteins on the bilayer was determined at different time points. The number of channel proteins on the bilayer was monitored every 5 minutes for about 20-30 minutes after bilayer formation, during which more channel proteins continued to insert onto the bilayer. When the bilayer conductance stabilized, meaning that there was less than 10 % change in conductance during subsequent conductance measurements, the conductance was monitored every 15 minutes instead. The average number of channel protein between each two consecutive measurements was calculated, and multiplied by the time elapsed between the two measurements, to approximate the channel time elapsed between the two measurements. The sum of all the channel time between the measurements gave the channel time of the bilayer. As each conductance measurement took less than 10 seconds to complete, this ensured that the interruption to the membrane potential application was at a minimum.

At the same time, when the DNA signal translocated across bilayers in droplet networks, signal concentrations in the droplets (C) could be determined as the DNA signals were fluorescently-labelled (Fig. 3.8). This allowed real time monitoring

of the DNA concentration in droplets when the electric potential is applied to the bilayer. f at different membrane potentials could therefore be determined from signal concentration in the droplets (C) and the channel time of the bilayer. .

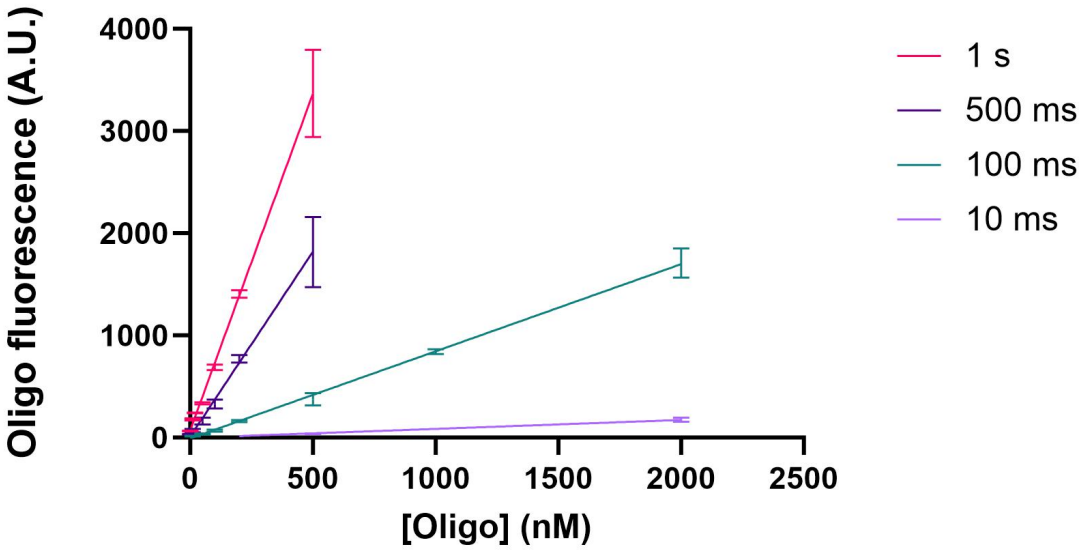


Figure 3.8: A calibration curve relating measured fluorescence intensity of Alexa-488 labelled signal to the signal concentration. The best fit line was constructed using the mean fluorescence at each DNA concentration tested, and the error bars were the standard deviation (n = 3).

It is important to note that when membrane potential was used to stimulate signal entry across channel proteins pores in bilayers, the sign of the membrane potential was reversed every 2s. For example, applying 120 mV meant that +120 mV was applied for 2 s, followed by -120 mV for 2s, and the cycle was repeated. The alternation the potential was necessary to prolong the lifetime of the electrodes, by preventing depletion of AgCl coating on the thin (0.1 mm diameter) electrodes. Depleted Ag/Agcl electrodes would appear white, which was distinct from the silver colour of unoxidized silver wires, or the black colour of Ag/AgCl electrodes. We did not observe depletion of electrodes when a voltage cycle was used. As the DNA concentration in receiver droplet was at most 10 nM compared to 300 µM in the signalling droplet, when the voltage was reversed, the rate of DNA translocation from the receiver droplet to the signal droplet was expected to be negligible.

Additional photos showed how the droplets were positioned in the setup when membrane potential was applied across the bilayers (Fig. 3.9, A to B). As shown in

the photos, the droplets were in a lipid-in-oil solution in a PMMA well. Ag/AgCl electrodes were inserted into the droplets and were connected by insulated copper wires to the amplifier at the back of the photo. The amplifier generated the membrane potential and measured the current through the bilayer. The copper wires were also secured onto micromanipulators visible on the sides of the photo. This allowed the position of the electrodes and the droplets to be controlled by the manipulator. The setup was placed under an inverted microscope for simultaneous bright field and fluorescnece imaging.

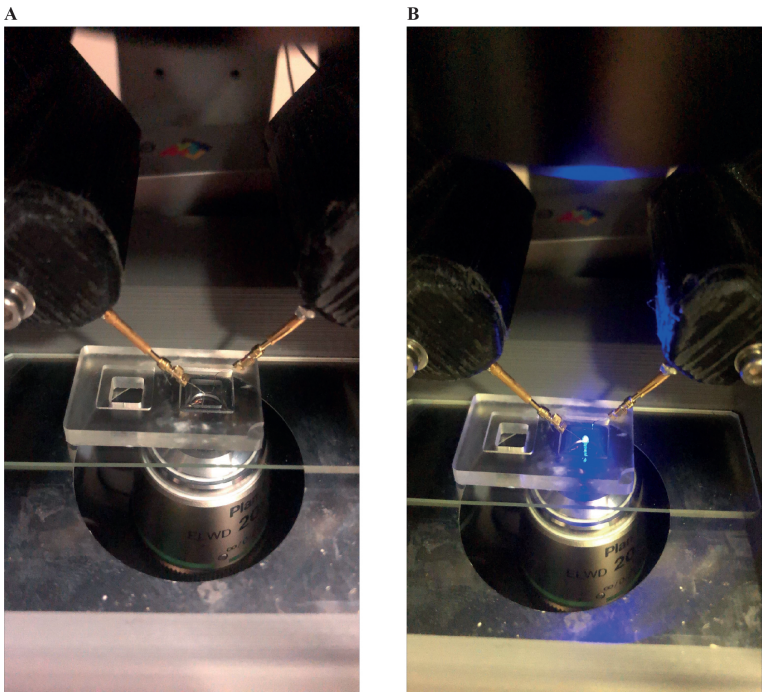


Figure 3.9: Photos of the droplet electrophysiology setup with an inverted microscope (A) without LED illumination, (B) with LED illumination. The droplets were in the lipid-in-oil solution in a PMMA chamber. The droplets were connected by Ag/AgCl wires to micromanipulators that could change the position of the droplets.The eOne amplifier can be seen at the back of the photo.

3.5.5 Summary

Overall, we demonstrated the ability to engineer droplet networks where gene activation only occurred in response to specific stimulus such as bilayer disruption and membrane potential.

In the future, signal entry across αHL pores could be controlled by the choice of mutant, where the correct mutant has to be present for signal entry to occur, even

when the applied potential and channel density on the bilayers were similar.

3.6 Chapter summary and outlook

In this chapter, we studied RNA and protein expression in aqueous droplets in a lipid-in-oil solution. RNA expression decreased in the lipid-in-oil solution, which could be increased by washing the silicone oil. Protein expression was not affected by expression in the lipid-in-oil solution. We showed that the DNA signal and the defective genes could be used to produce the protein pore α-hemolysin (αHL), which inserted into DIBs and allowed dye transfer between two compartments separated by the DIBs. Two mechanisms were used to control the access of ssDNA signals to the gene expression machinery. Firstly, the bilayer could be disrupted by adjusting the oil content to decrease the lipid solubility. Secondly, membrane potential could be used to regulate the entry of the ssDNA signal across channel protein pores embedded in the bilayers, thereby restricting the DNA signal to selected droplets.

Chapter 4

Further studies and applications

4.1 Introduction

This chapter describes preliminary studies for further applications using ssDNA for gene activation. In section 4.2, we discuss potential use of ssDNA signal and defective genes to construct temperature-controlled gene activation devices. In section 4.3, we discuss the use of DNA signal and defective gene to produce proteins that modify functions of biological cells. In section 4.4, we discuss the use of membrane potential to direct signal entry into droplets encapsulating in vitro transcription (and translation) systems. Finally, in section 4.5, we discussed potential use of dynamic covalent thiol-disulphide interchange chemistry to selectively deliver the DNA signals across channel proteins in lipid bilayers.

4.2 Thermoresponsive activation of defective genes

There was a lot of recent interest in using temperature to control gene activation in the synthetic biology community. To date, most of the published work relied on using naturally existing temperature-sensitive transcription activators or repressors to control gene activation with temperature, with potential applications in biosensing and bioproduction (*117*, *118*).

We envisioned that the ssDNA signals and the defective genes could be engineered for temperature-dependent gene activation, since the complementation of

the DNA signals to the defective gene was a temperature-sensitive process. The DNA signals were not expected to bind to the defective genes above the melting temperature of the DNA signals. As a result, gene activation would not occur above the melting temperature of the signals.

As a proof of concept, we investigated gene activation by the DNA signals at different temperatures. Since all of the DNA signals used in this thesis had a melting temperature of at least 47 °C, Hi-T7 RNA polymerase was used instead of the standard T7 RNA polymerase, so that transcription could be studied at higher temperatures. Hi-T7 RNA polymerase was a thermostable version of T7 RNA polymerase developed by NEB, and the polymerase was reported to be active from 37 °C to 56 °C (*78*).

The DNA signals s1, s2 and s6 had calculated melting temperatures of 58 °C, 86 °C, and 47 °C respectively. When incubated with the defective Broccoli (B4) at different temperatures, s1 and s2 were able to activate the defective Broccoli at 51 °C, but s3 could not, as 51 °C was higher than the melting temperature of the s3 signal (Fig. 4.1).

Unlike naturally occurring temperature-sensitive transcription activators and repressors, melting temperature of the DNA signals could be precisely controlled by the signal sequence and the salt concentration (especially concentration of magnesium ions) in the buffer (*50*), allowing construction of more precise temperature-controlled devices in the future.

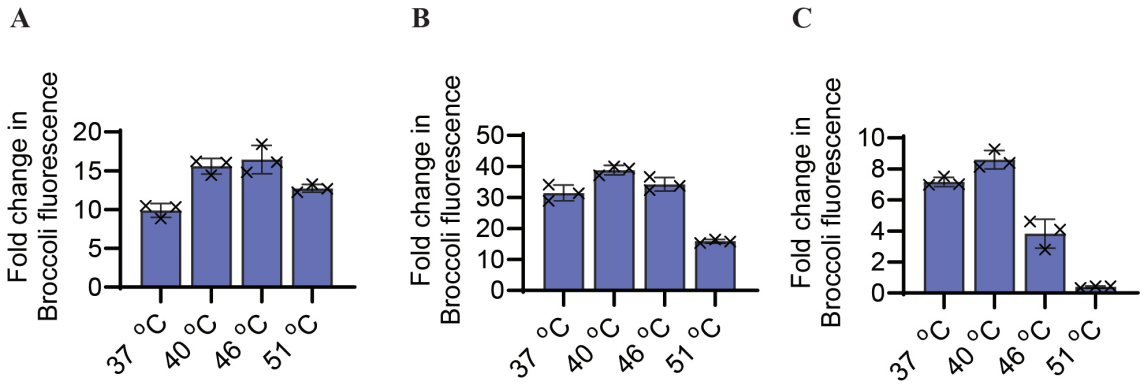


Figure 4.1: Bar graphs of fold change in Broccoli fluorescence intensity compared to the control with no signal, when the Broccoli signal (A) s1, (B) s2, (C) s6 was mixed with the defective Broccoli in bulk after 3 hours at different temperatures. In the bar graphs, technical replicates are displayed by crosses and the heights of the bars are the mean. The error bars show the standard deviation.

4.3 Interfacing DNA signalling with cells

We envisioned using DNA signal and defective genes to produce protein products that influence functions of cells. For example, we investigated killing of rabbit red blood cells by α-hemolysin produced from the defective genes.

α-hemolysin was produced from the DNA signal and the defective genes in IVTT mix, and the IVTT mix was diluted before adding to the rabbit red blood cells. The killing of red blood cells was monitored in real time by monitoring the absorbance (*119*). Cell lysis was observed even at 6400 fold dilution of the IVTT mix. This was a promising pilot expeirment and showed the possibility of interfacing the DNA signalling system with biological cells.

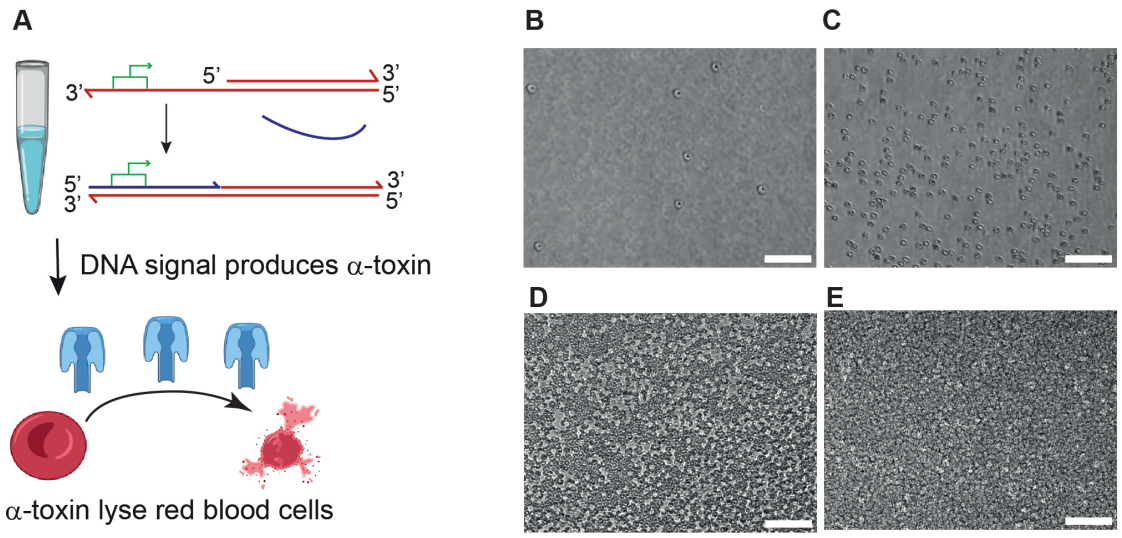


Figure 4.2: Microscopy images of rabbit red blood cells killed by α-hemolysin toxin produced by DNA signal (FS) and defective α-hemolysin gene (αHLm). The IVTT mix is diluted (A) 200, (B) 1600, (C) 6400 (D) 25600 fold. Scale bars, 50 µm.

4.4 One pot signalling

In the previous chapter, a membrane potential was used to control signal entry into receiver droplets, and the receiver droplets were subsequently detached from the signalling droplet and supplemented with the PURE system to initiate gene production.

Our next goal was to redesign the signal and receiver droplets so that IVT mix (for the production of RNA aptamers from defective genes) or IVTT mix (for the production of proteins from defective genes) was present in the receiver droplets during the signal entry (Fig. 4.3). The advantages of such design would be discussed, together with our initial steps towards this goal.

The advantage of embedding the defective gene and transcription (and translation) mix in the receiver droplet was that this would allow construction of more sophisticated droplet networks with more droplets with different compositions.

For example, in a droplet network where a signal droplet was surrounded by receiver droplets, the signal would only enter a receiver droplet when the membrane potential was present between the signal droplet and the receiver droplet, and that the αHL mutant pore with a high translocation rate was present on the bilayer. This would allow spatial patterning of gene production in the receiver droplets,

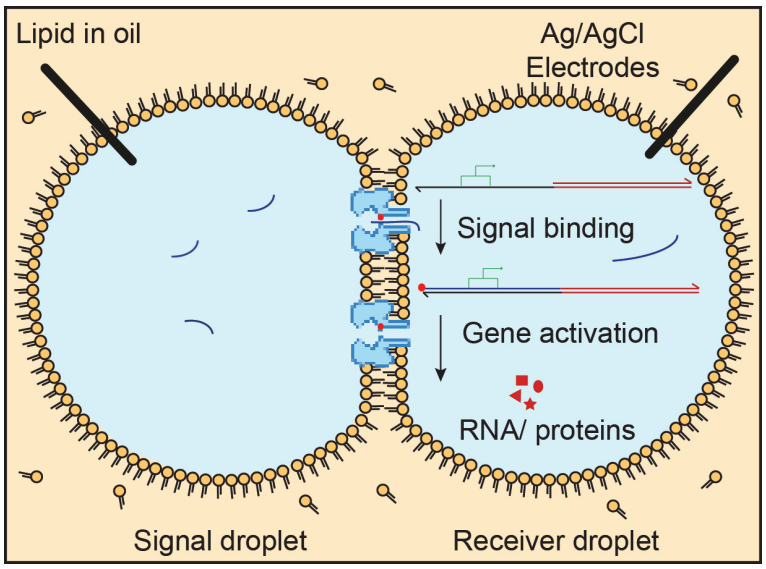


Figure 4.3: A schematic of membrane potential controlling DNA signal entry across bilayers. The defective gene and the transcription (and translation) mix were already present in the receiver droplet, and the translocated signal could activate gene production when the the droplets were still connected with a bilayer and the membrane potential was still applied to control signal entry.

where the pattern was controlled by the pattern of membrane potential (Fig. 4.4A). Alternately, different defective genes, such as defective Cherry/ defective mNG, or defective Broccoli/defective Pepper, could be present in different receiver droplets. The membrane potential would allow signal entry into the receiver droplets, which would produce different products in the droplets (Fig. 4.4B).

Apart from having multiple receiver droplets, we could also design droplet networks with multiple signal droplets surrounding a receiver droplet. Each signal droplet contained different ssDNA signals, and the pattern of membrane potential would decide which signal could enter the receiver droplet. The signal could then selectively activate gene production in the receiver droplet, using the strategies for selective gene activation outlined in chapter 2 (Fig. 4.5).

Of course, droplet networks with multiple signal droplets and receiver droplets could also be designed. Ultimately, this would lead to droplet networks where environmental stimulus would be converted to patterns of membrane potential on bilayers, which then activated gene activation on-demand. Each receiver droplet would produce different products, and the droplets would exhibit collaborative properties where the different products would produce synergistic effects in response to the

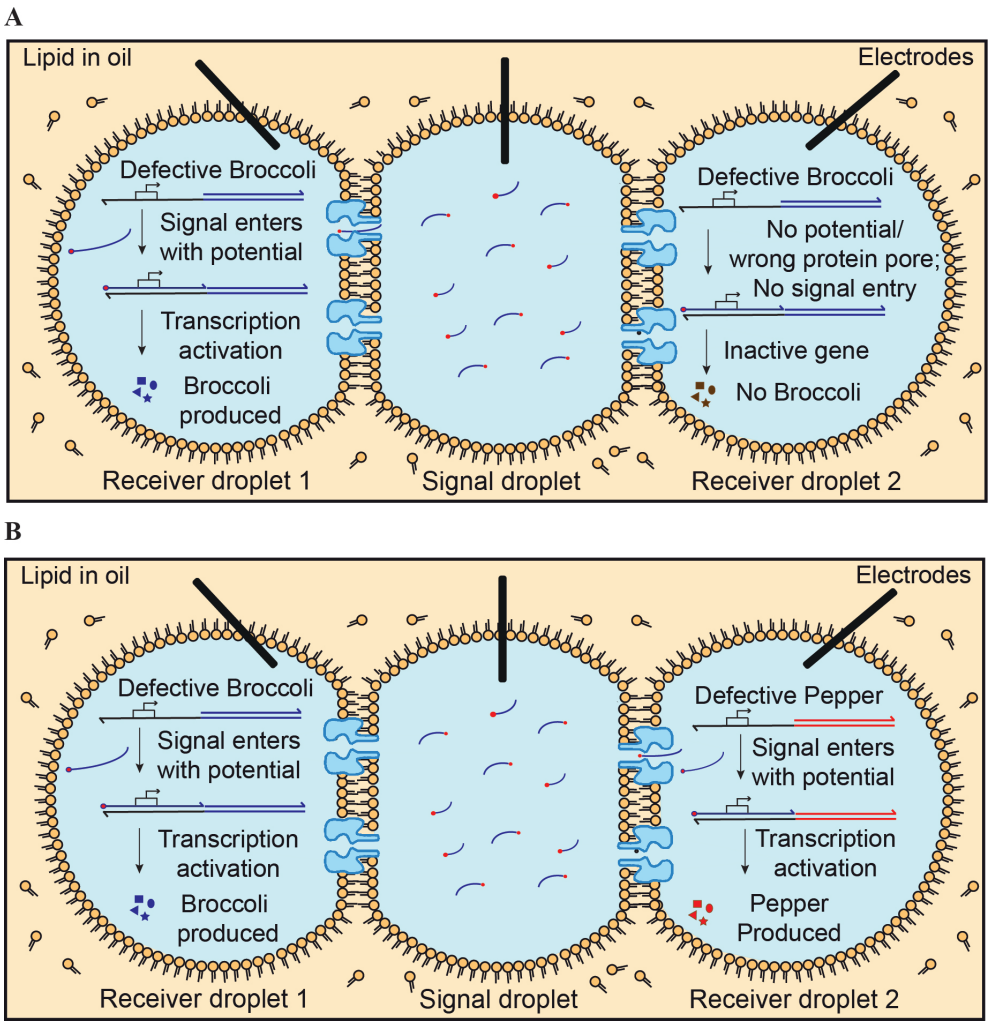


Figure 4.4: (A) A schematic of selective entry of the DNA signal across lipid bilayers in droplet networks. The ssDNA signal would only pass through bilayers with membrane potential and the correct channel protein pore. (B) A schematic of differentiated gene activation in droplet networks. The membrane potential allowed signal entry into both receiver droplets, different genes were produced in each receiver droplet.

stimulus.

4.4.1 Membrane potential control across multiple bilayers

The current amplifier used in the lab only had two terminus for simultaneous voltage application and current recording. At the same time, we also only had two micromanipulators that could control movement of the droplets. It was important that some of the electrode were mobile, as the droplets would coalesce instantaneously if they were directly in contact with each other when added to the lipid-in-oil solution, since the lipid monolayer was not formed around each droplet. Therefore, the

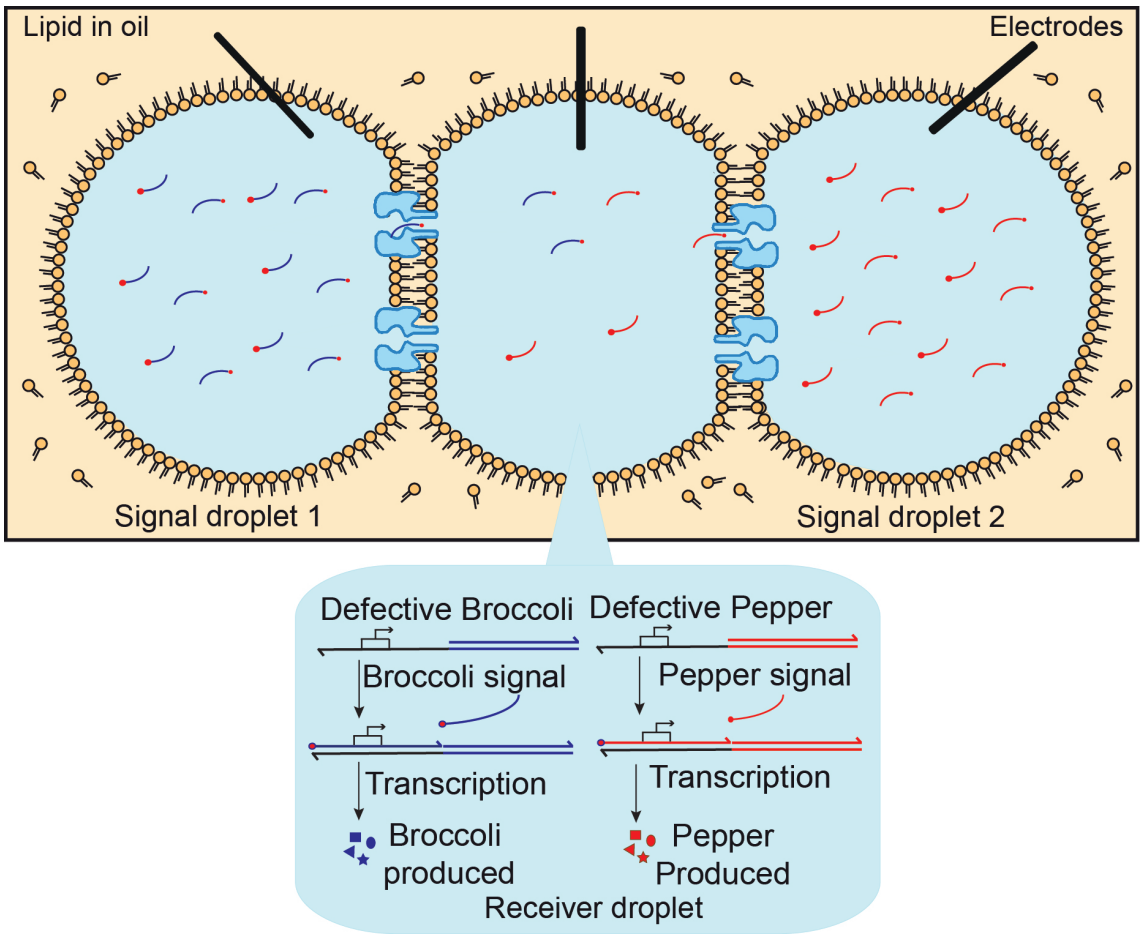


Figure 4.5: (A) A schematic of selective gene activation in droplet networks. Broccoli signal was present in signal droplet 1, Pepper signal was present in signal droplet 2, both defective Broccoli and Pepper were present in receiver droplet. If a membrane potential was present on the bilayer connecting the signal droplet 1 and the receiver droplet, Broccoli signal would enter across the bilayer and activate Broccoli production. Similarly, if a membrane potential was present on the bilayer connecting the signal droplet 2 and the receiver droplet, the Pepper signal would enter the receiver droplet and activate Pepper production. Both Broccoli and Pepper would be produced if the membrane potential was present on both bilayers.

electrodes had to be positioned away from each other when droplets were added to the electrodes to allow time to form the monolayer. Subsequently, the micromanipulators controlled the movement of the droplets, and allowed the droplets to come into contact to form lipid bilayers between them. We designed a setup that allowed three droplets, with two separate membranes, to be controlled by the amplifier and the two manipulators (Fig. 4.6A). The wires attached to the top and the bottom droplets were each secured on a separate micromanipulator, while the middle droplet was secured on the PMMA chamber by blue-tag, and was therefore immobile (Fig. 4.6B). Before the droplets were added to the lipid-in-oil solution, the top and bot-

tom electrodes were positioned away from the middle electrode, so that the droplets would not come into contact with each other before the lipid monolayer formation was complete. The top and bottom electrodes with the droplets were then moved in the lipid-in-oil solution by the manipulators, to each form a lipid-bilayer with the center droplet. In terms of electrical connection to the amplifier, the middle droplet was connected directly to the cis-terminus of the amplifier, while the top and the bottom droplets were each connected to the trans terminus of the amplifier through a switch (Fig. 4.6, C to D). Therefore, depending on the whether the switches were on or off, membrane potential could be applied to either or both membranes, while the remaining membrane would have no membrane potential. The limitation of this system compared to a multichannel amplifier was that both membranes would have either zero or equal potentials, but this was sufficient for our applications.

4.4.2 Osmolarity of IVT(T) solution

If the osmolarity of the signal and the receiver droplets were not balanced, an osmotic pressure would be exerted on the bilayer, potentially leading to bilayer rupture (*42*). Even if the bilayer could withstand the osmotic pressure, the droplet sizes would change over time due to osmosis (*80*), as a result the concentration of the components in the droplets would change. Therefore, it was important to know and to balance the osmolairty of the in vitro transcription (and translation) mix, before using them in droplets. It was also important to note that when multiple pores were present on the bilayer, the concentration of small molecules in the signal droplet and the receiver droplet would equilibrate over time. Therefore, the starting concentration of small molecules in the signal droplet and receiver droplet should be equal, so the concentrations will not change with time due to diffusion across bilayers, which could also result in an osmotic pressure.

The osmolarity of the PURExpress IVTT solution was already determined from our lab to be around 1000 mOsm (*2*, *42*). We measured the osmolarity of the IVT mix and several selected components of the IVT mix (Fig. 4.7). The T7 RNAP mix was the component with the highest osmolarity (750 mOsm). This was perhaps

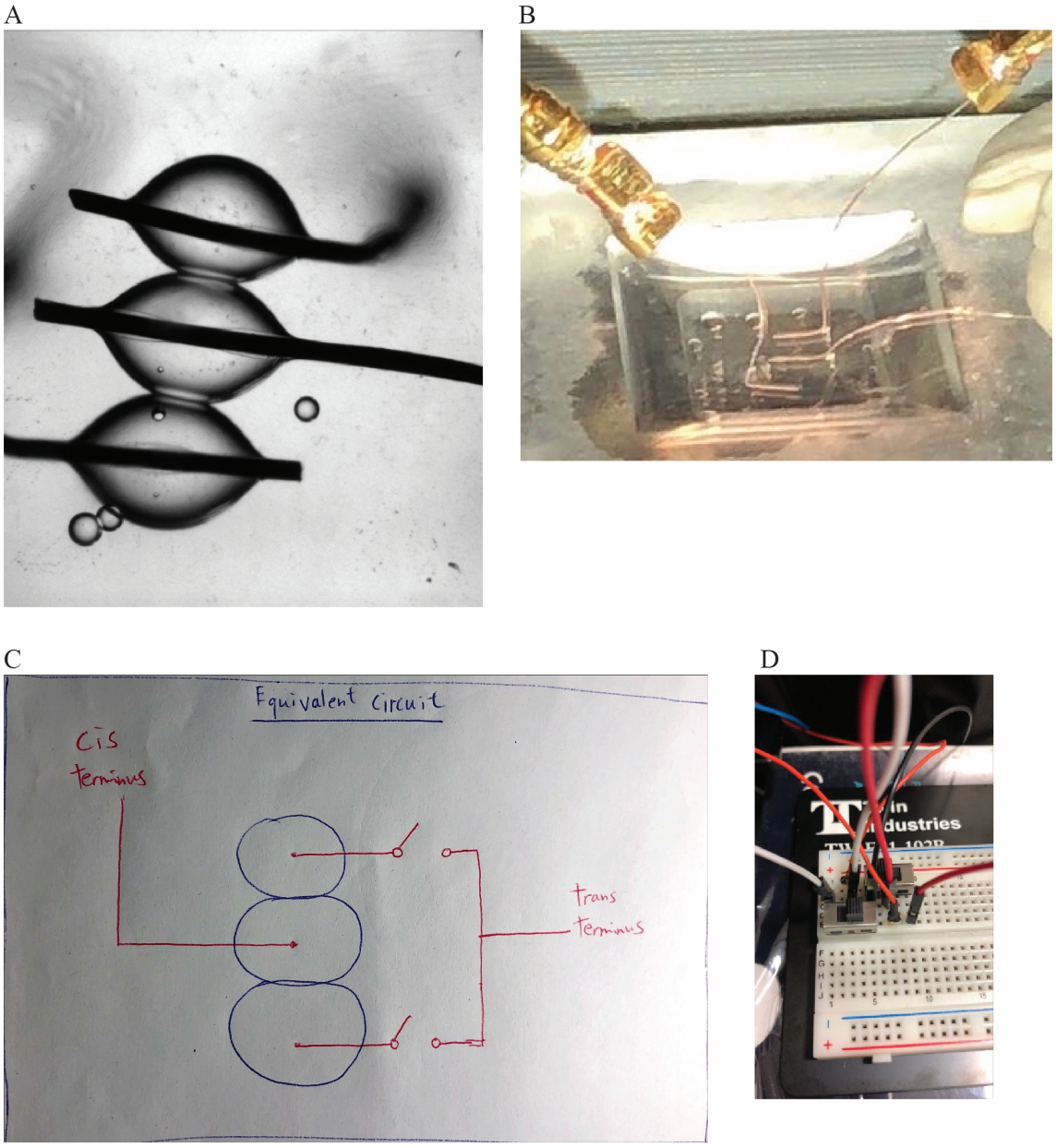


Figure 4.6: Signalling setup with 3 droplets. (A) A bright field microscopy image of three droplets with electrodes inserted into each of the droplets. The droplets were connected by droplet interface bilayers. (B) A photo showing the electrodes connected to the droplets in the lipid-in-oil solution. The wires connected to the top and the bottom droplets were secured on a micromanipulator. The wires connected to the middle droplet was secured to the imaging chamber by bluetag. The other droplets in the chamber came from droplets that failed to adhere to the electrodes. (C) An equivalent circuit diagram of the setup. The droplet in the middle was connected to the cis terminus of the amplifier, while the droplets on top and bottom were separately connected to the trans terminus of the amplifier through a switch. (D) A photo of the solderless breadboard with the two switches connecting top and bottom droplets to the trans terminus.

because the IVT solution contained 5 % glycerol by volume, equivalent to 0.5 M.

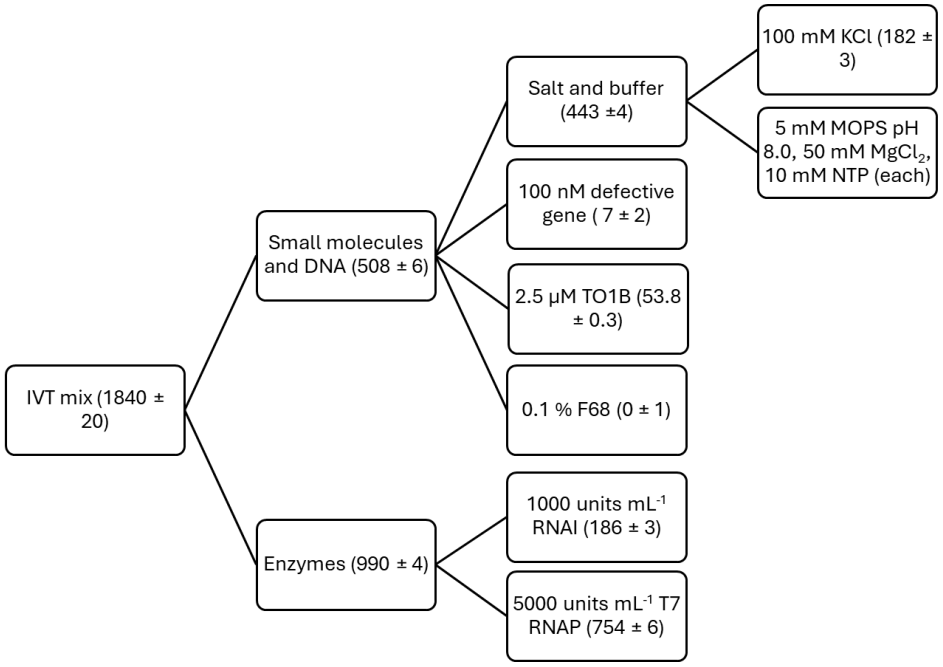


Figure 4.7: A composition map of the IVT mix. The mean and standard deviation of the osmolarity of some of the components in mOsm were listed in the table. The means and the standard deviations were calculated from three measurements of the osmolarity.

Therefore, in the following experiments, we would use the same concentration of the small molecules and buffer in both the signal droplet and the receiver droplet. The signal droplet would not contain T7 RNAP and RNAI, but would be supplemented with glycerol such that the glycerol concentration in the signal droplets and the receiver droplets was the same.

4.4.3 Stability of droplet interface bilayers

One crucial requirement for using the membrane potential to deliver the DNA signal across the bilayer was that the bilayer needed to remain stable when the membrane potential was applied. We designed a stability test to quantify the stability of bilayers. In the stability test, 10 minutes after formation of the bilayer, a membrane potential increasing by 1 mV per second was applied to the bilayer until the bilayer ruptured. The breakdown voltage indicated the voltage-dependent stability of the bilayer. A bilayer would be assigned breakdown voltage of 0 mV if it ruptured in the 10 minutes of incubation time. A breakdown voltage higher than the signalling

voltage at 60 mV would be needed for use in signalling.

We investigated the stability of bilayers formed from DPhPC lipid when the droplets contained the IVT mix. It was found that the IVT components formed stable bilayers that brokedown above the signalling voltage (condition 1), but the bilayers were no longer stable when the T7 RNA polymerase was also present in the droplets (condition 2). Since the polymerase was supplied with triton detergent, we removed the detergent with a detergent removal column, but this did not improve the stability (condition 3). We found that reducing the amount of T7 RNAP added to the droplets (condition 4), or doubling the amount of salt to 100 mM KCl (condition 5), improved the bilayer stability (Fig. 4.8).

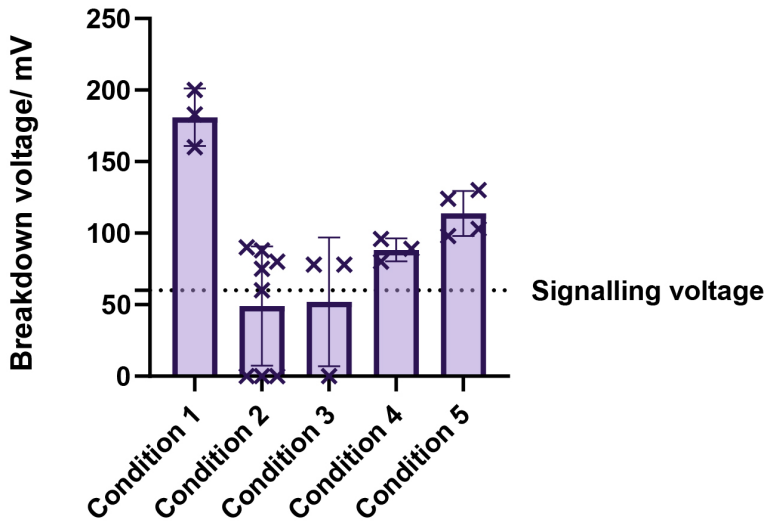


Figure 4.8: A bar graph of the breakdown voltage of droplet interface bilayers formed from DPhPC lipid when different components were present in the droplets. Condition 1: buffer B (20 mM MOPS pH 8.0, 50 mM $MgCl_2$, 2 mM spermidine, 10 mM DTT, 10 mM NTP (each), 50 mM KCl). Condition 2: buffer B with 5000 units mL^{-1} T7 RNA polymerase. Condition 3: buffer B with 5000 units mL^{-1} detergent-removed T7 RNA polymerase. Condition 4: buffer B with 2500 units mL^{-1} detergent-removed T7 RNA polymerase. Condition 5: buffer B with 2500 units mL^{-1} detergent-removed T7 RNA polymerase, with an additional 50 mM KCl. In the bar graph, technical replicates are displayed by crosses and the heights of the bars are the mean. The error bars show the standard deviation.

We also investigated the stability of droplet interface bilayers formed with IVTT mix (PurExpress). The IVTT mix consisted of three solutions, solution A, solution B, and RNAse inhibitor (RNAI). The solution A consisted of mostly salt and small molecules used in the IVTT reaction, while the solution B consisted of the enzymes and ribosomes used in the reaction. We found that while the solution A or a mixture

of the solution A and the RNase inhibitor formed stable bilayers with DPhPC lipids, the bilayer was not stable with the complete IVTT mix, or with a mixture of the solution A and solution B. This suggested that solution B was destabilising the bilayer. Adding supplements to the IVTT mix, such as with 2% PEG4000, did not significantly improve the bilayer stability (Fig. 4.9A). Different lipids, such as PEG lipid (*120*) or POPC lipid (*28*), were reported to improve stability of droplet interface bilayers. Therefore, we tested different lipid mixtures in the oil phase, such including POPC lipid or PEG lipids in the oil phase. Those lipid supplements improved the bilayer stability formed with the IVTT mix (Fig. 4.9B).

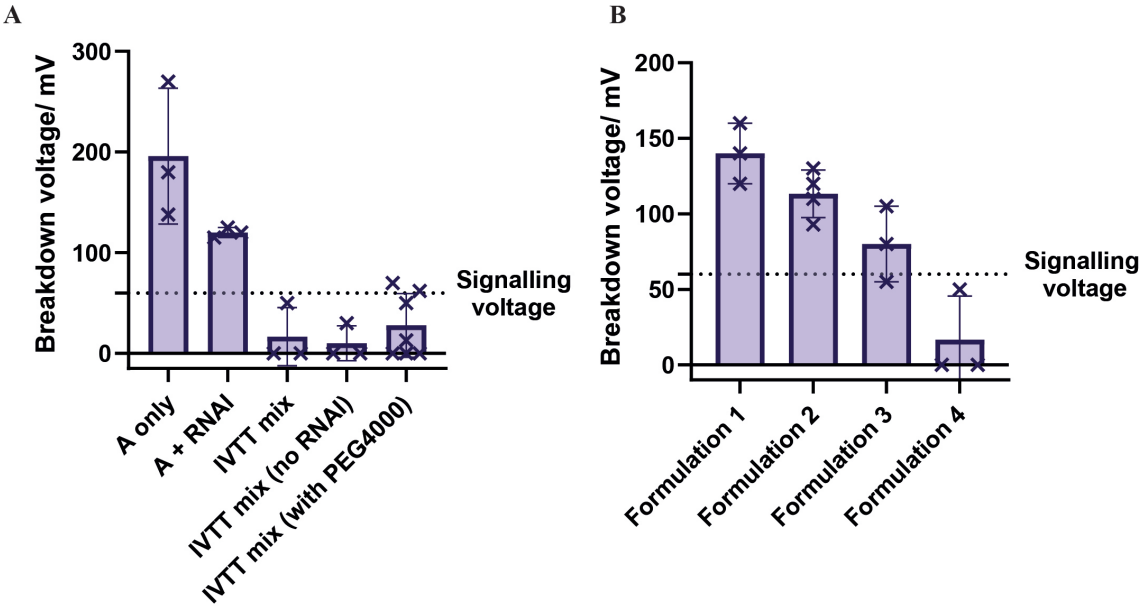


Figure 4.9: Stability of the droplet interface bilayers formed with the IVTT mix. (A) A bar graph of the brekadown voltage of bilayers formed from DPhPC lipid when different components were present in the droplets. (B) A bar graph of the breakdown voltage of bilayers, with different formulation of lipid in the oils solution, when the IVTT mix was present in the droplets. Formulation 1: 1:1:0.3125 (w/w/w) DPhPC:POPC:PEG2000PE. Formulation 2: 1:1:0.2 (w/w/w) DPhPC:POPC:PEG1000PE. Formulation 3: 1:1 (w/w) DPhPC:POPC. Formulation 4: DPhPC only

4.4.4 DNA signal capture at different lipid compositions

We evaluated using the DNA signal for gene activation in IVTT mix by using lipid compositions that generated stable bilayer. We developed a pore blockade assay experiment to investigate if the DNA signal could be captured by the αHL pores when the lipid composition changed. The assay used a straptavidin-bound DNA

signal (s13) (more on the straptavidin bound signal in the next session), which was known to be captured by αHL pores in the presence of a membrane potential due to the negatively charged DNA signal. However, the straptavidin-bound signal could not translocate across the pores, due to the bulky size of the straptavidin protein. As a result, the ionic current through the pore would decrease when those constructs were in the pore lumen, as they physically obstruct the ionic current through the pore.

We used this to develop an assay to verify if the DNA signals could be captured by the αHL pores. Without the DNA signals, the 111N/113R pores had a rectification effect. The current through the 111N/113R hemolysin pores was higher when a positive potential was applied to the trans side (the protein inserted from the cis side) of the bilayer, as compared to when a negative potential of the same magnitude was applied. We defined rectification factor as the current through the bilayer when a positive voltage was applied to the trans side, divided by the current through the bilayer when a negative voltage was applied to the trans side.

We analysed the rectification factor of multiple 111N/113R αHL channels on a bilayer formed from DPhPC lipid. Without the straptavidin-bound signal, the rectification factor was higher than one. When the straptavidin bound signal was present, the rectification factor decreased, as the straptavidin-bound DNA signal was expected to block the pores only when a positive potential was applied to the trans side of the bilayer (Fig. 4.10A).

The same set of experiments were repeated in a bilayer formed from DPhPC lipids supplemented with PEG1000 lipid. This lipid mixture was previously found to give stable bilayers when IVTT mix was present in the droplets. Surprisingly, the rectification factor remained similar regardless of whether the straptavidin-bound oligonucleotide was present (Fig. 4.10B). It was also surprising to find that the rectification factor was very different from the rectification factor of bilayers formed from DPhPC lipid only.

The experiments were again repeated in bilayers formed from a mixture of DPhPC and POPC lipids. The rectification factor of the bilayer was measured

in the presence of the straptavidin-bound oligonucleotide. Similarly, the rectification factor was high, suggesting that the DNA signals were not captured by the pores (Fig. 4.10C).

While further investigation would be required to establish the interaction of the DNA signal and protein pores when the lipid composition was altered, it was clear from the above experiments that the electrical behaviours of the protein pores on bilayers supplemented with PEG lipid and POPC lipid were different from bilayers with DPhPC lipid only. It remained to be investigated if the DNA signal could still translocate across the protein pores in those lipid compositions.

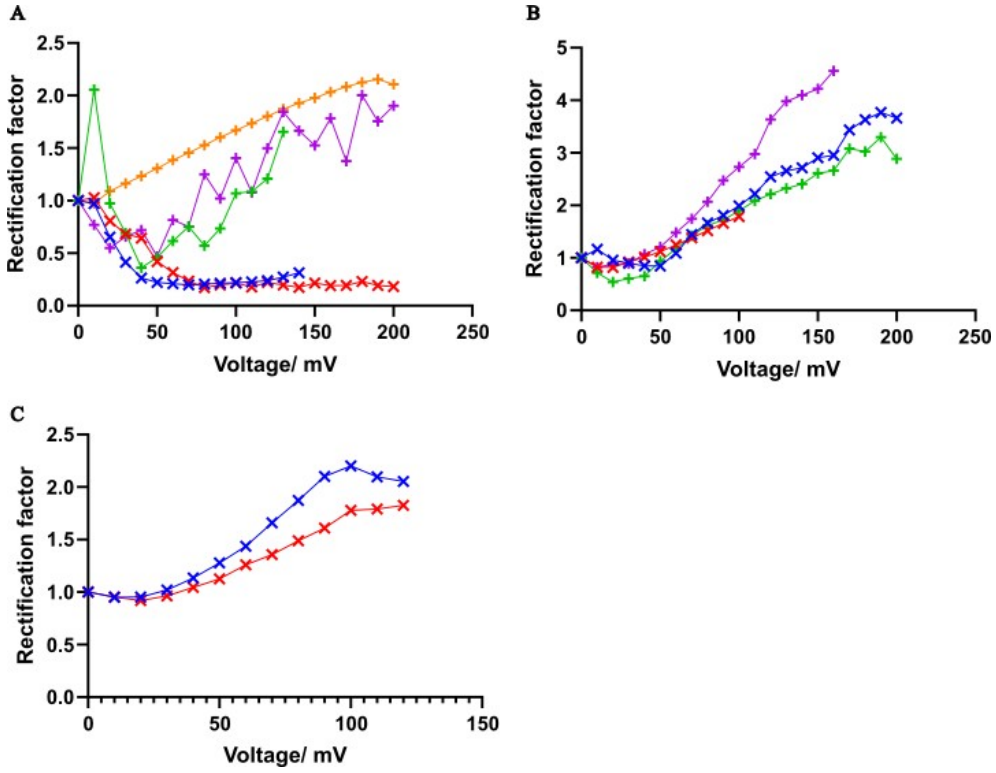


Figure 4.10: Graphs of rectification factor of bilayers consisting of αHL pores, with (+) or without (x) straptavidin-bound DNA signal, when the bilayer was formed with (A) DPhPC lipids only, (B) DPhPC with 10% (by mass) PEG1000 lipid, (C) DPhPC:POPC 1:1 (w/w) lipid. Each line was data obtained from a different bilayer. (+) indicates samples with straptavidin-bound signal. (x) indicates samples without straptavidin-bound signal.

During preparation for those experiments, it was observed that the properties of a mixed 1:1 DPhPC:POPC (w/w) lipid film would change over time even when it was stored at -80 °C. We found that the older lipid films (more than 1 month) were no longer soluble in pentane, while a freshly made lipid film was able to (Fig. 4.11). We could not find relevant literature on what could be occurring to the lipids, and

we also could not obtain an answer from the manufacturer (Avanti polar lipids). While POPC contained unsaturated double bond, the bond should stable at -80 °. It was very likely that the changes observed were due to hydration of the lipid films from moisture in the air, which altered the lipid solubility in pentane. Therefore, prolonged storage of lipid films were avoided.

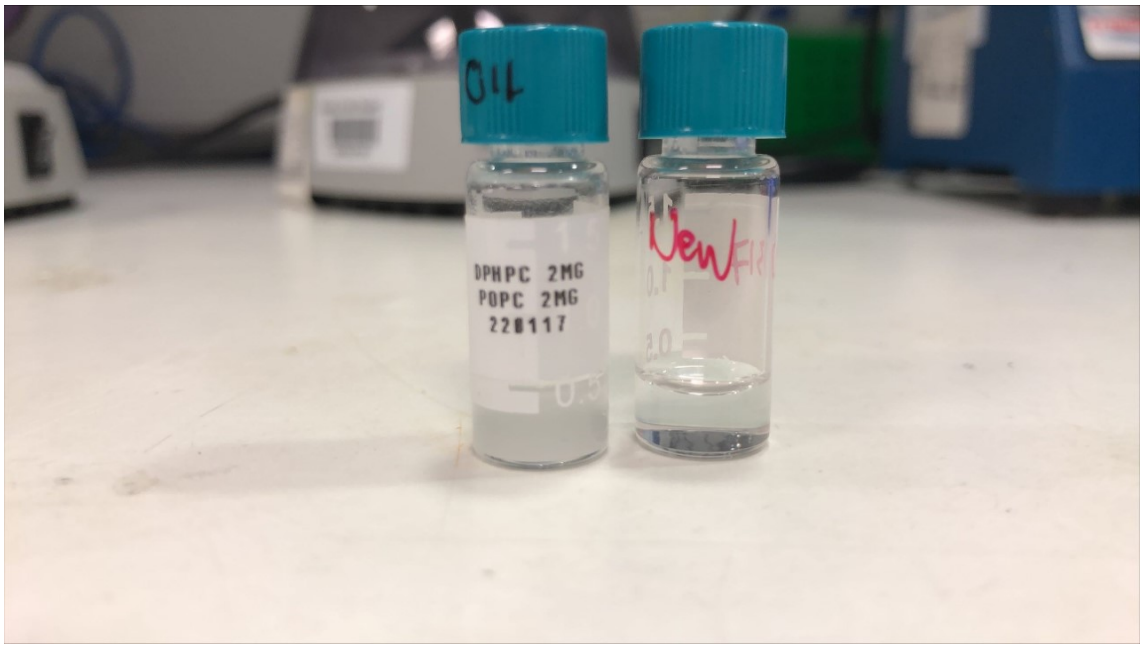


Figure 4.11: A photo of glass vials with 0.5 mL of pentane added to 4 mg of 1:1 DPhPC: POPC (w/w) lipid film. The lipid film was either stored for over a month at -80 °(left), or prepared within 48 hours (right).

4.4.5 Spermdidine deformed the signal droplets

It was observed that the signal droplets deformed when the signal droplet contained IVT components (all components without the T7 RNAP) (Fig. 4.12). The IVT mix contained 2 mM spermidine, which was a polycation. It was very likely that coacervates/ precipitates would form from interactions between the high concentration (150 µM) of the DNA signal - a polyanion - and the spermidine (*121*). There was also an additional 40 mM NTP (10 mM each), and 10 mM free magnesium ions in the solution, those components could also interact with the DNA signal/spermidine complex and precipitate. While the signal droplets no longer deformed when the spermidine was no longer used in our system, it was not obvious how the precipitation/coacervate formation affected the morphology of the droplets. Spermidine was

not used in subsequent experiments.

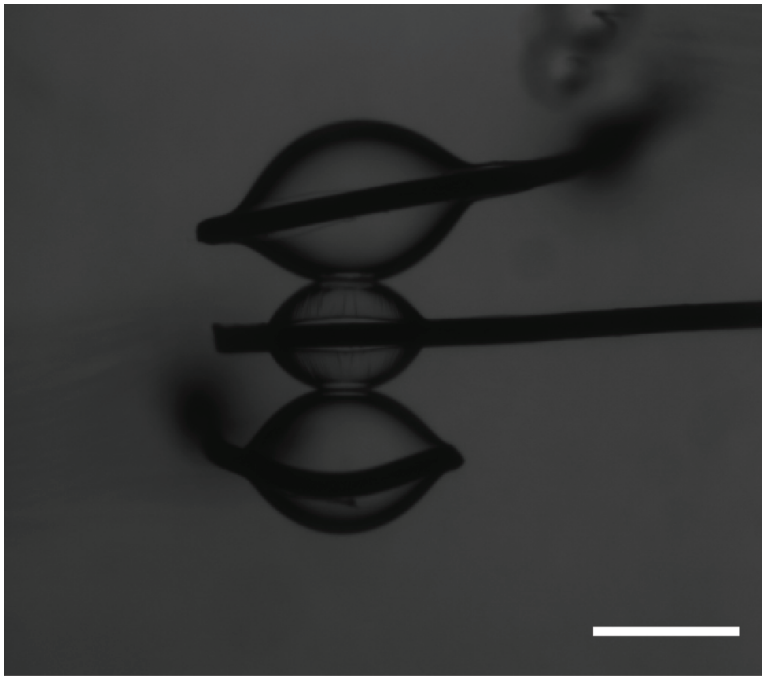


Figure 4.12: (A) A microscope image of the signal droplet (center) surrounded by two receiver droplets (top and bottom), when the droplets contained spermidine. Scale bar, 500 µm.

4.4.6 T7 RNAP degraded on Ag/AgCl wire

Finally, we investigated IVT expression on Ag/AgCl electrodes in a lipid-in-oil solution, and found that T7 RNAP lost activity within 15 minutes in contact with the electrodes.

To test the IVT activity as droplets on Ag/AgCl electrodes in the lipid-in-oil solution, we first added the signal (without the IVT mix) to the electrode and incubated the signal for 15 minutes, during which there was no increase in fluorescence as expected. The IVT mix was then added to the droplet containing the signal, and an increase in fluorescence was observed after 15 minutes (Fig. 4.13A). In another set of experiments, we first added the IVT mix to the electrode, and incubated the mix for 15 minutes, during which there was no increase in fluorescence, as expected. We then added the signal to the droplet on the electrode, and incubated the reaction for another 15 minutes. Surprisingly, there was no increase in fluorescence after the 15 minute incubation, despite the fact that all components necessary for gene expression were present in the droplet. Subsequently, we added extra IVT mix to the

droplets and observed increase in fluorescence after another 15 minutes (Fig. 4.13B). This result suggested that the first IVT mix in the droplets lost activity within 15 minutes of incubation on the electrodes, but the second IVT mix was able to express RNA before its activity was completely lost, as all the components required for gene expression was present. In another set of experiments, a mixture of the signal and the IVT mix was incubated on the electrode (Fig. 4.13C). The droplet fluorescence increased in the first 15 minutes, and stopped increasing afterwards. This supported our hypothesis that the IVT mix lost activity on the electrodes in 15 minutes.

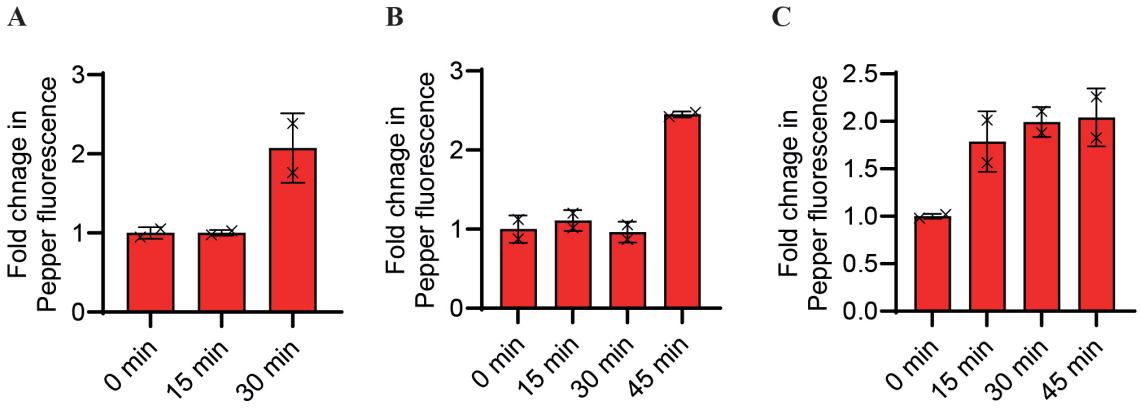


Figure 4.13: Bar graphs of fold change in the fluorescence of the Pepper aptamer in droplets incubated on Ag/AgCl electrodes over time, compared to the sample fluorescence at 0 min. (A) Droplet with the signal only was incubated on the electrode for 15 minutes, the IVT mix was then added, and the droplet was further incubated for another 15 minutes. (B) Droplet with the IVT mix was incubated on the electrodes for 15 minutes, the signal was then added, and the droplet was further incubated for another 15 minutes, before more IVT mix was added, and the droplet was incubated for a further 15 minutes. (C) Droplet with both the signal and the IVT mix was incubated on the electrode and imaged periodically.

To rule out that the lipid-in-oil solution was degrading the IVT mix, similar experiments were repeated in a lipid-in-oil solution without the electrodes. In the first set of experiments, the signal was incubated in the lipid-in-oil solution for 15 minutes, prior to adding IVT mix to the droplet. Increase in fluorescence was observed 15 minutes after adding the IVT mix to the droplet (Fig. 4.14A). In the second set of experiments, the IVT mix was incubated in the lipid-in-oil solution for 15 minutes, prior to adding the signal to the droplet. Unlike the previous example where the droplets were incubated on the electrodes, increase in fluorescence was observed 15 minutes after adding the signal to the droplet. In the third set of

experiments, a mixture of the signal and the IVT mix was incubated in the lipid-in-oil solution. Increase in fluorescence was observed even after 30 minutes in the oil solution (Fig. 4.14B), and the fluorescence increase was a lot higher (around 6 fold) compared to the same sample incubated on the electrodes (around 2 fold). In the final set of experiments, the signal and the IVT mix were incubated in separate droplet in the lipid-in-oil solution for 15 minutes, before the two droplets were fused to initiate the IVT reaction. Increase in fluorescence was observed 15 minutes after fusing the two droplets (Fig. 4.14C).

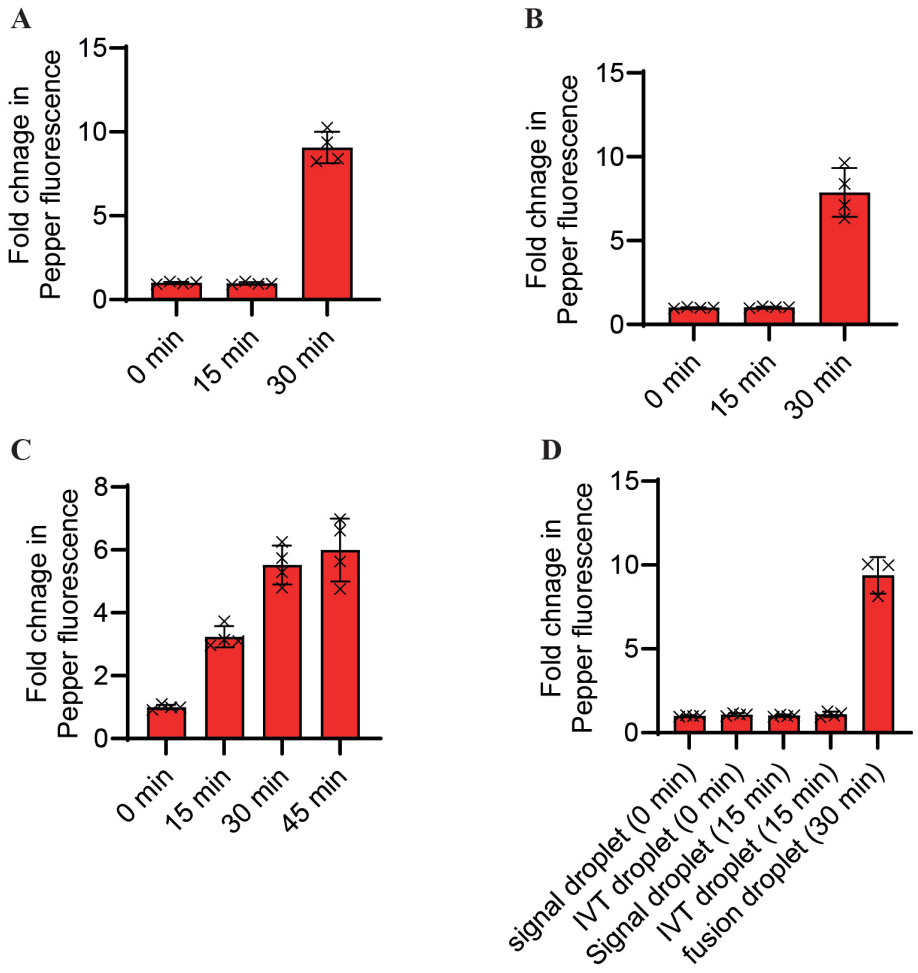


Figure 4.14: Bar graphs of fold change in the fluorescence of the Pepper aptamer in droplets incubated in lipid-in-oil solution, compared to the sample fluorescence at 0 min. (A) Droplets with the signal only was incubated for 15 minutes, the IVT mix was then added, and the droplets were further incubated for another 15 minutes. (B) Droplets with the IVT mix were incubated for 15 minutes, the signal was then added, and the droplets was further incubated for another 15 minutes. (C) Droplets with both the signal and the IVT mix were incubated. (D) Droplets with the signal and droplets with the IVT mix were separately incubated in the lipid-in-oil solution for 15 minutes, before the two droplets were fused together and incubated.

To investigate which component in the IVT mix degraded on the electrodes, the signal and the IVT mix (without the T7 polymerase) were mixed, and added to the electrode to form droplets. The droplets were incubated for 15 minutes, with no increase in fluorescence. Addition of T7 RNA polymerase to the droplets led to an increase in fluorescence after an additional 15 minutes incubation (Fig. 4.15A). In another set of experiments, we first added the solution containing only T7 RNA polymerase to the electrodes to form droplets, and the droplets were incubated for 15 minutes, during which there was no increase in droplet fluorescence. A mixture of the signal and the IVT mix (without the T7 polymerase) was then added to the droplets on the electrode. There was no increase in fluorescence after another 15 minutes of incubation. Following that, additional T7 RNA polymerase was added to the droplets, and an increase in fluorescence was observed after another 15 minutes of incubation (Fig. 4.15B). The two results combined indicated that the T7 RNAP was the component that lost activity when in contact with the electrodes, while the other components remained active. We finally tested if pretreatment of the electrode with BSA could prevent degradation of the IVT mix on the electrodes, as BSA was commonly used to prevent non-specific binding interactions (*122*), unfortunately the prevention did not prevent activity loss of the T7 RNA polymerase (Fig. 4.15C).

It was not known how the polymerase lost activity when in contact with the electrodes, since Ag/AgCl electrode had not been used in IVT(T) solution before. It was plausible that ions or nanoparticles leaking out from the electrode degraded the T7 RNA polymerase. For example, silver nanoparticles were known to inhibit enzymes such as ribosome (*123*), so they might have similar impact on the polymerase. It was also plausible that the physical surface of the electrode caused the polymerase to degrade. To continue this study, different combination of polymerases and electrodes could be screened to identify conditions where the polymerases were not degraded by the electrodes.

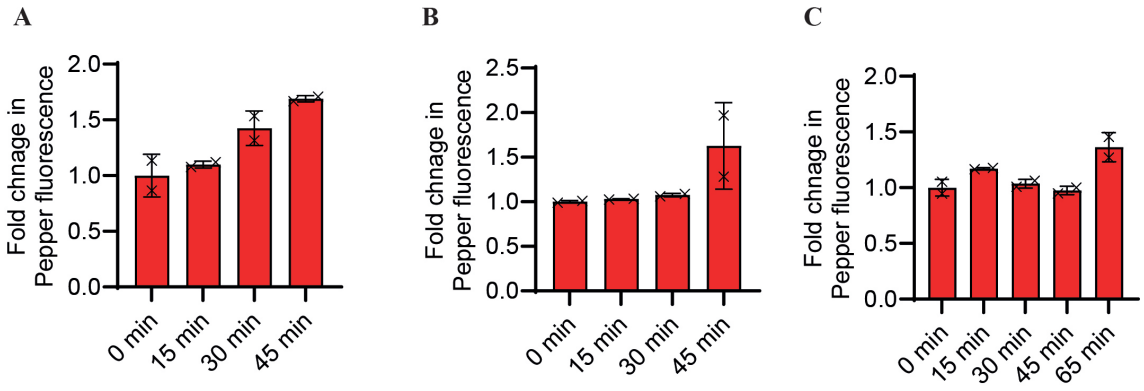


Figure 4.15: Bar graphs of fold change in the fluorescence of the Pepper aptamer in droplets incubated on the Ag/AgCl electrodes over time, compared to the sample fluorescence at 0 min. (A) Droplets with a mixture of the signal and the IVT mix (without T7 RNA polymerase) were incubated on the electrode for 15 minutes, the T7 RNA polymerase was then added, and the droplets were further incubated for another 15 minutes. (B) Droplets with the signal and the IVT mix (without T7 RNA polymerase) were incubated on the electrodes for 15 minutes, the T7 RNA polymerase was then added, and the droplets were further incubated for another 15 minutes, before more T7 RNA polymerase was added, and the droplet were incubated for a further 15 minutes. (C) Droplets with both the signal and the IVT mix were incubated on the electrodes and imaged periodically. The electrodes were pretreated with BSA solution.

4.5 Selective signalling by covalent chemistry

We designed a system where different types of signals could translocate through different types of protein pores, therefore activating gene production in different receiver droplets. This could potentially be achieved by the use of dynamic covalent chemistry to control entry of the DNA across protein pores on lipid bilayers, such that matching pairs of the signal and protein pores were required for signal entry.

We designed pairs of a signal precursor and a membrane-embedded nanoreactor—a signal processor—for selective transmembrane signalling. The signal precursor had a protein stopper linked to the signal via a reactive recognition site (Fig. 4.16A). The signal processor was an engineered protein nanopore with a catalytic site which could react with the recognition site on the signal precursor, only when the two were in close proximity.

The signal precursor would enter the signal processors on bilayers when a membrane potential was applied, but unprocessed signal precursors were not able to translocate freely across the signal processors on the bilayer, unless the recognition

site on the signal precursor and the catalytic site on the signal processor were in close proximity, which would allow the catalytic site to react with the recognition site to release the signal (Fig. 4.16B).

Different signal precursors could be designed by changing the linker length between the stopper and the recognition site, such that the position where the recognition site was positioned relative to the signal processor would vary as the membrane potential was applied to the signal precursor. Different signal processors could be designed by changing the position of the catalytic site. As a result, orthogonal pairs of signal precursor and signal processors could be designed, where each type of signal precursors could only be processed by specific type of signal processors, since the reaction to release the signal could only occur if the recognition site on the precursor and the catalytic site on the processor were in close proximity (Fig. 4.16C).

The signal precursors could be placed in the signal droplet in the lipid-in-oil solution, and the signal droplet was separated from the receiver droplet by a lipid bilayer. The receiver droplet had defective genes and IVT(T) mix for gene expression. The signal processors would be on the bilayer. An applied membrane potential would allow the signal precursors to enter the signal processors on the bilayer, and the signal precursors would be processed to release the signal if the signal precursor and processors pair matched with each other. The released signal would complement defective genes in the receiver droplet, thereby activating gene expression to produce RNA (and proteins) (Fig. 4.16D).

While different types of channel protein pores could theoretically be used to build this selective signalling platform (*114*), we chose to engineer our transmembrane signalling platform based on chemistry of α-hemolysin because this protein was extensively modified and investigated in our research group. α-hemolysin was a heptameric bacterial transmembrane protein first identified from Strepylococcus aureus. It spanned the membrane by forming β-barrel and had a rigid structure. Its rigid structure and low intrinsic noise allowed the pore to be modified to study chemical reactions or translocation of polymers. The different types of covalent chemistry studied in the αHL nanoreactor included boronic acid binding to monosaccharides (*124*),

cycloaddition reactions (*125*, *126*), oxime formation (*127*), S-Nitrosothiol chemistry (*128*), thiol-arsenic chemistry (*129*), Poly(disulfide)s oligomerization (*130*) and thiol-disulphite interchange reaction (*131*).

It followed that many different types of chemistry could be used for signal release. For example, the recognition site could be a peptide/thioester, and the catalytic site could have a catalytic triad to hydrolyse the peptide/thioester. Nevertheless, we would specifically use signal precursors with biotin—straptavidin binding motif at the terminus of a peptide segment, which was conjugated to a DNA oligonucleotide by strain-promoted azide-alkyne cycloaddition, and consisted of a disulfide bond which could be broken by cysteine residues in the pore. The disulfide was installed between the peptide and the oligonucleotide with the sulfur atom Sα proximal to the peptide carrier and the sulfur atom Sβ proximal to the DNA signal (Fig. 4.16E). The processor was an engineered αHL containing cysteine residues that could release the signal by thiol-disulfide interchange reaction. By varying the length of the peptide segment, the disulfide substrate could react site-selectively with different α-hemolysin cysteine mutants. For example, as the straptavidin prevented the substrate from translocating through the nanopore, shorter peptide linkers would allow the disulfide to react selectively with the α-hemolysin mutants with cysteine residues closer to the entrance of the pore, whereas longer peptide linker would allow the disulfide to react selectively with α-hemolysin mutants with cysteine residues further from the entrance of the pore. We chose those components to build our signalling platform among other possible chemistry in αHL pores, because macromolecule immobilization in αHL pores were commonly used in our group, firstly to immobilze oligonucleotides in the pore for nucleic sensing applications (*132*), and later used to characterize selective thiol-disulphide interchange reaction within αHL channel protein nanoreactors on a single-molecule level (*133*). An applied potential across the bilayer caused the signal precursor to enter the nanorector from the signal droplet. The signal precursor was processed by breaking the disulphide bond on the precursor, and the released signal entered the receiver droplet to activate gene production, thereby converting a chemical signal input into different outputs within

receiver cells.

We envisioned that even if it was difficult to use the released signal to activate transcription and translation reaction due to reasons discussed in the previous section, it might still be possible to use the released signal to trigger other types of response in the receiver droplets, for example, by interaction with a molecular beacon to displace a fluorescence quencher from a fluorophore with DNA strand-displacement reaction, thereby activating fluorescence in the receiver droplet (Fig. 4.17).

The catalytic signal processing cycle of the signal processor consisted of four steps. In the first step, the signal entered the signal precursor due to the membrane potential on the bilayer. In the second step, a cysteine residue in the catalytic site of the signal processor attacked the disulphide in the recognition site of the signal precursor. As there were two sulphur atoms and two possible attack locations on the disulphite, the attack would either release the signal, or the linker and stopper, from the signal processor. The released signal would translocate across the pore due to the applied potential, while the linker and stopper were uncharged and could diffuse freely out of the signal processor from the signal entry side. In the third step, another cysteine in the recognition site would attack the newly formed disulphide, releasing the remainder of the signal precursor. This regenerated the unoccupied signal processor, with a newly formed disulphide bond in the signal processor. In the last step, the oxidized pore was reduced by DTT in the solution, thereby regenerating the reduced pore that could be used in subsequent cycles (Fig. 4.19A).

We synthesized the signal precursor carrying the DNA signal (s12), and the signal precursor before straptavidin binding was characterized by LC-MS (Fig. 4.18, A to B).

The rate of each step in the catalytic signal processing cycle could be determined from monitoring the current flowing through the signal processor. An ionic current flowed through the signal processor when the membrane potential was applied across the pore. The current was reduced when the pore lumen was blocked. The beginning of the trace showed the open pore current of the signal processor when the pore

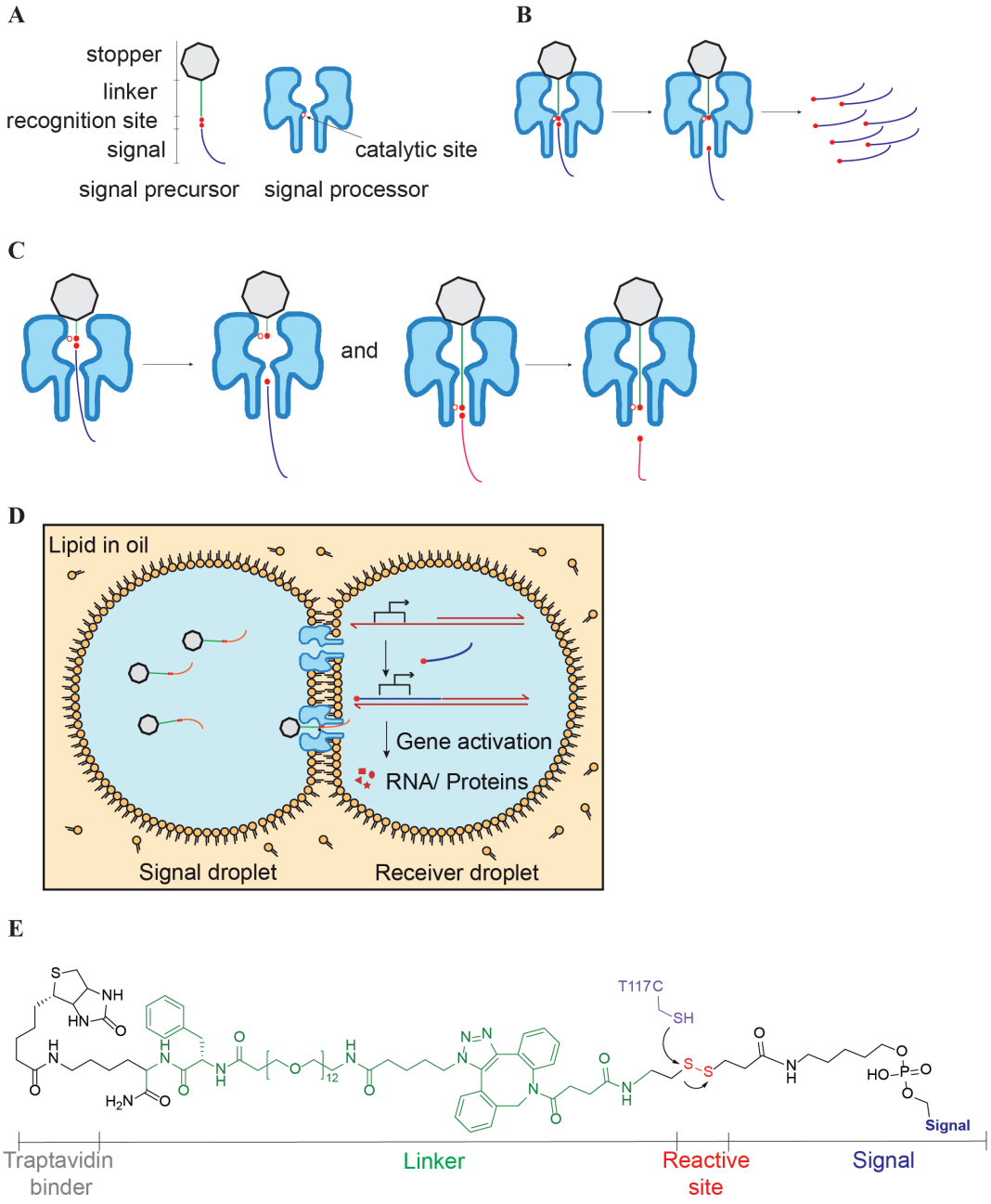


Figure 4.16: Schematics of selective ssDNA signal entry using dynamic covalent chemistry. (A) A schematic of the signal precursor and the signal processor. The signal precursor was covalently attached to a bulky stopper which prevented it from translocating freely across the channel protein pores in bilayer. (B) The signal processor had a catalytic site that could react with the recognition site on the signal precursor, thereby allowing signal translocation across bilayers. (C) Orthogonal pairs of the signal precursor and the signal processors could be designed, by varying the linker length on the precursor and the position of catalytic site on the processor. The length of the linker and position of catalytic site determined if the recognition site on the precursor could reach and react with the catalytic site on the processor. (D) The released signal could selectively activate transcription in the receiver droplet by complementing the defective genes.(E) A chemdraw diagram of the signal precursor, which consisted of a straptavidin-binding biotin moiety, a PEG linker, the disulphite recognition site, and the ssDNA signal.

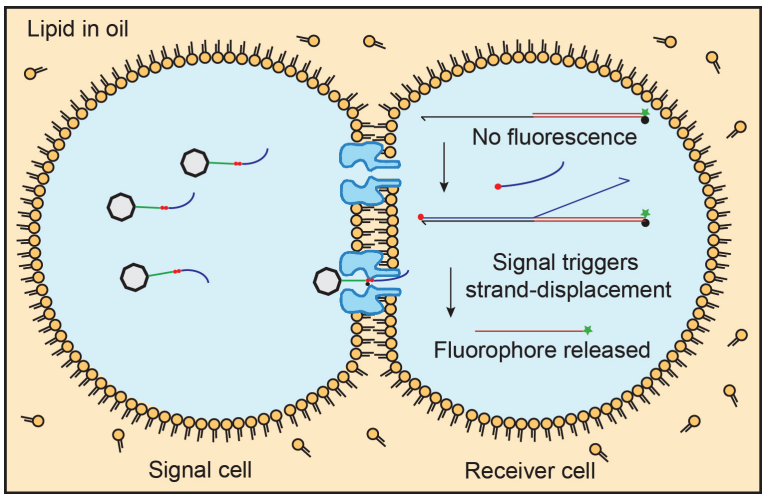


Figure 4.17: A schematic of selective signal entry across droplet interface bilayers using dynamic covalent chemistry. The released signal activated receiver cell fluorescence by DNA strand displacement reaction of a molecular beacon.

lumen was empty. (i) Signal precursor entered the pore, blocking the pore and led to a decrease in current. (ii) The signal was released from the pore, which reduced the degree of pore blockade and slightly increased the current through the pore. (iii) The rest of the signal precursor was released from the pore, the current through the pore returned to the open pore level. Please note that we were not able to identify the oxidized form of the unoccupied signal processor from the reduced form of the unoccupied signal processor from the current trace. This step was assumed to be quick as the DTT concentration was high in the recording chamber (5 mM) (Fig. 4.19B).

The signal processing rate was previously reported at pH 8.5, which was different from the pH used in IVTT (IVTT mix had pH 7.4). We therefore investigated the kinetics of the signal processing cycle at on a single-molecule level using the new conditions, and found that each protein pore can process signal at a rate of 1.5 s^{-1} per channel at 120 mV, which was 1000 times slower than the rate of unbound ssDNA translocation through 111N/113R protein pores, as discussed in previous chapter (Fig. 4.19C). Therefore, to activate responses in receiver droplets with processed signals, the signal processing rate had to be increased by many folds, or alternatively the receiver droplets had to be optimized so they would respond to an even lower signal concentrations.

The signal processing rate was expected to increase by changing the reaction

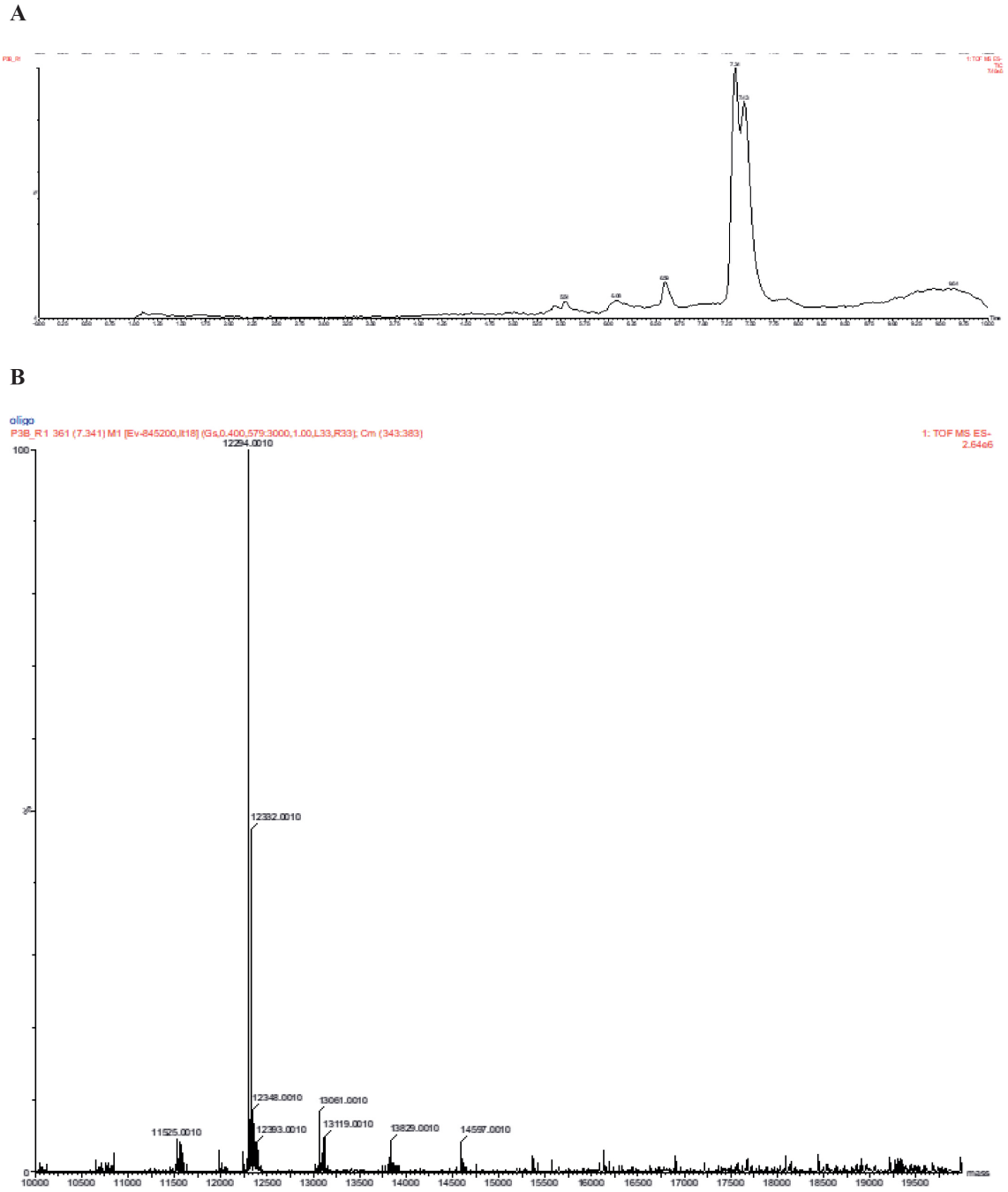


Figure 4.18: LC-MS characterization of the peptide DNA conjugate. (A) Chromatogram of the sample. (B) Mass deconvolution spectra of the sample. Calculated mass: 12293 Da, observed mass: 12294 Da.

conditions. The rate of the first step, signal entry step, was expected to increase by increasing the membrane potential and the signal concentration, and by additional mutations in the pore (such as E113N/N113R as described previously). The rate of the second step, signal release, was expected to increase with the number of cysteine residues in the pore. As αHL was a heptameric pore, it was possible to install multiple cysteine residues proximal to the disulphide bonds of the unprocessed DNA signal. The rate of the third step, linker release, the nucleophilic attack on the signal-pore complex by another cysteine residue in the pore, was the slowest step in the signal processing cycle. The rate could also potentially be increased by engineering more cysteine residues near the catalytic site, or by screening different combination of signal precursor and signal processor αHL mutants to increase the rate.

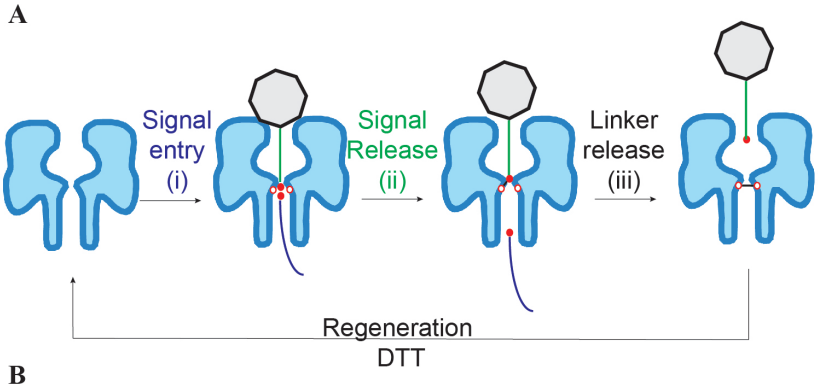
4.5.1 Increasing the number of pores on the membrane

One could imagine that another method to increase the signal translocation rate across the bilayer was to increase the number of pores on the bilayer. However, We noted from several experiments that the conductance of the setup with hemolysin pores on the scale of $10^4 - 10^5$ within an intact bilayer was comparable the conductance when the bilayer was ruptured. To illustrate what this meant for our experiments, we could represent the setup as two electrical components in series. The first component was the membrane with conductance G_M and resistance R_M. Denoting the conductance per pore as G_p, with n as the number of pores, it followed that:

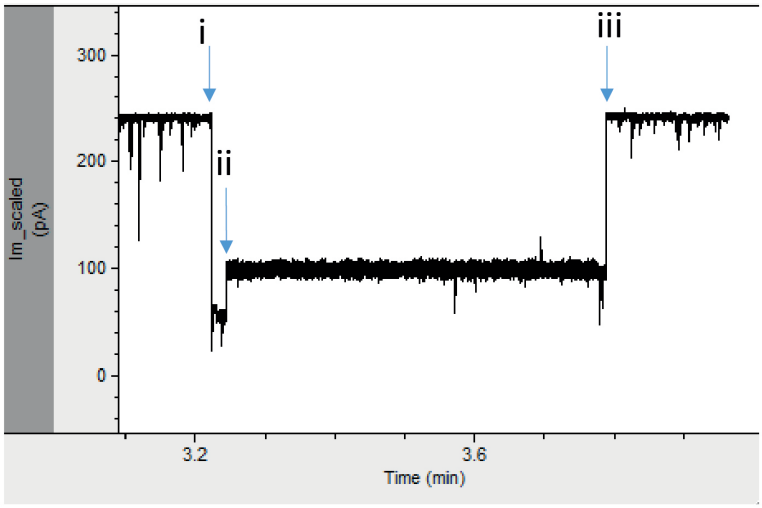
$$G_M = n\, G_p$$

The droplets contained NaCl and/or monopotassium glutamate (MPG). The main buffer in PurExpress was MKG, while the storage buffer of αHL contained NaCl. Denoting the single channel conductance per molar MPG and NaCl as G_{MPG} and G_{NaCl} respectively, assuming that the two salts did not interfere with each other, we could estimate the pore conductance as:

A



B



C

Applied potential	Mean waiting time of each step ± S.D.			
	Signal entry (A)/ s	Signal/linker release (B)/ s	Linker/signal release (C) / s	Complete cycle / s
150 mV	8.0 ± 1.3	0.943 ± 0.055	35.8 ± 6.0	46 ± 7.4 *s*
120 mV	55 ± 10	4.26 ± 0.77	29.5 ± 5.0	87 ± 16 *s*
100 mV	113 ± 19	0.82 ± 0.14	14.4 ± 2.5	130 ± 22 *s*

Figure 4.19: The catalytic signal processing cycle of the signal processor. (A) A schematic of the catalytic cycle of the signal processor. (i) The signal precursor entered the signal processor. (ii) The signal was released. (iii) The linker and stopper were released from the pore. DTT then reduced the disulphide bond between the two cysteine residues in the signal processor. Alternatively, the linker and stopper could be released first, followed by the signal (not shown). (B) A representative current recording of the signal processing cycle. The beginning of the trace showed the open pore current of the signal processor when the pore lumen was empty. (i) The signal precursor entered the pore (ii) The signal was released from the pore. (iii) The rest of the signal precursor was released from the pore.(C) A table of the average waiting time in each step in the signal processing cycle at different membrane potentials. The average waiting time was calculated from more than 30 events.

$$G_p = G_{MPG}\,[MPG] + G_{NaCl}\,[NaCl]$$

We note that single channel conductance per molar KCl and NaCl are approximately identical and was around 1 nS (*110*).

From measurement of more than 100 single chnanels, we obtained:

$$G_{MPG} = 0.22 \pm 0.06\,nS$$

Apart from the membrane, the rest of the setup had conductance G_{bg} and resistance R_{bg}. The background conductance/resistance included that of the electrodes, the agarose coating on the electrode, and the buffer in the droplet.

Without a bilayer (i.e. when two electrodes were inside a single droplet in the lipid-in-oil solution), the whole setup would have a total conductance G_{bg} and resistance R_{bg}.

When a bilayer was present between the two electrodes, the whole setup would have a total conductance G_T and resistance R_T.

$$G_T = \frac{(G_{bg}\,G_m)}{(G_{bg} + G_m\,)}$$

$$R_T = R_{bg} + R_m$$

An input voltage V was applied across the setup from the headstage. The conductance could be obtained by plotting the current against the applied potential.

When the bilayer was present, the input voltage (V) was distributed between the background (electrodes/agarose/buffer) (V_{bg}) and the membrane (V_m).

$$V = V_{bg} + V_m$$

The potential across the bilayer (V_m) could be expressed in terms of the input voltage (V), the conductance of the system when the bilayer was broken (G_{bg}), and

the total conductance of the system with an intact bilayer (G_T).

$$G_T = \frac{G_{bg}\, G_m}{G_{bg} + G_m}$$

Rearranging the equation gave;

$$V_m = \frac{G_T}{G_m} V = \frac{1 - G_T}{G_{bg}} V$$

Or, in terms of the resistance,

$$V_m = V \frac{R_m}{R_T} = V \frac{1 - R_{bg}}{R_T}$$

If $\frac{G_T}{G_{bg}} = 0.9$, then $\frac{V_m}{V} = 0.1$. This meant that when 100 mV was applied across the entire setup, only 10 mV would be applied to the membrane.

In scenarios where $G_{bg} \gg G_m$, such as when the number of protein pores were low, it followed that $G_T = G_m = n\, G_p$, where $\mathrm{G_T}$ was the total conductance and $\mathrm{G_p}$ was the conductance per pore.

However, when $\mathrm{G_e}$ and $\mathrm{G_m}$ were comparable, $R_T = R_m + R_{bg}$. Since $R_m = \frac{R_p}{n}$, where R_p was the resistance per pore, rearranging the equation led to:

$$n = \frac{R_p}{R_T - R_{bg}}$$

Or, in terms of the conductance:

$$n = \frac{1}{G_p \left(\frac{1}{G_T} - \frac{1}{G_E} \right)} = \frac{G_T\, G_e}{G_p (G_e - G_T)}$$

We evaluated the source of the background resistance in the system, as identifying the source of resistance might provide solution to minimize the resistance.

The resistance of the metal wires were directly measured with a multimeter and were less than 1 Ω, in other words, the conductance of the wires were larger than 1 S. Therefore, the metal wires had a negligible contribution to the background conductance, which was typically in the range of 1-10 µS.

Next, we filled a cuvette with 1 M potassium glutamate solution, and measured the total conductance of Ag/AgCl electrodes in the solution, while varying the distance between the electrodes and the length of electrodes immersed in the solution (Fig. 4.20, A to C). The electrodes with the agarose coating (Fig. 4.20A) gave much higher conductance than the electrodes without the agarose coating (Fig. 4.20B). The conductance increased when the length of the wires immersed in the solution increased. On the other hand, the distance between the electrodes did not have an obvious impact on the conductance. The experiment suggested that the electrochemical redox reaction on the electrode surface was the main source of background resistance in the system.

Finally, we evaluated the total conductance when both Ag/AgCl electrodes were in the same aqueous droplet in a lipid-in-oil solution. The background conductance was higher in a KCl solution than a MKG solution, and the conductance also increased with the concentration of the salt solution (Fig. 4.20D). We tested both 0.1 mm and 0.05 mm diameter Ag/AgCl wires in 500 mM KCl and 100 mM MKG solution, and there were no significant difference between the conductance of the two types of electrodes in the same solution (Fig. 4.20E).

To conclude, the redox reaction on the electrode was the main contributor to the background conductance. From the derived equations, it was theoretically possible to compensate for the voltage loss due to the background conductance, by applying an even higher voltage across the entire system. This would allow us to maintain a constant potential across the bilayer when the number of pores increased, and that the bilayer conductance was comparable to the background conductance. However, this would only be possible if the background conductance was consistent, and our data showed that the background conductance could vary across different measurements. The number of pores on the bilayer had to be controlled, such that the bilayer conductance remained less than around 20-30 % of the background conductance. Otherwise it would be difficult to control the potential across the bilayer. It is also not known if a potential difference between the electrode surface and the droplet could interfere with the signalling system.

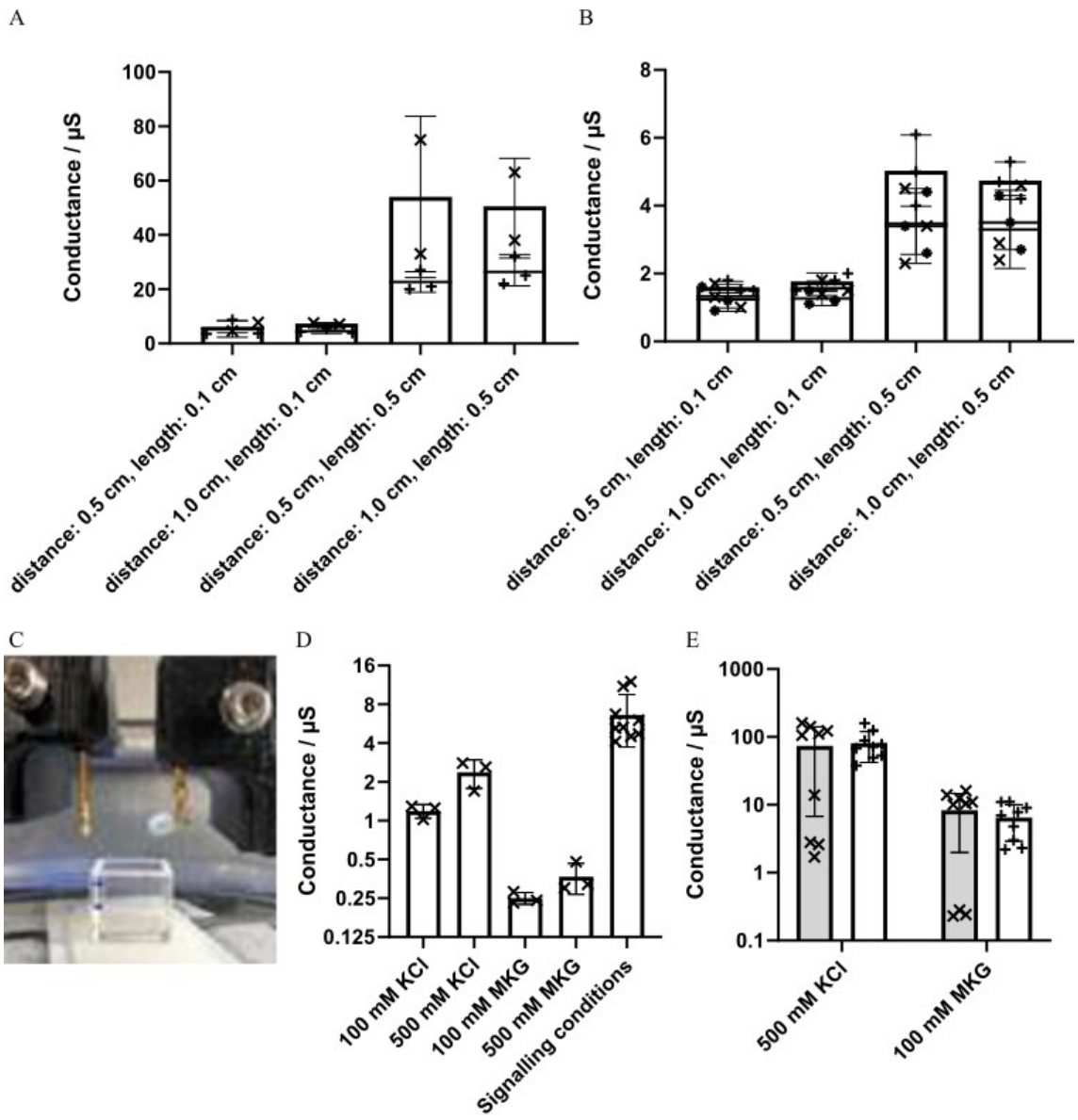


Figure 4.20: (A to C) A bar graph of the total conductance of Ag/AgCl electrodes in 1 M potassium glutamate solution, when the distance between the electrodes and the length of electrodes in the solution were varied. (A) Ag/AgCl electrodes with agarose coating, (B) Ag/AgCl electrodes without agarose coating. (C) Photo of the setup using micromanipulators to control the length of electrodes in the solution, as well as the distance between the electrodes. Measurements from the same pair of electrodes were labelled with the same symbol. (D) A bar graph of the total conductance of Ag/AgCl electrodes inserted into different droplets in the lipid-in-oil solution, when the droplet content was varied. Signalling condition was 0.2 M MKG and 300 mM NaCl. (E) A bar graph of the total conductance of Ag/AgCl electrodes inserted into droplet in a lipid-in-oil solution. Grey bars were measurements with Ag/AgCl electrodes with 0.1 mm diameter, while white bars were measurements with Ag/AgCl electrodes with 0.05 mm diameter. In the bar graph, the heights of the bars are the mean. The error bars show the standard deviation.

Overall, optimization of the signal processing rate and/or detection sensitivity of the processed signal would allow the work on covalent signalling to be continued.

Chapter 5

Conclusions and future directions

5.1 Perspectives

Our work demonstrated the efficient use of ssDNA signals for gene activation in synthetic tissues by complementing genes with a defective promoter. Selective gene activation was achieved by using different promoters or by using inhibitors to remove undesired signals. The DNA signal was further split in halves to construct complex logic gates (AND-OR-AND-OR-AND gates) controlling gene activation. ssDNA signal activated production of multiple RNA, proteins, and functional enzymes. Furthermore, we controlled signal entry between droplets in droplet networks by selectively disrupting the bilayer or applying a membrane potential to deliver signal across mutated αHL pores in the bilayer (Fig. 5.1).

The use of ssDNA as a signalling molecule was desirable compared to other types of signals, since DNA sequences were highly programmable, and we showed that as few as 50 pM of ssDNA signal was sufficient for gene activation, in comparison to small molecules activators where typically µM to mM range of signal concentration was required (*3*). In addition, ssDNA had lower cost, longer shelf life and higher stability compared to other types of signals (e.g. RNA, small molecules) (*134*, *135*).

Our work also expanded our understanding of T7 and related polymerases, and their applications in synthetic biology. For example, we revealed that T7 promoter cannot tolerate strand breaks on the coding strand from -12 to -9 of the transcription start site. It remained unknown whether strand breaks were tolerated at other

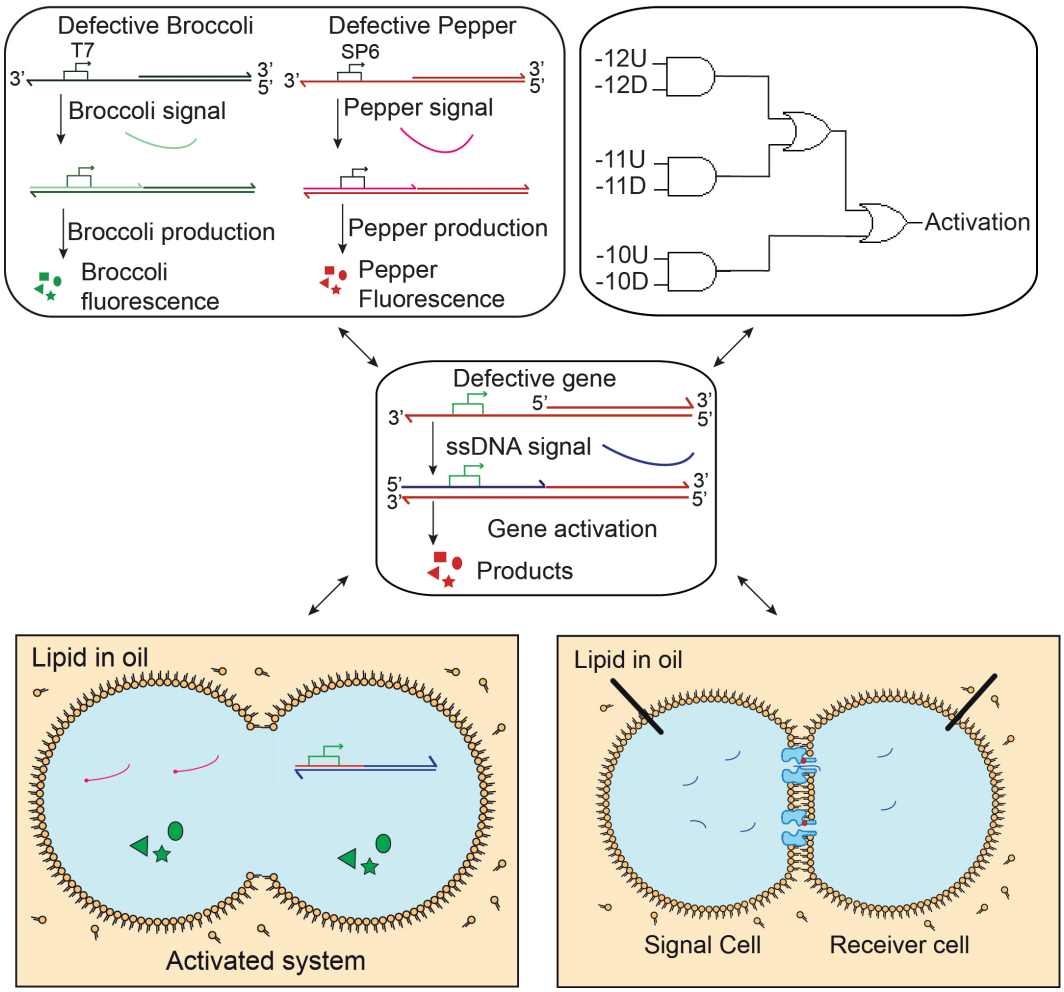


Figure 5.1: An illustration showing the main highlights in this thesis. ssDNA signal was used to activate gene production by complementing genes with a defective promoter (center). We demonstrated that ssDNA signals could selectively activate the defective genes (top left), and could be used to construct complex logic gates (top right). Furthermore, we demonstrated the control of the signal entry between droplets in droplet networks by selectively disrupting the bilayer (bottom left) or applying a membrane potential to deliver the signal across channel protein pores in the bilayer (bottom right).

locations on the promoter. We were also the first to demonstrate the combined use of RNA polymerase and DNA ligase in vitro, creating 3 orthogonal AND gates by splitting the ssDNA signal at different positions. It was plausible that even more orthogonal AND gates could be constructed by splitting the signal at other positions, and that the signal could be split in more than two halves.

We showed that the DNA signal and the defective genes could be separated by lipid bilayers in different droplet network compartments, and the defective genes could be activated by disrupting the bilayer. While we chose to disrupt the bilayer by perfusing the oil, lipid bilayers could be made sensitive to other environmental

stimuli, including temperature, light, redox states, and enzymes (reviewed in ((*4*))). In scenarios where preservation of membrane integrity was desired, we also demonstrated the use of membrane potential to deliver DNA signal across protein pores embedded in the bilayer. The membrane potential in this work was maintained by electrodes in synthetic cells, but it could also be generated by light-responsive proton pumps, asymmetric lipids, or by living cells (*38*, *136*). Droplet networks could be transferred from the lipid-in-oil environment to an aqueous environment, which would enable direct chemical communication between synthetic tissues and the aqueous surrounding (*84*).

Ultimately, our work lays the groundwork engineering multifunctional systems, where different set of genes would be activated in response to multiple triggers in the environment. While the stimuli could include changes in the chemistry of the external environment and changes in the membrane potential, as demonstrated in this thesis, other forms of stimuli, such as light, temperature and magnetism, can also be engineered to activate the droplet networks. Each droplet in the network could respond different from the stimuli, and the coordinated collective response of the droplets produces a desired functional output. We envisioned this would be useful in biotechnology and medicine, where precise control of droplet behaviors in presence of different stimuli was desired (Fig. 5.2).

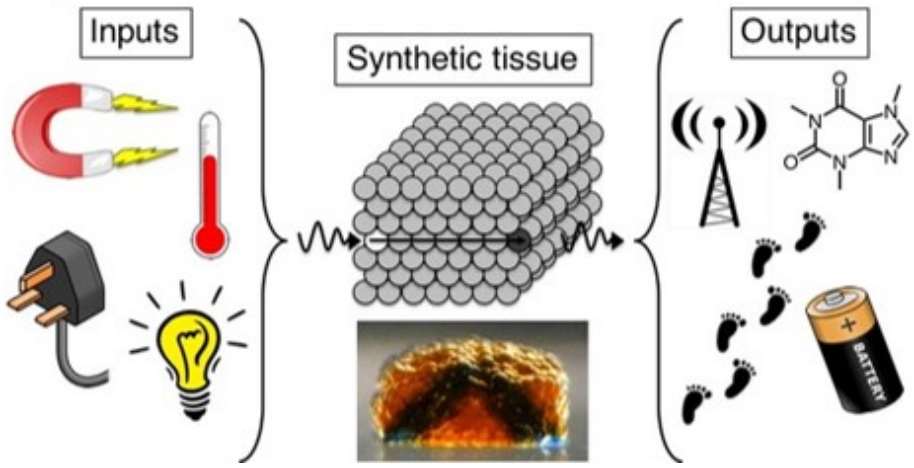


Figure 5.2: The future development of complex droplet networks. Each droplet would respond differently in the presence of multiple stimuli, such that the droplet network would produce a collective response towards the stimuli. The stimuli could include electrical forces, mechanical forces, light, temperature, or magnetism. The output included signalling, production of proteins/small molecules, battery power, movement, and could potentially control and interface with living cells. Figure reproduced from (*79*).

5.2 Future directions

We already discussed several potential directions that could branch out from the findings of this research, for applications in basic and synthetic biology. For example, in section 2.10 we discussed further investigating the effects of signal length on RNA yield. We also discussed probing tolerance of T7 promoter to single-strand breaks at other locations to construct additional AND gates. We also discussed expanding repertoire of orthogonal RNA aptamer - fluorophore dye pairs for signalling and other synthetic biology applications. We also discussed alternate experiments to use of the ssDNA signal as a transcription factor mimic to activate multiple genes, such as using the ssDNA signal to express split proteins, and to recreate the E.coli *lac* operon. We also discussed the potential loss of activity of in vitro transcription (and translation) mix in aqueous emulsions in lipid-in-oil solution, which mechanism remained unknown and needed to be investigated. In section 3.4 we discussed fabrication of next generation hydrogel structures with residual compartmentalization embedded in the structures using agarose beads.

In the previous chapter, we presented several preliminary work extending the gene activation system so that the activation becomes temperature-dependent 4.2.

We explored interfacing our system with biological cells 4.3. We discussed progress and challenges using membrane potential to control ssDNA movement across droplets with IVT(T) mix 4.4, and to use covalent chemistry to control DNA movement across bilayers 4.5.

In the following section, we propose a study of the kinetics and thermodynamics of the system presented in this study.

5.3 Kinetics and thermodynamics characterization of the system

When the DNA signal was used to produce fluorescent RNA aptamers, multiple processes contributed to the observed aptamer fluorescence, the kinetics and thermodynamics of each step remained to be investigated and quantified.

The first step in the gene activation process was the binding of the DNA signal or DNA signal fragments to the defective gene. The concentration and temperature dependence of this binding can be investigated by UV-vis spectrophotometry (*137*). In some experiments, this step was possibly followed by a strand displacement reaction or ligase repair, the process of which could be monitored by gel electrophoresis, as described in earlier chapters.

Next, the T7 RNAP was bound to the promoter complex and initiate transcription, the total concentration of RNA synthesized over time could be studied by qPCR or again by gel electrophoresis, gel electrophoresis could also confirm whether the full-length RNA transcript was the predominant product in the transcription reaction. Aside from synthesis of the full-length RNA transcript, other processes such as abortive initiation, background hydrolysis of NTP, and degradation of T7 RNAP had been reported to occur over time in the IVT reaction (*138*).

Thirdly, the correctly transcribed aptamer had to fold correctly to bind successfully to the small molecule dye. The aptamer-dye binding is a bimolecular process that depends on the binding equilibrium constant between the aptamer and the fluorophore, and could be affected by temperature, as well as ion concentrations,

especially potassium and magnesium, in the reaction mixture. The small-molecule dye fluorescences in the presence of an excitation light. The dye would have different quantum yield and brightness in the bound and unbound form (*68*). There is also the possibility of self-quenching if the concentration of bound fluorophore was too high.

When the DNA signal was used to produce fluorescence proteins, the observed fluorescence of the IVTT mixture was further affected by the rate of protein translation and protein maturation. the transcribed RNA was further translated into proteins. The total concentration of proteins can be estimated by using radioactive amino acids to label the protein, or by other methods such as ELISA and western blot (*139*). The protein has to undergo maturation to become fluorescent, which is a first-order process. Similar to bound aptamers, each fluorescent protein has different quantum yield and brightness.

When the DNA signal was used to produce αHL that inserted into the bilayers to facilitate dye transfer across the bilayer, the rate of dye transfer increased with the number of αHL on the bilayer. The number of αHL pores on the bilayer was expected to increase overtime as more αHL monomers were produced in the IVTT reaction, and the number of αHL was expected to eventually plateau towards the end of the IVTT reaction when protein production was ceased. However, the protein concentration in the IVTT droplet, as well as the number of channel proteins on the bilayer, was not quantified.

While distinct components of this process, such as DNA binding (*87*, *140*), DNA strand displacement reaction (*141*, *142*), RNA transcription (*138*), aptamer-fluorophore binding, and fluorophore brightness (*68*, *74*), were separately modelled in the past, experimentally verifying the relevant thermodynamic and kinetic parameters, and model our ssDNA signalling system by building on existing models would help us better predict the behaviour of the DNA signalling system, and potentially allow us to improve the signal sensitivity and optimize the product yield. It would be advantageous to continue the study on the kinetics and thermodynamics parameters using a microfluidic flow system, such as one described by the Huck

group (*143*), as such system allowed precise control and variation of concentrations of DNA constructs, transcription components, and translation components, while also providing measurement of the product formation rate in real time.

Chapter 6

Methods and materials

This chapter describes the conditions used in this thesis. Unless otherwise specified, the manufacturer's instructions were followed when commercial kits and columns are used. Unless otherwise specified, experiments were carried out at room temperature (23 ±1 °C).

6.1 Chemical and reagents

6.1.1 Suppliers

All reagents were obtained from Merck unless otherwise specified. mCherry, mNeonGreen, lactase and αHL plasmids were gifts from Michael Booth group. The plasmids have PURExpress control template backbone (*78*). ssDNA shorter than 200 nt were purchased from biomers, Merck and IDT. T7 RNA polymerase, SP6 RNA polymerase, T3 DNA ligase, T4 DNA ligase, Monarch DNA Gel extraction kit, Monarch PCR cleanup kit, Phusion High-Fidelity DNA Polymerase, PURExpress, murine RNase inhibitor were purchased from New England Biolabs. DreamTaq Green PCR Master mix and DreamTaq PCR Master mix was purchased from ThermoFisher. All lipids were purchased from Avanti Polar lipids. DFHBI-1T was purchased from Torcris. HBC620 was purchased from MedChemExpress. TO1B was purchased from Applied Biological Materials. Nuclease-free water was purchased from Ambion. QIAprep Spin Miniprep Kit was purchased from Qiagen. Crimp-terminals were pur-

chased from RS components. GelRed® Nucleic Acid Gel Stain was purchased from Biotium. Bl21(de3)pLysS competent cells and XL 10-Gold ultracompetent cells was purchased from Agilent.

6.1.2 Conditions of enzymes

The supplied conditions of enzymes are important in this work for reasons outlined previous. T3, T7, SP6 RNAP, Murine RNase Inhibitor are purchased from NEB. The enzymes are supplied in the following conditions: T7 RNAP: 50000 units/ mL T7 RNAP, 50 mM Tris-HCl, 100 mM NaCl, 20 mM β-me, 1 mM EDTA, 50 % glycerol, 0.1% (w/v) Triton X-100, pH 7.9 at 25 °C. T3 RNAP: 50000 units/ mL T7 RNAP, 50 mM Tris-HCl, 100 mM NaCl, 20 mM β-me, 1 mM EDTA, 50 % glycerol, 0.1% (w/v) Triton X-100, pH 7.9 at 25 °C SP6 RNAP: 20000 units/mL SP6 RNAP, 50 mM Tris-HCl, 100 mM NaCl, 20 mM β-me, 1 mM EDTA, 50 % glycerol, 0.1% (w/v) Triton X-100, pH 7.9 at 25 °C RNAI: 40000 units/ mL RNAI, 20 mM HEPES-KOH, 50 mM KCl, 8 mM DTT, 50 % glycerol, pH 7.6 at 25 °C T3 DNA ligase: 3,000,000 units/mL T3 DNA ligase, 10 mM Tris-HCl, 50 mM KCl, 0.1 mM EDTA, 1 mM DTT, 50 % glycerol, pH 7.4 at 25 °C T4 DNA ligase: 400,000 units/mL T4 DNA ligase, 10 mM Tris-HCl, 50 mM KCl, 0.1 mM EDTA, 1 mM DTT, 50 % glycerol, pH 7.4 at 25 °C Salt-T4 DNA ligase: 400,000 units/mL Salt-T4 DNA ligase, 10 mM Tris-HCl, 50 mM KCl, 0.1 mM EDTA, 1 mM DTT, 50 % glycerol, pH 7.4 at 25 °C

6.1.3 Activity of enzyme and enzyme inhibitors

NEB definitions are used for protein activity. For T3, T7 and SP6 RNAP, one unit is the amount of enzyme that incorporates 1 nmol ATP into acid-insoluble material in a total reaction volume of 50 µL in 1 hour at 37 °C. For RNAI, one unit is the amount of Murine RNase Inhibitor required to inhibit the activity of 5 ng of RNase A by 50 %. RNase A activity is measured with hydrolysis of cytidine 2',3'-cyclic monophosphate. For T3 DNA ligase, one unit is the amount of enzyme required to give 50 % ligation of 100 ng HindIII fragments of λ DNA in a total reaction volume

of 20 µL in 1 minute at 25 °C. For T4 DNA ligase, one unit is the amount of enzyme required to give 50 % ligation of 300 µg/mL HindIII segments of λ DNA in a total reaction volume of 20 µL in 30 minutes at 16 °C. For salt-T4 DNA ligase, one unit is the amount of enzyme required to give 50 % ligation of 6 µg of Lambda-HindIII DNA in a total reaction volume of 20 µL in 30 minutes at 25 °C.

6.1.4 Components of the PURE system

The detailed components of the PURE system is as follows: Solution A: 0.2 mM each 20 amino acids, 108 OD_{260} mL^{-1} E. Coli tRNA mixtures, 4 mM ATP, 4 mM GTP, 2 mM CTP, 2 mM UTP, 40 mM creatine phosphate, 20 mg mL^{-1} formyl donor, 100 mM HEPES-KOH, pH 7.6, 200 mM potassium glutamate, 26 mM magnesium acetate, 4 mM spermidine, 2 mM DTT. Solution B: Solution B contains 690 mg mL^{-1} alanyltRNA synthetase, 20 mg mL^{-1} arginyl-tRNA synthetase, 220 mg mL^{-1} asparaginyl-tRNA synthetase, 80 mg mL^{-1} aspartate-tRNA synthetase, 12 mg mL^{-1} cysteinyl-tRNA synthetase, 38 mg mL^{-1} glutaminyl-tRNA synthetase, 126 mg mL^{-1} glutamyltRNA synthetase, 96 mg mL^{-1} glycyl-tRNA synthetase, 8 mg/ mL histidyl-tRNA synthetase, 400 mg mL^{-1} isoleucyl-tRNA synthetase, 40 mg mL^{-1} leucyl-tRNA synthetase, 64 lysyl-tRNA synthetase, 21 mg mL^{-1} methionyl-tRNA synthetase, 170 mg mL^{-1} phenylalanyl-tRNA synthetase, 100 mg mL^{-1} prolyl-tRNA synthetase, 19 mg mL^{-1} seryl-tRNA synthetase, 63 mg mL^{-1} threonyl-tRNA synthetase, 11 mg mL^{-1} tryptophanyl-tRNA synthetase, 6 mg mL^{-1} tyrosyl-tRNA synthetase, 18 mg mL^{-1} valyl-tRNA synthetase, 200 mg mL^{-1} methionyl-tRNA formyltransferase, 100 mg mL^{-1} initiation factor 1, 400 mg mL^{-1} initiation factor 2, 100 mg mL^{-1} initiation factor 3, 500 mg mL^{-1} elongation factor G, 1,000 mg mL^{-1} elongation factor Tu, 500 mg mL^{-1} elongation factor Ts, 100 mg mL^{-1} release factor 1 , 100 mg mL^{-1} release factor 3, 100 mg mL^{-1} ribosome recycling factor, 40 mg mL^{-1} creatine kinase, 30 mg mL^{-1} myokinase, 11 mg mL^{-1} nucleotide diphosphate kinase, 10 mg mL^{-1} pyrophosphatase, T7 RNAP, and 12 mM ribosome (*76*, *78*).

6.2 General Methods

6.2.1 Agarose gel electrophoresis

Agarose gel electrophoresis was used for DNA samples. 1 % agarose gel was used for >200 nt samples. 3 % agarose gel was used for >200 nt samples. The gel was made in TAE and Gel-Red. Home-made gel loading buffer (10 % glycerol, 3.33 mM Tris pH 8.0, 10 mM EDTA, 0.08 % SDS, 0.005 % (w/v) bromophenol blue was used to load DNA samples onto the gel, unless the sample was in DreamTaq Green PCR Master Mix (Thermofisher), which can be loaded directly onto the gel. The gel was run in TAE buffer at 120 V for 70 minutes. The bands were imaged with Gel Doc XR^+ (Bio-Rad) and analysed with Image lab (Bio-Rad).

6.2.2 Nanodrop spectrophotometers

DNA concentration and salt content were analyzed by nanodrop (ND-1000 spectrophotometer, Marshall scientific). Protein concentrations were also determined with the same instrument.

6.2.3 Calculation of DNA melting temperature

DNA melting temperature in PCR reaction mix was calculated with webtools provided by the manufacturers. Melting temperature in IVT and IVTT mix was estimated with Tm for oligos calculator (Promega), using 100 nM primer concentration, 10 mM $MgCl_2$ and 50 mM KCl. 10 mM $MgCl_2$ was chosen as there were 50 mM of $MgCl_2$ and 40 mM of NTP in the transcription mixture, therefore the concentration of free Mg^{2+} was 10 mM.

6.2.4 Fluorescence measurements

Unless otherwise specified, epifluorescence microscopy (Leica DMI 8) was used to determine fluorescence intensity of reaction samples. For samples incubated in bulk solution, 200 nL of the solution was added to a lipid-in-oil solution in a PMMA chamber at the end of the incubation to determine the fluorescence intensity. The

lipid was 1,2-diphytanoyl-sn-glycero-3-phosphocholine (DPhPC) or 1:1 (mass ratio) DPhPC:1-palmitoyl-2-oleoyl-glycero-3-phosphocholine (POPC), and the oil was 1:1 (v/v) hexadecane: silicone oil (AR20). Samples incubated in lipid-in-oil mixture or samples embedded in organogel were directly imaged under the microscope. Fluorescence images were acquired with 10x objective and maximum fluorescent light intensity. Fluorescence intensity was analyed with image J (NIH). The following excitation and emission filters were used:

Setting	Used for	Excitation (nm)	Emission (nm)
GFP	Alexa488, DFHBI-1T, TO1, TO1B, TO3B, HBC530, mNeonGreen, mVenus	450-490	500-550
TXR	TAMRA, mCherry, HBC620	540-580	592-668

Table 6.1: Epifluorescence settings of Leica DMI 8

Fold change and normalized fluorescence intensity

The fold change in fluorescence intensity of a sample compared to the control was calculated as the fluoresence intensity of the sample divided by the mean fluorescence intensity of the controls. Where appropriate, the control conditions used to calculate the fold change are specified in the figure captions.

The normalized fluorescence intensity of a sample was calculated using the following formula:

$$\frac{(I - I_C)}{(I_{max} - I_C)} \times 100$$

where I, I_c, and I_{max} were the fluorescence intensity of the sample, the mean fluorescence intensity of the no signal controls, and the mean fluorescence intensity of the condition with the highest mean fluorescence intensity, respectively. After normalization, the mean of the normalized fluorescence intensity of the condition

with the brightest mean fluorescence intensity would be 100, while the mean of the normalized fluorescence intensity of the controls with no signal would be 0.

6.2.5 Molecular Biology

Plasmid Propagation

XL 10-Gold Ultracompetent cells (10 µL) were thawed on ice for 15 minutes, and incubated with plasmids with ampicillin resistance gene (10 ng) on ice for 10 min. The cells were spread on LB LB-agar plates with ampicillin (100 µg/mL) or carbenicillin (50 µg/mL) for 16 hours at 37 °C. Single colony was picked to grow in LB for 16 hours at 37 °C and the plasmids were extracted with QIAprep Spin Miniprep Kit.

Plasmid mutagenesis

αHL WT/D8H6 plasmid was described previously (*144*). It contained inducible wild-type αHL gene with a D8H6 tag at the C-terminus in a pT7 vector with ampicillin resistance gene. New mutants used in this thesis was constructed from αHL WT/D8H6 plasmid by QuikChange II Site-directed mutagenesis kit (Agilent). Plasmid sequences were confirmed by Sanger sequencing (Source BioScience).

alpha-hemolysin expression and purification

Bl21(de3)pLysS competent cells (10 µL, Agilent) were thawed on ice for 10 minutes, and were then incubated with with αHL plasmids (10 ng) on ice for 15 minutes. The cells were spread on LB agar plates with carbenicillin (50 µg mL^{-1}) and chloramphenicol (34 µg mL^{-1}), and grown for 16 hours at 37 °C.

Single colonies were picked and grown in LB culture (200 mL) with carbenicillin (50 µg mL^{-1}) and chloramphenicol (34 µg mL^{-1}) at 37 °C until $OD_{600\ nm}$ = 0.6 - 0.8. Protein expression was induced by adding 1 mM IPTG and the cells were further grown at 18 °C for 16 hours. The culture was centrifuged (3800 g, 20 min, 4 °C) to collect the cell pallet.

From this step onwards, all steps were performed on ice or in a 4 °C cold room. If

the protein had cysteine residues, 1 mM DTT was included in all subsequent buffers used for protein purification.

Cell pallet from each 200 mL culture was suspended in 5 mL lysis buffer (50 mM Tris pH 8, 150 mM NaCl, 10 mM imidazole, 0.1 % (v/v) Triton X-100). 5 mM $MgCl_2$, 1 mg mL^{-1} lysozyme, 0.5 µL benzonase were then added to the lysis buffer. The lysate was stirred for 30 min, and sonicated 3 times for 30 s, with 30 s intervals between. The lysate was centrifuged (29000 g, 45 min) and the supernatant was loaded onto a Ni^{2+}-NTA column (2 mL) pre-equilibrated with the lysis buffer. The lysate was mixed with the beads for 1 hour and the lysate was allowed to flow through. The beads ware washed 3 times with 15 mL of wash buffer (50 mM Tris pH 8.0, 500 mM NaCl, 10 mM imidazole, 0.1 % (v/v) Triton X-100), and the protein was eluted slowly with 6 mL elution buffer (50 mM Tris pH 8.0, 500 mM NaCl, 250 mM imidazole, 0.1 % v/v Triton X-100).

Proteins were further purified on a HiLoad 26/60 Superdex 200 column (GE Healthcare) connected to an Akta system (Cytiva). The column was equilibrated and ran with storage buffer (10 mM Tris pH 8.0, 150 mM NaCl). Heptamers and monomers elute as separate fraction and were collected separately.

Protein concentration was measured by nanodrop (ND-1000 spectrophotometer, Marshall scientific). Protein purity was analyzed by SDS-PAGE, by adding protein samples to Laemmli buffer (Bio-Rad) and running with TGX buffer on 4–15 % Mini-PROTEAN® TGX™ Precast Protein Gels (Bio-Rad). The gels were stained with InstantBlue™ Coomassie Stain (abcam) to visualize the protein bands. The purified proteins were flash frozen in liquid nitrogen and stored as aliauots at -80 °C until use.

6.3 Nucleic acid and protein sequences

6.3.1 RNA Aptamer sequences

Aptamer	Sequence (5'-3')
Broccoli(*68*)	GAGACGGUCGGGUCCAGAUAUUCGUAUCUGUC GAGUAGAGUGUGGGCUCC
Spinach(*68*)	GACGCAACUGAAUGAAAUGGUGAAGGACGGGU CCAGGUGUGGCUGCUUCGGCAGUGCAGCUUGU UGAGUAGAGUGUGAGCUCCGUAACUAGUCGCG UC
Mango (MangoIII-A10U) (*72*)	GGUACGAAGGAAGGUUUGGUAUGUGGUAUAUU CGUAC
Peach (PeachI)(*73*)	GGAAUCCCUGAAGGAUGUGGGGGAGGGAGAAG GGAUUCC
Pepper(*74*)	CCAAUCGUGGCGUGUCGGCCUGCUUCGGCAGG CACUGGCGCCG
DIR2s-Apt5(*101*)	GGAUGCGCCUUGAAAAGCCUGCUUCGGCAGCU GGUGAAUGACAGCUAUGGCGCAUCC

Table 6.2: RNA aptamer sequences

6.3.2 DNA sequences

DNA	Sequences (5'-3')
s1	gaatttaatacgactcac
s2	gaatttaatacgactcacaatcgggagacggtcgggtccagata
s3	gaattatttaggtgacactatagaaatccccaatcgtggcgtg
s4	gaatttaatacgactcacaatcggggtacgaaggaagg
s5	cagtctaatacgactcactccgggatccccaatcgtggcgtgtc
s6	taatacgactcac
s7	atccgtaatacgactcaccgagggagacggtcgggtccagata
s8	aaaaaaaaaaaaaaaaaaaaaaaaaaaaaaaaaaaaaa
s9	tctgataatacgactcactatagggagacggtcgggtccag
s10	[phos]gccacgattggggatttctatagtgtcacctaaataattc
s11	[phos]gacccgaccgtctcccgattgtgagtcgtattaaattc
s12	gaaattaatacgactcactatagggtctagaaataatttt
s13	[Alexa-488]gaaattaatacgactcactatagggtctagaaataatttt
s14	aaaaaaaaaaaaaaaaaaaattcccccccccccccccccccccttaaaaaaaaa attcccccccccccttaaaaaaaaaattcccccccccc
-12U	gaatttaatac

-12D	[phos]gaactcacaatcgggagacggtcgggtccagata
-11U	gaatttaatacg
-11D	[phos]actcacaatcgggagacggtcgggtccagata
-10U	gaatttaatacga
-10D	[phos]ctcacaatcgggagacggtcgggtccagata
-9U	gaatttaatacgac
-9D	[phos]tcacaatcgggagacggtcgggtccagata
I1	tatctggacccgaccgtctcccgattgtgagtcgtattaaattc
I2	gacacgccacgattggggatcccggagtgagtcgtattagactg
I3	ccttccttcgtaccccgattgtgagtcgtattaaattc
I4	ctggacccgaccgtctcCCTATAGTGAGTCGTATTATCAGA
B1	gaatttaatacgactcacaatcgggAGACGGTCGGGTCCAGATATTCGTATCTGT CGAGTAGAGTGTGGGCTCC
B2	tctgataatacgactcactatagggAGACGGTCGGGTCCAGATATTCGTATCTGT CGAGTAGAGTGTGGGCTCC
B3	gaatttaatacgactcacaatcgggagacggtcgggtcCAGATATTCGTATCTGT CGAGTAGAGTGTGGGCTCC
B4	gaatttaatacgactcacaatcgggagacggtcgggtccagataTTCGTATCTGT CGAGTAGAGTGTGGGCTCC
P1	gaattatttaggtgacactatagaaatccccaatcgtggcgtgTCGGCCTGCTTC GGCAGGCACTGGCGCCGGGATTTC
P2	cagtctaatacgactcactccgggATCCCCAATCGTGGCGTGTCGGCCTCTCCCA ATCGTGGCGTGTCGGCCTCTCTTCGGAGAGGCACTGGCGCCGGAGAGGCACTGGC GCCGGGATC
P3	gaattatttaggtgacactatagaaatccccaatcgtggcGTGTCGGCCTGCTTC GGCAGGCACTGGCGCCGGGATTTC
M1	gaatttaatacgactcacaatcggggTACGAAGGAAGGTTTGGTATGTGGTATAT TCGTAC
R1	gtttaactttaagaaggaggtatacatatggtgag

R2	gatatagttcctcctttcagcaaaaaacccctca
R3	gaaattaatacgactcactatagggtctagaaa
R4	gtttaactttaagaaggaggtatac
R5	gatatagttcctcctttcagcaaaaaacc
C1	gaaattaatacgactcactatagggtctagaaataattttGTTTAACTTTAAGAA GGAGGTATACATATGGTGAGCAAGGGCGAGGAGGATAACATGGCCATCATCAAGG AGTTCATGCGCTTCAAGGTGCACATGGAGGGCTCCGTGAACGGCCACGAGTTCGA GATCGAGGGCGAGGGCGAGGGCCGCCCCTACGAGGGCACCCAGACCGCCAAGCTG AAGGTGACCAAGGGTGGCCCCCTGCCCTTCGCCTGGGACATCCTGTCCCCTCAGT TCATGTACGGCTCCAAGGCCTACGTGAAGCACCCCGCCGACATCCCCGACTACTT GAAGCTGTCCTTCCCCGAGGGCTTCAAGTGGGAGCGCGTGATGAACTTCGAGGAC GGCGGCGTGGTGACCGTGACCCAGGACTCCTCCCTGCAGGACGGCGAGTTCATCT ACAAGGTGAAGCTGCGCGGCACCAACTTCCCCTCCGACGGCCCCGTAATGCAGAA GAAGACCATGGGCTGGGAGGCCTCCTCCGAGCGGATGTACCCCGAGGACGGCGCC CTGAAGGGCGAGATCAAGCAGAGGCTGAAGCTGAAGGACGGCGGCCACTACGACG CTGAGGTCAAGACCACCTACAAGGCCAAGAAGCCCGTGCAGCTGCCCGGCGCCTA CAACGTCAACATCAAGTTGGACATCACCTCCCACAACGAGGACTACACCATCGTG GAACAGTACGAACGCGCCGAGGGCCGCCACTCCACCGGCGGCATGGACGAGCTGT ACAAGTAATGAGGATCCCGGGAATTCTCGAGTAAGGTTAACCTGCAGGAGGCCTT TAATTAAGGTGGTGCGGCCGCGCTAGCGGTCCCGGGGGATCGATCCGGCTGCTAA CAAAGCCCGAAAGGAAGCTGAGTTGGCTGCTGCCACCGCTGAGCAATAACTAGCA TAACCCCTTGGGGCCTCTAAACGGGTCTTGAGGGGTTTTTTGCTGAAAGGAGGAA CTATATC

G1	gaaattaatacgactcactatagggtctagaaataattttGTTTAACTTTAAGAA GGAGGTATACATATGGTGAGCAAGGGCGAGGAGGATAACATGGCCTCTCTCCCAG CGACACATGAGTTACACATCTTTGGCTCCATCAACGGTGTGGACTTTGACATGGT GGGTCAGGGCACCGGCAATCCAAATGATGGTTATGAGGAGTTAAACCTGAAGTCC ACCAAGGGTGACCTCCAGTTCTCCCCCTGGATTCTGGTCCCTCATATCGGGTATG GCTTCCATCAGTACCTGCCCTACCCTGACGGGATGTCGCCTTTCCAGGCCGCCAT GGTAGATGGCTCCGGATACCAAGTCCATCGCACAATGCAGTTTGAAGATGGTGCC TCCCTTACTGTTAACTACCGCTACACCTACGAGGGAAGCCACATCAAAGGAGAGG CCCAGGTGAAGGGGACTGGTTTCCCTGCTGACGGTCCTGTGATGACCAACTCGCT GACCGCTGCGGACTGGTGCAGGTCGAAGAAGACTTACCCCAACGACAAAACCATC ATCAGTACCTTTAAGTGGAGTTACACCACTGGAAATGGCAAGCGCTACCGGAGCA CTGCGCGGACCACCTACACCTTTGCCAAGCCAATGGCGGCTAACTATCTGAAGAA CCAGCCGATGTACGTGTTCCGTAAGACGGAGCTCAAGCACTCCAAGACCGAGCTC AACTTCAAGGAGTGGCAAAAGGCCTTTACCGATGTGATGGGCATGGACGAGCTGT ACAAGTAATGAGGATCCCGGGAATTCTCGAGTAAGGTTAACCTGCAGGAGGCCTT TAATTAAGGTGGTGCGGCCGCGCTAGCGGTCCCGGGGGATCGATCCGGCTGCTAA CAAAGCCCGAAAGGAAGCTGAGTTGGCTGCTGCCACCGCTGAGCAATAACTAGCA TAACCCCTTGGGGCCTCTAAACGGGTCTTGAGGGGTTTTTTGCTGAAAGGAGGAA CTATATC

A1	gaaattaatacgactcactatagggtctagaaataattttGTTTAACTTTAAGAA GGAGGTATACATATGGCAGATTCTGATATTAATATTAAAACCGGTACTACAGATA TTGGAAGCAATACTACAGTAAAAACAGGTGATTTAGTCACTTATGATAAAGAAAA TGGCATGCACAAAAAAGTATTTTATAGTTTTATCGATGATAAAAATCACAATAAA AAACTGCTAGTTATTAGAACAAAAGGTACCATTGCTGGTCAATATAGAGTTTATA GCGAAGAAGGTGCTAACAAAAGTGGTTTAGCCTGGCCTTCAGCCTTTAAGGTACA GTTGCAACTACCTGATAATGAAGTAGCTCAAATATCTGATTACTATCCAAGAAAT TCGATTGATACAAAAAACTATATGAGTACTTTAACTTATGGATTCAACGGTAATG TTACTGGTGATGATACAGGAAAAATTGGCGGCCTTATTGGTGCAAATGTTTCGAT TGGTCATACACTGAACTATGTTCAACCTGATTTCAAAACAATTTTAGAGAGCCCA ACTGATAAAAAAGTAGGCTGGAAAGTGATATTTAACAATATGGTGAATCAAAATT GGGGACCATACGATCGAGATTCTTGGAACCCGGTATATGGCAATCAACTTTTCAT GAAAACTAGAAATGGTTCTATGAAAGCAGCAGATAACTTCCTTGATCCTAACAAA GCAAGTTCTCTATTATCTTCAGGGTTTTCACCAGACTTCGCTACAGTTATTACTA TGGATAGAAAAGCATCCAAACAACAAACAAATATAGATGTAATATACGAACGAGT TCGTGATGATTACCAATTGCATTGGACTTCAACAAATTGGAAAGGTACCAATACT AAAGATAAATGGACAGATCGTTCTTCAGAAAGATATAAAATCGATTGGGAAAAAG AAGAAATGACAAATTAATGAGGATCCCGGGAATTCTCGAGTAAGGTTAACCTGCA GGAGGCCTTTAATTAAGGTGGTGCGGCCGCGCTAGCGGTCCCGGGGGATCGATCC GGCTGCTAACAAAGCCCGAAAGGAAGCTGAGTTGGCTGCTGCCACCGCTGAGCAA TAACTAGCATAACCCCTTGGGGCCTCTAAACGGGTCTTGGAGGGGTTTTTTGCTG AAAGGAGGAACTATATC

Table 6.3: DNA sequences. All sequences are from 5' to 3'. Lower case denotes single-stranded sequences, upper case denotes double-stranded sequences. [phos]: phosphorylated 5' end. [Alexa-488]: Alexa-488 modified 5' end.

6.3.3 Protein sequences

WT/D8H6 ADSDINIKTGTTDIGSNTTVKTGDLVTYDKENGMHKKVFYSFIDDKNHNKKLLVIRTKG
TIAGQYRVYSEEGANKSGLAWPSAFKVQLQLPDNEVAQISDYYPRNSIDTKEYMSTLTYGFNGNVTGDD
TGKIGGLIGANVSIGHTLKYVQPDFKTILESPTDKKVGWKVIFNNMVNQNWGPYDRDSWNPVYGNQLFM
KTRNGSMKAADNFLDPNKASSLLSSGFSPDFATVITMDRKASKQQTNIDVIYERVRDDYQLHWTSTNWK
GTNTKDKWTDRSSERYKIDWEKEEMTNDDDDDDDDHHHHHH

6.4 Defective gene synthesis

Defective genes were made by annealing two ssDNA of different lengths. For short defective genes (<200 nt), DNA strands were purchased commercially. Equal amount of each ssDNA in annealing buffer (100 mM NaCl, 10 mM Tris pH 8.0, 1 mM EDTA) were held at 98 °C for 10 s and cooled at a rate of 0.1 °C s^{-1} to 20 °C. (Veriti 96 Well Thermal Cycler, Applied biosystems). For longer defective genes (>200 nt), the coding strands were made from a two-step PCR. In the first step, a standard exponential PCR (peqSTAR 2X PCR thermocycler, VWR) was used to make ds-DNA template containing the coding strand and it's complementary strand. The PCR used DreamTaq Green PCR master mix with primers R1 and R2, following the manufacturer's recommendations. The dsDNA product was purified by agarose gel electrophoresis with Monarch Gel Extraction kit and further purified by Monarch PCR cleanup kit, eluting in nuclease free water. In the second step, linear PCR was used to amplify the coding strand from the dsDNA template. The linear PCR used DreamTaq PCR master mix with primer R4. Unless otherwise specified, [Primer] = 2500 nM, [dsDNA template] = 8 ng μL^{-1}, and no. of thermocycles = 20. The ssDNA product was immediately separated from dsDNA template by agarose gel electrophoresis. ssDNA bands were crushed with polypropylene pestle (Bellco glass) in a solution with 300 mM sodium acetate (pH 5.2) and 1 mM EDTA. The mixture was incubated at 37 °C for 16 hours, and the gel fragments were removed from the solution by centrifugation in proteus clarification mini spin column (Protein Ark). The ssDNA containing filtrate was concentrated and buffer exchanged to annealing

buffer (100 mM NaCl, 10 mM Tris pH 8.0, 1 mM EDTA), using amicon ultra 30 k centrifugal filters (Millipore). The template strand was made in a similar process, except that primers R3 and R2 were used in the first PCR step, and primer R5 was used in the second PCR step. The two ssDNA were annealed to form defective genes using the same annealing protocol. After annealing, the long defective genes were purified by Zeba spin desalting columns (ThermoFisher), eluting in TE buffer (10 mM Tris pH 8.0, 1 mM EDTA). They were further purified with Monarch PCR cleanup kit, eluting in nuclease free water.

6.5 RNA production from defective genes

To estimate strength of signal binding to defective genes, DNA melting temperature was calculated using online calculator from Promega (57), with the following settings: 100 nM primer concentration, 10 mM $MgCl_2$, and 50 mM KCl.

6.5.1 Defective gene activation by DNA signal

To study the final fluorescence intensity when different concentrations of defective Broccoli and Broccoli signal were used, defective Broccoli (B1) and DNA signal (s1) were added to 10 mM Tris pH 8.0, 50 mM $MgCl_2$, 1 mM DTT, 10 mM NTP (each), 60 µM DFHBI-1T, 50 mM KCl, and 5000 units mL^{-1} T7 RNA polymerase. The mixture was incubated at 37 °C for 3 hours prior to fluorescence measurement. To study fluorescence activation of different fluorophores by different aptamers, 100 nM of either defective Broccoli (B1), defective Mango (M1), or defective Pepper (P2), were added to 100 nM DNA signal (s1), 20 mM MOPS pH 8.0, 50 mM $MgCl_2$, 2 mM spermidine, 1 mM DTT, 10 mM NTP (each), 50 mM KCl, and 5000 units mL^{-1} T7 RNA polymerase, in the presence of either 60 µM DFHBI-1T, 5 µM HBC620 or 2.5 µM TO1B. The mixture was incubated at 37 °C for 3 hours prior to fluorescence measurement.

6.5.2 Selective gene activation using multiple polymerases

To study selective activation of defective Broccoli with T7 promoter (B1) and defective Pepper with SP6 promoter (P1), 100 nM Broccoli signal (s2) and/or 100 nM Pepper signal (s3) were added to 5 mM MOPS pH 8.0, 50 mM $MgCl_2$, 2 mM spermidine, 1 mM DTT, 10 mM NTP (each), 50 mM KCl, 100 nM defective Broccoli (B1), 100 nM defective Pepper (P1), 60 µM DFHBI-1T, 5 µM HBC620, 5000 units mL^{-1} T7 RNA polymerase, and 2000 units mL^{-1} SP6 RNA polymerase. The mixture was incubated at 37 °C for 3 hours prior to fluorescence measurement. To study selective activation of defective Mango with T7 promoter (M1) and defective Pepper with SP6 promoter (P1), 100 nM Mango signal (s4) and/or 100 nM Pepper signal (s3) were added to 20 mM MOPS pH 8.0, 50 mM $MgCl_2$, 2 mM spermidine, 1 mM DTT, 10 mM NTP (each), 50 mM KCl, 100 nM 11BM, 100 nM 31PPM, 60 µM DFHBI-1T, 5 µM HBC620, 2500 units mL^{-1} T7 RNA polymerase, and 2000 units mL^{-1} SP6 RNA polymerase. The mixture was incubated at 37 °C for 3 hours prior to fluorescence measurement.

6.5.3 Selective gene activation using inhibitors

To study selective activation of defective Broccoli (B1) and defective Pepper (P2) with T7 promoter, 100 nM of either Broccoli signal (s2), Pepper signal (s5), or Universal signal (s6) were added to 5 mM MOPS pH 8.0, 50 mM $MgCl_2$, 1 mM DTT, 10 mM NTP (each), 50 mM KCl, 5000 units mL^{-1} T7 RNA polymerase, with either 100 nM defective Broccoli (B1), 1 uM Pepper signal inhibitor (I2) and 60 µM DFHBI-1T; or 100 nM defective Pepper (P2), 1 uM Broccoli signal inhibitor (I1) and 5 µM HBC620. The mixture was incubated at 37 °C for 3 hours prior to fluorescence measurement. In the agarose gel electrophoresis analysis of strand displacement reaction, Pepper signal (s5) and defective Broccoli (B1) were first incubated at 37 °C for 30 minutes. Pepper signal inhibitor (I2) was then added and the mixture was incubated at 37 °C for a further 60 minutes before loading the samples onto agarose gel for analysis. To study selective activation of defective Mango (M1) and defective Pepper (P2) with T7 promoter, 100 nM of either Pepper

signal (s5), Mango signal (s4), Universal signal (s7), or polyA signal (s8), were added to 20 mM MOPS pH 8.0, 50 mM $MgCl_2$, 1 mM DTT, 10 mM NTP (each), 50 mM KCl, 5000 units mL^{-1} T7 RNA polymerase, with either 100 nM defective Mango (M1), 1 µM Pepper signal inhibitor (I2) and 2.5 µM TO1B; or 100 nM defective Pepper (P2), 1 µM Mango signal inhibitor (M1) and 5 µM HBC620. The mixture was incubated at 37 °C for 3 hours prior to fluorescence measurement. To study selective activation of defective Broccoli (B2), defective Mango (M1) and defective Pepper (P2) with T7 promoter, 100 nM of either Pepper signal (s5), or Mango signal (s4), or Broccoli signal (s9), were added to 20 mM MOPS pH 8.0, 50 mM $MgCl_2$, 1 mM DTT, 10 mM NTP (each), 50 mM KCl, 5000 units mL^{-1} T7 RNA polymerase, with either 100 nM defective Mango (M1), 1 µM Pepper signal inhibitor (I2), 1 µM Broccoli signal inhibitor (I4), and 2.5 µM TO1B; or 100 nM defective Pepper (P2), 1 µM Mango signal inhibitor (M1), 1 µM Broccoli signal inhibitor (I4), and 5 µM HBC620; or 100 nM defective Broccoli (B2), 1 µM Mango signal inhibitor (M1), 1 µM Pepper signal inhibitor (I2), and 60 µM DFHBI-1T. The mixture was incubated at 37 °C for 3 hours prior to fluorescence measurement.

6.5.4 Activation of inverse defective genes

To study fluorescence intensity of inverse defective Pepper (P3), 100 nM Pepper signal (s10) was mixed with 5 mM MOPS pH 8.0, 50 mM MgCl2, 2 mM spermidine, 1 mM DTT, 10 mM NTP (each), 50 mM KCl, 5000 units mL^{-1} T7 RNA polymerase, 5 µM HBC620, 100 nM inverse defective Pepper (P3), with or without 40,000 units mL^{-1} T4 DNA ligase. The mixture was incubated at 37 °for 3 hours prior to fluorescence measurement. To study fluorescence intensity of inverse defective Broccoli (B3), 100 nM Broccoli signal (s11) is mixed with 5 mM MOPS pH 8.0, 50 mM MgCl2, 2 mM spermidine, 1 mM DTT, 10 mM NTP (each), 50 mM KCl, 5000 units mL^{-1} T7 RNA polymerase, 60 µM DFHBI-1T, 100 nM inverse defective Broccoli (B3), with or without 40,000 units mL^{-1} T4 DNA ligase. The mixture was incubated at 37 °for 3 hours prior to fluorescence measurement.

6.5.5 Complex logic gates by splitting the DNA signal

To study fluorescence intensity of logic gates, 1 µM each signal fragments were added to 5 mM MOPS pH 8.0, 50 mM $MgCl_2$, 1 mM DTT, 10 mM NTP (each), 50 mM KCl, 5000 units mL^{-1} T7 RNA polymerase, 100 nM defective Broccoli (B4), and 60 µM DFHBI-1T, with or without 300,000 units mL^{-1} T3 DNA ligase. The mixture was incubated at 37 °C for 3 hours prior to fluorescence measurement.

6.5.6 Signal length effect on defective genes

To study the effect of signal length on the fluorescence intensity of the Broccoli aptamer, 1 µM each signal fragments were added to 10 mM Tris pH 8.0, 50 mM $MgCl_2$, 1 mM DTT, 10 mM NTP (each), 50 mM KCl, 5000 units mL^{-1} T7 RNA polymerase, 100 nM defective Broccoli (B4), and 60 µM DFHBI-1T. The mixture was incubated at 37 °C for 3 hours prior to fluorescence measurement.

6.6 Protein production from defective genes

6.6.1 DNA signal activates defective genes

To investigate the effect of signal concentration on the activation of defective mNG (G1), DNA signal (s12) and defective mNG (G1) were mixed with 1x PURExpress In Vitro Protein Synthesis Mix, and 1000 units mL^{-1} murine RNAse inhibitor. The mixture was incubated at 37 °C for 3 hours prior to fluorescence measurement.

6.6.2 DNA signal as a transcription factor mimic

To investigate DNA signal as a transcription factor mimic, 100 nM DNA signal (s12) was added to either 10 nM defective mCherry (C1), 10 nM defective mNG (G1), or 5 nM defective mCherry (C1) and 5 nM defective mNG (G1), with 1x PURExpress In Vitro Protein Synthesis Mix, and 1000 units mL^{-1} murine RNAse inhibitor. The mixture was incubated at 37 °C for 3 hours prior to fluorescence measurement. To immobilize the protein production system in organogel, 10 mg/mL of Polystyrene-

block-poly(ethylene-ran-butylene)-blockpolystyrene (SEBS, average Mw 118000) in hexadecane, containing 2 wt % Span80 was melted at 50 °C. 30 µL of this solution was added to a 96 well plate with blackened sides and clear bottom (Corning 3603) and left to solidify to coat the bottom of the well. Then, 40 µL of the polymer solution was added to the prepared PURExpress solution, the solutions were quickly emulsified by agitation and the resulting emulsion transferred to the pre-coated well and left to set for 5 min. The emulsions were then incubate at 37 °C for 3 hours prior to fluorescence imaging.

6.7 Aqueous droplet networks in lipid-in-oil solution

6.7.1 Preparation of lipid films

2 mL glass vials (Supelco) were washed carefully with isopropyl alcohol, gently dried under a stream of nitorgen, and desiccated for at least 1 hour before use. Lipid films were prepared by dissolving lipid powder in chloroform and aliquoting the solution into the 2 mL glass vials. The chloroform was evaporated very gently under a stream of nitrogen. To make lipid film consisting of multiple types of lipids, after evaporating the chloroform to deposit the first lipid, the vials were desiccated under vacuum for at least 1 hour, before chloroform solution of another lipid was added to the vials. The chloroform was again evaporated gently under a stream of nitrogen, and the vials were desiccated under vacuum for at least 1 hour. This process was repeated until all required lipids were added to the vials. Then, the vials were desiccated under vacuum overnight, and were either used immediately, or they were filled with argon, sealed with teflon tape, and stored at -80 °C. Lipid films consisting of any lipid labelled hydroscopic by the manufacturer, such as POPC lipid, should not be stored as lipid films for more than 2 weeks before use.

6.7.2 Preparation of oil solution

Hexadecane and silicon oil AR20 were filtered through 0.22 µm filters (Corning). If the oil was subsequently used for droplets containing IVT mix, 3 mL of the silicone oil (AR20) was shaken vigorously with 12 mL of 10 mM HCl solution in a 15 mL falcon tube. The mixture was allowed to settle for 1 minute, then centrifuged (2900 g, 3 min). The aqueous solution was carefully removed. The silicone oil was then washed with 12 mL of 10 mM KOH solution, and then with a buffer solution (5 mM MOPS pH 8.0, 50 mM $MgCl_2$, 100 mM KCl) in the same manner. Finally, the silicone oil solution was aliquoted to 1.5 mL microcentrifuge tubes and centrifuged (24000 g, 5 min) to ensure complete sepration of the aqueous and the oil phase.

6.7.3 Preparation of lipid-in-oil solution

Lipid films were brought to room temperature before opening the glass vials to prevent condensation on the interior surface of the glass vials. The hexadecane was added to the lipid films first, followed by the silicone oil. The solution was mixed by vortexing for 30 s and then sonicating (Branson 2800 ultrasonic bath 230 V) for 1 hr. The solution was further vortexed for 30 s before use.

6.7.4 Formation of droplet interface bilayers - without electrodes

If electrical recording was not required, the lipid-in-oil solution was added to a PMMA well. Aqueous droplets were added to the solution by pipette (> 200 nL droplets) or by Hamilton gastight syringe (<200 nL droplets, Hamilton). To form DIBs, droplets were brought together by tilting the well and allowing droplets to come into contact by gravity.

6.7.5 Formation of droplet interface bilayers - with electrodes

Aqueous droplets for electrical recording were prepared in a similar manner except that electrodes were inserted into the droplets.

Electrodes preparation

To prepare Ag/Agcl electrodes for the recording, silver wires (0.1 mm diameter) were tied or soldered onto male crimp-terminal (TE Connectivity 1-66506-0, RS components). The tips of the wires were incubated in sodium hypochloride (15 %) for 15 min to form Ag/AgCl electrodes. The electrodes were rinsed by dipping in water, and coated with hydrogel by dipping in melted agarose (1 %) twice with 5 minute interval in between.

Setup for electric recording

The male crimps-terminals connected to the wire were plugged into female crimp-terminal. The female crimp-terminals were soldered to a cable that connected to eONE amplifier (Elements, serial no. E1HC0005), controlled by a computer running Elements Data Reader software (Elements, 3.8.18). The electric signal was sampled at 10 kHz and filtered at 1.25 kHz with HW analog low pass filter and without additional digital filters. The cable connecting the female crimp-terminal to the amplifier was also secured to a micromanipulator (Narishige, NMN-21) that controlled movement of the electrodes. The electrodes were positioned in the lipid-in-oil solution in a PMMA well using the micromanipulators.

Droplet interface bilayer formation

Aqueous droplets were added to the electrodes using a pipette or hamilton syringe. The droplets would spontaneously adhere to the hydrogel coating on the electrode. The droplets were then brought together by moving the micromanipulators to form DIB between the droplets. Bilayer formation was monitored by measuring the bilayer capacitance using the triangular function on the software, with the following parameters: Vamp = 50 mV, TPeriod = 100 ms.

Estimation of number of channel protein

The total number of channel proteins on the bilayer was approximated from the bilayer conductance, assuming that the bilayer conductance was the conductance of

a single channel at the same salt concentration multiplied by the number of channels on the bilayer. The conductance was measured using the seal test function on the software, with the following parameters: Vpulse = 20 mV, Discard (% of Tpu) = 30.00, Tpulse = 1000 ms, Thold = 1000 ms. We note that this method has a lower detection limit of 100 nS. After bilayer formation, the conductance was measured every 5 minutes until the conductance was stabilized (less than 10 % change in conductance between subsequent measurements), after which the conductance was measured every 15 minutes.

Stability test

A stability test was used to quantify the voltage-dependence of bilayer stability when the contents in the aqueous droplets or the lipid-in-oil solution were varied. In the test, the membrane potential across the bilayer increased at a rate of 1 mV s^{-1} from 0 mV until the bilayer ruptured, the point of which was indicated by a sudden coalescence of the two droplets, and a sudden increase in electric current.

Membrane potential application

In each signalling cycle, the required potential was applied for 2 s, followed by application of the opposite potential for 2 s. The process was repeated until the desired DNA concentration in the receiver droplet was reached.

Simultaneous electrical and fluorescence studies

Nikon Eclipse TE2000-S with pE-300 LED and Hammatsu EM-CCD digital camera C9100 were used to image droplet connected to electrodes. The following fluorescent cubes were used:

Setting	Used for	Excitation filter (nm)	Barrier filter (nm)
V2A	BFP	380-420	450
GFP-L	sulphonated fluorescein, broccoli, mNeonGreen, mVenus	460-500	510
TXR	TAMRA, mCherry	540-580	600-660

6.7.6 IVT expression in lipid-in-oil solution compared to expression in bulk

To investigate the effects of silicone oil treatment on IVT expression of the Mango aptamer, the silicone oil was either unwashed, washed with water three times, or washed with acid, base, and buffer (acid-base-buffer wash). To wash the silicone oil with water, 3 mL of the AR20 silicone oil was shaken vigorously with 12 mL of water in a 15 mL falcon tube. The mixture was allowed to settle for 1 minute, centrifuged (2900 g, 3 min), and the aqueous phase was carefully removed. This process was repeated 2 additional times. Finally, the silicone oil solution was aliquoted to 1.5 mL microcentrifuge tubes and centrifuged (24000 g, 5 min) to ensure complete sepration of the aqueous and the oil phase.

To wash the silicone oil with acid-base-buffer wash, 3 mL of the silicone oil (AR20) was shaken vigorously with 12 mL of 10 mM HCl solution in a 15 mL falcon tube. The mixture was allowed to settle for 1 minute, then centrifuged (2900 g, 3 min). The aqueous solution was carefully removed. The silicone oil was then washed with 12 mL of 10 mM KOH solution, and then with a buffer solution (5 mM MOPS pH 8.0, 50 mM $MgCl_2$, 2 mM spermidine, 100 mM KCl) in the same manner. Finally, the silicone oil solution was aliquoted to 1.5 mL microcentrifuge tubes and centrifuged (24000 g, 5 min) to ensure complete sepration of the aqueous

and the oil phase.

To study IVT expression in lipid-in-oil solution compred to expression in the bulk solution, 100 nM defective Mango (M1) and 100 nM DNA signal (s7) were added to 5 mM MOPS pH 8.0, 50 mM $MgCl_2$, 2 mM spermidine, 1 mM DTT, 10 mM NTP (each), 100 mM KCl, 2.5 µM TO1B, and 5000 units mL^{-1} T7 RNA polymerase. The mixture was either incubated as a bulk solution, or as 200 nL droplets in 1:1 (v/v) hexadecane: silicone oil solution, with different treatments of the silicone oil. The mixture was at 25 °C for 22 hours prior to fluorescence measurement.

6.7.7 IVTT expression in lipid-in-oil solution compared to expression in bulk

To evaluate IVTT expression as aqueous droplets in lipid-in-oil solution compared to expression in a bulk solution, 0.1 ng/ µL linear double-stranded mVenus template was added to 1x Purexpress with 1000 units mL^{-1} murine RNAse inhibitor. The mixture was either incubated directly as a bulk solution in a PCR tube, or 200 nL aqueous droplets were added to different lipid-in-oil mixtures using a pipette. The bulk mixture and aquoues in oil droplets were incubated at 37 °and imaged after 3 hours, 6 hours, and 19 hours.

6.7.8 DNA signal activated hemolysin production in droplet networks

To activate αHL production using DNA signal in droplet networks, the signal droplet (200 nL) contained 4 ng μL^{-1} defective αHL (A1), 1x PURExpress In Vitro Protein Synthesis mix, and 1000 units mL^{-1} murine RNAse inhibitor, with or without 20 nM DNA signal (s12). The reservoir droplet (200 nL) contained 1x solution A of PURExpress In Vitro Protein Synthesis Mix, 200 mM potassium monoglutamate, and 0.33 mM NBDG. The two droplets were separately pipetted into a lipid-in-oil solution with 10 mg/mL 1:1 (mass ratio) DPhPC: POPC in 1:1 (v/v) hexadecane: silicone oil (AR20). The droplets were gently brought together to allow lipid bilayer formation between the droplets. The constructs were then incubated at 37 °C and

imaged periodically.

6.7.9 Droplet networks with droplet-hydrogel bilayers

Droplet networks formed from droplet-hydrogel bilayers were constructed adapting protocol outlined in (*83*). The signal droplet (200 nL) contained 70 µM DNA signal (s6), 6.25 % glycerol, 1 % ultra-low gelling agarose (melted), 5 mM MOPS pH 8.0, 50 mM $MgCl_2$, 1 mM DTT, 10 mM NTP (each), 50 mM KCl, 2.5 µM TO1B and 0.1 % F68. The receiver droplet (200 nL) contained 100 nM defective Mango (M1), 5000 units mL^{-1} T7 RNA polymerase, 1000 units mL^{-1} murine RNAse inhibitor, 1 % ultra-low gelling agarose (melted), 5 mM MOPS pH 8.0, 50 mM $MgCl_2$, 1 mM DTT, 10 mM NTP (each), 50 mM KCl, 2.5 µM TO1B and 0.1 % F68. Similarly, the two cells were separately pipetted into a lipid-in-oil solution with 10 mg mL^{-1} 1:1 (mass ratio) DPhPC: POPC in 1:1 (v/v) hexadecane: silicone oil (AR20), gently brought together, and incubated for 10 minutes at 25 °C to form bilayer between the droplets. The droplets were then kept at 4 °C for 30 minutes, and activated by perfusing the lipid-in-oil solution with pure silicone oil (AR20) solution to break the bilayers. The constructs were kept at 4 °C for 60 minutes, and then incubated at 37 °C for 3 hours prior to fluorescence imaging.

To form droplet networks with immbolized fluorophores, the signal droplet (300 nL) contained 70 µM DNA signal (s6), 6.25 % glycerol, 1 % ultra-low gelling agarose (melted), 5 mM MOPS pH 8.0, 50 mM $MgCl_2$, 1 mM DTT, 10 mM NTP (each), 50 mM KCl, and 0.1 % F68. The defective gene droplet (300 nL) contained 100 nM defective Mango (M1), 5000 units mL^{-1} T7 RNA polymerase, 1000 units mL^{-1} murine RNAse inhibitor, 1 % ultra-low gelling agarose (melted), 5 mM MOPS pH 8.0, 50 mM $MgCl_2$, 1 mM DTT, 10 mM NTP (each), 50 mM KCl, and 0.1 % F68. The fluorophore droplet (300 nL) contained 60 % volume of fluorophore sepharose beads solution, 6.25 % glycerol, 1 % ultra-low gelling agarose (melted), 5 mM MOPS pH 8.0, 50 mM $MgCl_2$, 1 mM DTT, 10 mM NTP (each), 50 mM KCl, and 0.1 % F68.

6.7.10 Membrane potential controlled entry across protein pores

To prepare the droplet network for DNA signal translocation across channel protein pores in droplet interface bilayers, signal droplets (200 nL) contained 100 mM NaCl, 0.21 mg mL^{-1} αHL monomer and 300 µM DNA signal (s13). Receiver droplets (200 nL) contained 100 mM NaCl. The two droplets were separately pipetted onto electrode tips in the lipid-in-oil solution, and gently brought together to form a lipid bilayer between the droplets using the micromanipulator. The lipid-in-oil solution used was 10 mg/mL 1:1 (mass ratio) DPhPC: POPC in 1:1 (v/v) hexadecane: silicone oil (AR20). The signalling droplet was held at 0 mV, while the voltage in the receiver droplet alternated between +120 mV and -120 mV.Signalling was stopped when the channel time reached 15,000 channel hours. The two droplets were carefully separated, and the receiver droplet was supplemented to a final 1x PURExpress In Vitro Protein Synthesis mix, 1000 units mL^{-1} murine RNAse inhibitor and 3.33 ng μL^{-1} defective mCherry (C1). The receiver droplet was incubated at 37 °C for 3 hours prior to fluorescence measurement.

6.7.11 Rectification factor of bilayer formed from different lipids

To investigate rectification factor of bilayers with multiple protein pores, with or without straptavidin-bound oligo, 200 nM straptavidin-bound s12 signal was present in the same droplet as αHL monomers. 500 mM KCl was used in the droplets. The following voltage clamp protocol was applied to the droplets: 10 mV (10 s), -10 mV (10 s), 20 mV (10 s), -20 mV (10 s), 30 mV (10 s), -30 mV (10 s) etc, until the bilayer ruptured. At each voltage level, the current at the last two second of the recording was used to calculate the rectification factor, to avoid measurement of capacitative currents.

6.7.12 Spermidine in signalling droplet

To investigate the morphology of droplets containing IVT mix, droplet interface bilayers were formed between the signal droplet and two receiver droplets. The signal droplet contained 175 µM Mango (s4), 20 mM MOPS pH 8.0, 50 mM $MgCl_2$, 2 mM spermidine, 1 mM DTT, 10 mM NTP (each), 50 mM KCl, 50 mM NaCl, 2.5 µM TO1B, and 150 µg/mL 111N/113R αHL mutant monomers. The receiver droplet contained 100 nM defective Mango (M1), 20 mM MOPS pH 8.0, 50 mM $MgCl_2$, 2 mM spermidine, 1 mM DTT, 10 mM NTP (each), 100 mM KCl, 2.5 µM TO1B, and 5000 units mL^{-1} T7 RNA polymerase.

6.7.13 T7 RNAP degradation on electrodes

To test the overall IVT activity as droplets on Ag/AgCl electrodes in lipid-in-oil solution using Pepper aptamer as the readout, the signal solution contained 1 µM s17, 10 mM Tris pH 8.0, 100 mM KCl. The IVT solution contained 10 mM Tris pH 8.0, 50 mM $MgCl_2$, 1 mM DTT, 10 mM NTP (each), 100 mM KCl, 50 nM P2, 1000 units mL^{-1} murine RNAse inhibitor, 5000 units mL^{-1} T7 RNA polymerase. The lipid-in-oil solution was 10 mg/mL DPhPC in 1:1 (v/v) hexadecane: washed silicone oil (AR20), with 1 µM HBC620. After coating the electrodes with agarose, the electrodes were immersed in a solution of 100 mM KCl, 10 mM tris pH 8.0 for at least 15 minutes prior to use. In the first set of experiments, the signal solution (150 nL) was first added to the electrode to form droplet, and the droplet was incubated for 15 minutes. The IVT solution (150 nL) was then added to the droplets, and the mixture was incubated for another 15 minutes. In the second set of experiments, the IVT solution (150 nL) was first added to the electrode to form droplet, and the droplet was incubated for 15 minutes. The signal solution (150 nL) was then added to the droplets, and the mixture was incubated for another 15 minutes.Then, more IVT solution (300 nL) was added to the droplet, and the droplet was further incubated for 15 minutes. In the third set of experiments, a mixture of the IVT solution and the signal solution (150 nL) was added to the electrode to form droplet, and the droplet was incubated over time. As a control to the above set of

experiments, the experiments were repeated with the solution added to a lipid-in-oil solution to form droplets. The droplets were not in contact with the electrodes.

To verify which IVT component lost activity on the Ag/AgCl electrode using Pepper aptamer as the readout, the signal and IVT mix (without T7 RNA polymerase) contained 10 mM Tris pH 8.0, 50 mM $MgCl_2$, 1 mM DTT, 10 mM NTP (each), 100 mM KCl, 50 nM P2, 1 µM s17, 1000 units mL^{-1} murine RNAse inhibitor. The T7 RNA polymerase solution contained 10 mM Tris pH 8.0, 1 mM DTT, 100 mM KCl, 5000 units mL^{-1} T7 RNA polymerase. In the first set of expeirments, the signal and the IVT mix (without T7 RNA polymerase) (150 nL) was first added to the electrode to form droplet, and the droplet was incubated for 15 minutes. The T7 RNA polymerase solution (150 nL) was then added to the droplets, and the mixture was incubated for another 15 minutes. In the second set of experiments, the T7 RNA polymerase solution (150 nL) was first added to the electrode to form droplet, and the droplet was incubated for 15 minutes. The the signal and the IVT mix (without T7 RNA polymerase) (150 nL) was then added to the droplets, and the mixture was incubated for another 15 minutes. Then, more T7 RNA polymerase solution (300 nL) was added to the droplet, and the droplet was further incubated for 15 minutes. In the third set of experiments, a mixture of the signal and IVT mix (without T7 RNA polymerase), and the T7 RNA polymerase solution (150 nL) was added to the electrode to form droplet, and the droplet was incubated over time. To test if presaturating the electrode with BSA improved fluoresnece expression on the electrodes, the electrodes were immersed in a solution of 100 mM KCl, 10 mM Tris pH 8.0, 5% (W/w) BSA for at least 15 minutes prior to use.

6.8 Single-channel electrical Recording

6.8.1 Recording chamber preparation

Single αHL channel electrophysiology recordings were performed on black lipid membranes, prepared with the Montal-Mueller method (*145*).To prepare Ag/AgCl wires, silver wires (1 mm diameter) were inserted into male crimp. The wires were incu-

bated in sodium hypochloride (15 %) overnight to form Ag/AgCl electrodes. To prepare black lipid membranes, two polyoxymethylene compartments were separated by a 25 µm thick polytetrafluoroethylene film (Goodfellow Cambridge Limited) containing an 100 µm diameter aperture. The aperture was treated with 1% (v/v) hexadecane in pentane. Each compartment were then filled with the required buffer. Ag/AgCl electrodes were connected to each compartment through a salt bridge formed from 1 M KCl in 1 % Agarose.

6.8.2 Electrical recording

Current recordings of the planar bilayer were performed with Axopatch 200B amplifier (Axon Instruments) connected to CV203BU headstage (Axon Instruments). Signals were digitized with Digidata 1550B digitizer (Molecular Devices), connected to a computer running the pCLAMP 10.7 software suite (Molecular Devices). The sampling rate was at least 5 times the filtering rate. A lowpass Bessel filter (80 dB/decade) was used for filtering. pCLAMP software was used for data analysis. The cis compartment was connected to the ground.

6.8.3 Lipid bilayer formation

To form bilayer on the aperture, DPhPC Lipid (1 mg mL^{-1}) in pentane were added to both compartments and bilayers were formed on the aperture by skillfully pipetting the mixtures in both compartments. The bilayer formation was monitored by applying a triangular voltage waveform, with the following parameters: maximum voltage = 10 mV, minimum voltage = -10 mV, Voltage gradient = 1 mV ms^{-1}.

6.8.4 Single channel recording

To obtain single protein pore on the bilayer, the protein was repetitively added to the cis compartment and the compartment gently stirred, until electric current through a single channel was detected by the amplifier. The cis compartment was rapidly and carefully perfused with the same recording buffer, to prevent additional insertions of channel proteins on the bilayer. If multiple insertion occurred, the

bilayer was broken by briefly applying a pulse of high voltage (1 V, 100-200 ms), and the process repeated until a stable single channel was obtained.

6.8.5 Translocation rate of ssDNA across different mutant pores

To study translocation rate of ssDNA (s14) across different αHL mutants, both compartments in the chamber contained 1 M KCl, 25 mM Tris pH 8.0, and 100 µM EDTA. The protein and subsequently the ssDNA (s14) were added to the cis compartment, and the current through the single channel pore at different voltages were recorded.

6.8.6 Synthesis of signal precursor

The signal precursor was synthesized using a similar method as described in (*146*). DBCO magnetic beads (20 nmol, 0.67 mg resin, 67 µL suspension) was washed with water three times to remove Kathon in the suspension. Peptide P3 (10 mM, 2 µL) was incubated with 5'-DBCO modified DNA signal (1 mM, 10 µL) for 1 hr. The reaction mixture was added to the magnetic beads and incubated (1 hr). Water (488 µL) was added to facilitate separation of magnetic beads from peptide oligo conjugate and the conjugate was lyophilized (Christ alpha 2-4 LDplus). The peptide oligo conjugate was characterized with LC-MS (UPLC-MS Waters XEVO G2-QTOF (ESI-negative); Acquity UPLC Oligonucleotide BEH C18 Column: 2.1 mm x 50 mm, 1.7 µM (particle size); linear gradient: 0-70% eluant B in eluant A over 8 min, flow rate: 0.2 mL min^{-1}; eluant A: 8.6 mM TEA, 200 mM HFIP in 5% methanol/water (v/v); eluant B: 20% eluant A in methanol). Traptavidin (2.11 mg/mL) in phosphate-buffered saline was buffer exchanged into buffer B (44 mM Tris-HCl, 6.6 mM $MgCl_2$, pH 7.9) using Amicon Ultra – 0.5 mL centrifugal filters (10 K). Traptavidin (40 µM, 10 µL) in buffer B was added to the peptide oligo conjugate (400 µM, 1 µL) in water. The reaction mix was incubated for 30 min and frozen at -20 °before use.

6.8.7 Signal processing rate of catalytic cycle

To determine the mean waiting time of each step in the catalytic signal processing cycle at physiologically relevant pH, a planar lipid bilayer was formed from DPhPC lipid in the recording chamber. The cis (grounded) side of the recording chamber contained 2 M KCl, 50 mM HEPES pH 7.6, 50 µM EDTA, and 200 nM signal precursor, heptameric $(115143)_1(\mathrm{WT})_6$ mutant, with a final pH 7.4. The trans side of the recording chamber contained 2 M KCl, 50 mM HEPES pH 7.6, 50 µM EDTA, and 5 mM DTT. A single channel insertion was obtained on the bilayer, and the membrane potential was applied continuously when the current was recorded.

Bibliography

1. Karoui, H., Patwal, P. S., Pavan Kumar, B. V. & Martin, N. *Chemical Communication in Artificial Cells: Basic Concepts, Design and Challenges* 2022.

2. Smith, J. M., Chowdhry, R. & Booth, M. J. Controlling Synthetic Cell-Cell Communication. *Frontiers in Molecular Biosciences* **8,** 1321. ISSN: 2296889X (2022).

3. Buddingh', B. C. & Van Hest, J. C. Artificial Cells: Synthetic Compartments with Life-like Functionality and Adaptivity. *Accounts of Chemical Research* **50,** 769–777. ISSN: 15204898 (2017).

4. Sato, W., Zajkowski, T., Moser, F. & Adamala, K. P. Synthetic cells in biomedical applications. *Wiley Interdisciplinary Reviews: Nanomedicine and Nanobiotechnology* **14,** e1761. ISSN: 19390041 (Mar. 2022).

5. Ioannou, I. A. *et al.* Nucleated synthetic cells with genetically driven intercompartment communication. *Proceedings of the National Academy of Sciences of the United States of America* **121,** e2404790121. ISSN: 10916490 (36 Sept. 2024).

6. Pilkington, C. P., Gispert, I., Chui, S. Y., Seddon, J. M. & Elani, Y. Engineering a nanoscale liposome-in-liposome for in situ biochemical synthesis and multi-stage release. *Nature Chemistry 2024 16:10* **16,** 1612–1620. ISSN: 1755-4349 (10 July 2024).

7. Malouf, L. *et al.* Sculpting DNA-based synthetic cells through phase separation and phase-targeted activity. *Chem* **9,** 3347–3364. ISSN: 2451-9294 (Nov. 2023).

8. Fabrini, G. *et al.* Co-transcriptional production of programmable RNA condensates and synthetic organelles. *Nature Nanotechnology 2024,* 1–9. ISSN: 1748-3395 (July 2024).

9. Leathers, A. *et al.* Reaction-Diffusion Patterning of DNA-Based Artificial Cells. *Journal of the American Chemical Society* **144,** 17468–17476. ISSN: 15205126 (Sept. 2022).

10. Miller, M. B. & Bassler, B. L. Quorum Sensing in Bacteria. *Annual Review of Microbiology* **55,** 165–199. ISSN: 0066-4227 (Oct. 2002).

11. Bevan, P. Insulin signalling. *Journal of cell science* **114,** 1429–30. ISSN: 0021-9533 (2001).

12. Huelsken, J. The Wnt signalling pathway. *Journal of Cell Science* **115,** 3977–3978. ISSN: 00219533 (Nov. 2002).

13. Kholodenko, B. N. Cell-signalling dynamics in time and space. *Nature Reviews Molecular Cell Biology* **7,** 165–176. ISSN: 14710072 (Mar. 2006).

14. Lentini, R. *et al.* Two-Way Chemical Communication between Artificial and Natural Cells. *ACS Central Science* **3,** 117–123. ISSN: 23747951 (2017).

15. Toparlak, D. *et al.* Artificial cells drive neural differentiation. *Science Advances* **6,** 4920–4938. ISSN: 23752548 (2020).

16. Aufinger, L., Brenner, J. & Simmel, F. C. Complex dynamics in a synchronized cell-free genetic clock. *Nature Communications* **13,** 1–9. ISSN: 20411723 (2022).

17. Ding, Y., Contreras-Llano, L. E., Morris, E., Mao, M. & Tan, C. Minimizing Context Dependency of Gene Networks Using Artificial Cells. *ACS Applied Materials and Interfaces* **10,** 30137–30146. ISSN: 19448252 (2018).

18. Scott, S. R. & Hasty, J. Quorum Sensing Communication Modules for Microbial Consortia. *ACS Synthetic Biology* **5,** 969–977. ISSN: 21615063 (2016).

19. Dupin, A. & Simmel, F. C. Signalling and differentiation in emulsion-based multi-compartmentalized in vitro gene circuits. *Nature Chemistry* **11,** 32–39. ISSN: 17554349 (2019).

20. Dupin, A. *et al.* Synthetic cell-based materials extract positional information from morphogen gradients. *Science Advances* **8,** 9228. ISSN: 23752548 (Apr. 2022).

21. Gaut, N. J. *et al.* Programmable Fusion and Differentiation of Synthetic Minimal Cells. *ACS Synthetic Biology* **11,** 855–866. ISSN: 21615063 (Feb. 2022).

22. Bhosale, S. *et al.* Photoproduction of proton gradients with π-stacked fluorophore scaffolds in lipid bilayers. *Science* **313,** 84–86. ISSN: 00368075 (2006).

23. Elani, Y., Law, R. V. & Ces, O. Vesicle-based artificial cells as chemical microreactors with spatially segregated reaction pathways. *Nature Communications 2014 5:1* **5,** 1–5. ISSN: 2041-1723 (2014).

24. Niederholtmeyer, H., Chaggan, C. & Devaraj, N. K. Communication and quorum sensing in non-living mimics of eukaryotic cells. *Nature Communications* **9,** 352666. ISSN: 20411723 (Dec. 2018).

25. Tang, T. Y. *et al.* Gene-Mediated Chemical Communication in Synthetic Protocell Communities. *ACS Synthetic Biology* **7,** 339–346. ISSN: 21615063 (2018).

26. Booth, M. J., Cazimoglu, I. & Bayley, H. Controlled deprotection and release of a small molecule from a compartmented synthetic tissue module. *Communications Chemistry 2019 2:1* **2,** 1–8. ISSN: 2399-3669 (Dec. 2019).

27. Hindley, J. W. *et al.* Building a synthetic mechanosensitive signaling pathway in compartmentalized artificial cells. *Proceedings of the National Academy of Sciences of the United States of America* **116,** 16711–16716. ISSN: 10916490 (Aug. 2019).

28. Cazimoglu, I., Booth, M. J. & Bayley, H. A Lipid-Based Droplet Processor for Parallel Chemical Signals. *ACS Nano* **15,** 20214–20224 (2021).

29. Lister, F. G., Le Bailly, B. A., Webb, S. J. & Clayden, J. Ligand-modulated conformational switching in a fully synthetic membrane-bound receptor. *Nature Chemistry* **9,** 420–425. ISSN: 17554349 (2017).

30. Langton, M. J., Keymeulen, F., Ciaccia, M., Williams, N. H. & Hunter, C. A. Controlled membrane translocation provides a mechanism for signal transduction and amplification. *Nature Chemistry* **9,** 426–430. ISSN: 17554349 (2017).

31. Langton, M. J., Williams, N. H. & Hunter, C. A. Recognition-Controlled Membrane Translocation for Signal Transduction across Lipid Bilayers. *Journal of the American Chemical Society* **139,** 6461–6466. ISSN: 15205126 (2017).

32. Langton, M. J., Scriven, L. M., Williams, N. H. & Hunter, C. A. Triggered Release from Lipid Bilayer Vesicles by an Artificial Transmembrane Signal Transduction System. *Journal of the American Chemical Society* **139,** 15768–15773. ISSN: 15205126 (2017).

33. Yasuga, H. *et al.* Logic gate operation by DNA translocation through biological nanopores. *PLoS ONE* **11.** ISSN: 19326203 (2016).

34. Adir, O. *et al.* Synthetic cells with self-activating optogenetic proteins communicate with natural cells. *Nature Communications* **13,** 1–13. ISSN: 20411723 (Apr. 2022).

35. Chakraborty, T. & Wegner, S. V. Cell to Cell Signaling through Light in Artificial Cell Communities: Glowing Predator Lures Prey. *ACS nano* **15,** 9434–9444. ISSN: 1936086X (June 2021).

36. Spriestersbach, A., Kubicek, J., Schäfer, F., Block, H. & Maertens, B. in *Methods in Enzymology* 1–15 (Academic Press Inc., June 2015).

37. Schild, V. R. *et al.* Light-Patterned Current Generation in a Droplet Bilayer Array. *Scientific Reports* **7,** 1–9. ISSN: 20452322 (Apr. 2017).

38. Hoskin, C. E., Schild, V. R., Vinals, J. & Bayley, H. Parallel transmission in a synthetic nerve. *Nature Chemistry* **14,** 650–657. ISSN: 17554349 (Apr. 2022).

39. Green, A. A., Silver, P. A., Collins, J. J. & Yin, P. Toehold Switches: De-Novo-Designed Regulators of Gene Expression. *Cell* **159,** 925–939. ISSN: 0092-8674 (4 Nov. 2014).

40. Hu, B. *et al.* Therapeutic siRNA: state of the art. *Signal Transduction and Targeted Therapy 2020 5:1* **5,** 1–25. ISSN: 2059-3635 (1 June 2020).

41. Chou, C., Young, D. D. & Deiters, A. Photocaged T7 RNA polymerase for the light activation of transcription and gene function in pro- and eukaryotic cells. *ChemBioChem* **11,** 972–977. ISSN: 14394227 (May 2010).

42. Booth, M. J., Schild, V. R., Graham, A. D., Olof, S. N. & Bayley, H. Light-activated communication in synthetic tissues. *Science Advances* **2,** e1600056–e1600056. ISSN: 23752548 (Apr. 2016).

43. Mazzotti, G., Hartmann, D. & Booth, M. J. Precise, Orthogonal Remote-Control of Cell-Free Systems Using Photocaged Nucleic Acids. *Journal of the American Chemical Society* **145,** 9481–9487. ISSN: 15205126 (May 2023).

44. Hartmann, D., Chowdhry, R., Smith, J. M. & Booth, M. J. Orthogonal Light-Activated DNA for Patterned Biocomputing within Synthetic Cells. *Journal of the American Chemical Society* **145,** 9471–9480. ISSN: 15205126 (May 2023).

45. Han, T., Chen, Q. & Liu, H. Engineered Photoactivatable Genetic Switches Based on the Bacterium Phage T7 RNA Polymerase. *ACS Synthetic Biology* **6,** 357–366. ISSN: 21615063 (Feb. 2017).

46. Segall-Shapiro, T. H., Meyer, A. J., Ellington, A. D., Sontag, E. D. & Voigt, C. A. A 'resource allocator' for transcription based on a highly fragmented T7 RNA polymerase. *Molecular Systems Biology* **10,** 742. ISSN: 1744-4292 (July 2014).

47. Gaut, N. J. *et al.* Programmable Fusion and Differentiation of Synthetic Minimal Cells. *ACS Synthetic Biology* **11,** 855–866. ISSN: 21615063 (Feb. 2022).

48. Monck, C., Elani, Y. & Ceroni, F. Genetically programmed synthetic cells for thermo-responsive protein synthesis and cargo release. *Nature Chemical Biology 2024 20:10* **20,** 1380–1386. ISSN: 1552-4469 (10 July 2024).

49. Adamala, K. P., Martin-Alarcon, D. A., Guthrie-Honea, K. R. & Boyden, E. S. Engineering genetic circuit interactions within and between synthetic minimal cells. *Nature Chemistry* **9,** 431–439. ISSN: 17554349 (2017).

50. Seeman, N. C. & Sleiman, H. F. *DNA nanotechnology* Nov. 2017.

51. Simmel, F. C. DNA-based assembly lines and nanofactories. *Current Opinion in Biotechnology* **23,** 516–521. ISSN: 09581669 (Aug. 2012).

52. Joesaar, A. *et al.* DNA-based communication in populations of synthetic protocells. *Nature Nanotechnology* **14,** 369–378. ISSN: 17483395 (Apr. 2019).

53. Yang, S. *et al.* Light-activated signaling in dna-encoded sender-receiver architectures. *ACS Nano* **14,** 15992–16002. ISSN: 1936086X (Nov. 2020).

54. Zambrano, A. *et al.* Programmable synthetic cell networks regulated by tuneable reaction rates. *Nature Communications* **13.** ISSN: 20411723 (Dec. 2022).

55. Gong, J., Tsumura, N., Sato, Y. & Takinoue, M. Computational DNA Droplets Recognizing miRNA Sequence Inputs Based on Liquid–Liquid Phase Separation. *Advanced Functional Materials* **32,** 2202322. ISSN: 16163028 (Sept. 2022).

56. Peruzzi, J. A., Jacobs, M. L., Vu, T. Q., Wang, K. S. & Kamat, N. P. Barcoding Biological Reactions with DNA-Functionalized Vesicles. *Angewandte Chemie - International Edition* **58,** 18683–18690. ISSN: 15213773 (Dec. 2019).

57. Wang, C., Yan, A., Wang, H., Su, Y. & Li, D. DNA-Mediated Membrane Fusion and Its Biological Applications: Sensing, Reaction Control and Drug Delivery. *Analysis & Sensing* **2,** e202200024. ISSN: 2629-2742 (Sept. 2022).

58. Maslak, M. & Martin, C. T. Kinetic Analysis of T7 RNA Polymerase Transcription Initiation from Promoters Containing Single-Stranded Regions. *Biochemistry* **32,** 4281–4285. ISSN: 15204995 (Apr. 1993).

59. Milligan, J. F., Groebe, D. R., Witherell, G. W. & Uhlenbeck, O. C. Oligoribonucleotide synthesis using T7 RNA polymerase and synthetic DNA templates. *Nucleic Acids Research* **15,** 8783–8798. ISSN: 03051048 (1987).

60. Kartje, Z. J., Janis, H. I., Mukhopadhyay, S. & Gagnon, K. T. Revisiting T7 RNA polymerase transcription in vitro with the Broccoli RNA aptamer as a simplified real-time fluorescent reporter. *Journal of Biological Chemistry* **296,** 100175–100176. ISSN: 1083351X (2021).

61. Kim, J., White, K. S. & Winfree, E. Construction of an in vitro bistable circuit from synthetic transcriptional switches. *Molecular Systems Biology* **2.** ISSN: 17444292 (2006).

62. Yang, S., Joesaar, A., Bögels, B. W., Mann, S. & de Greef, T. F. Protocellular CRISPR/Cas-Based Diffusive Communication Using Transcriptional RNA Signaling. *Angewandte Chemie - International Edition* **61,** e202202436. ISSN: 15213773 (June 2022).

63. Skinner, G. M., Baumann, C. G., Quinn, D. M., Molloy, J. E. & Hoggett, J. G. Promoter binding, initiation, and elongation by bacteriophage T7 RNA polymerase: A single-molecule view of the transcription cycle. *Journal of Biological Chemistry* **279,** 3239–3244. ISSN: 00219258 (5 Jan. 2004).

64. Kochetkov, S. N., Rusakova, E. E. & Tunitskaya, V. L. Recent studies of T7 RNA polymerase mechanism. *FEBS Letters* **440,** 264–267. ISSN: 00145793 (Dec. 1998).

65. Adler, S. & Modrich, P. T7-induced DNA polymerase. Requirement for thioredoxin sulfhydryl groups. *Journal of Biological Chemistry* **258,** 6956–6962. ISSN: 00219258 (1983).

66. Jorgensen, E. D., Durbin, R. K., Risman, S. S. & McAllister, W. T. Specific contacts between the bacteriophage T3, T7, and SP6 RNA polymerases and their promoters. *Journal of Biological Chemistry* **266,** 645–651. ISSN: 00219258 (1991).

67. Zhou, H. & Zhang, S. Recent Development of Fluorescent Light-Up RNA Aptamers. *Critical Reviews in Analytical Chemistry* **52,** 1644–1661. ISSN: 15476510 (2022).

68. Filonov, G. S., Moon, J. D., Svensen, N. & Jaffrey, S. R. Broccoli: Rapid selection of an RNA mimic of green fluorescent protein by fluorescence-based selection and directed evolution. *Journal of the American Chemical Society* **136,** 16299–16308. ISSN: 15205126 (Nov. 2014).

69. Warner, K. D. *et al.* Structural basis for activity of highly efficient RNA mimics of green fluorescent protein. *Nature Structural & Molecular Biology 2014 21:8* **21,** 658–663. ISSN: 1545-9985 (July 2014).

70. Song, W. *et al.* Imaging RNA polymerase III transcription using a photostable RNA-fluorophore complex. *Nature Chemical Biology* **13,** 1187–1194. ISSN: 15524469 (Sept. 2017).

71. Trachman, R. J. *et al.* Structure and functional reselection of the Mango-III fluorogenic RNA aptamer. *Nature Chemical Biology* **15,** 472–479. ISSN: 15524469 (Apr. 2019).

72. Dolgosheina, E. V. *et al.* RNA Mango aptamer-fluorophore: A bright, high-affinity complex for RNA labeling and tracking. *ACS Chemical Biology* **9,** 2412–2420. ISSN: 15548937 (Oct. 2014).

73. Kong, K. Y., Jeng, S. C., Rayyan, B. & Unrau, P. J. RNA Peach and Mango: Orthogonal two-color fluorogenic aptamers distinguish nearly identical ligands. *RNA* **27,** 604–615. ISSN: 14699001 (Mar. 2021).

74. Chen, X. *et al.* Visualizing RNA dynamics in live cells with bright and stable fluorescent RNAs. *Nature Biotechnology 2019 37:11* **37,** 1287–1293. ISSN: 1546-1696 (Sept. 2019).

75. Rees, H. C., Gogacz, W., Li, N. S., Koirala, D. & Piccirilli, J. A. Structural Basis for Fluorescence Activation by Pepper RNA. *ACS Chemical Biology* **17,** 1866–1875. ISSN: 15548937 (July 2022).

76. Yoshihiro Shimizu, T. U. in *Cell-Free Protein Production Methods and Protocols* (Humana Press, 2010).

77. Fisher, T. L., Terhorst, T., Cao, X. & Wagner, R. W. Intracellular disposition and metabolism of fluorescently-labled unmodified and modified oligouncleotides microijjected into mammalian cells. *Nucleic Acids Research* **21,** 3857–3865. ISSN: 03051048 (Aug. 1993).

78. Inc., N. E. B. *2021.22 NEB Catalogue and Technical Reference* (2021).

79. Booth, M. J., Restrepo Schild, V., Downs, F. G. & Bayley, H. Functional aqueous droplet networks. *Molecular BioSystems* **13,** 1658–1691 (Aug. 2017).

80. Villar, G., Graham, A. D. & Bayley, H. A tissue-like printed material. *Science* **340,** 48–52. ISSN: 10959203 (Apr. 2013).

81. Holden, M. A., Needham, D. & Bayley, H. Functional bionetworks from nanoliter water droplets. *Journal of the American Chemical Society* **129,** 8650–8655. ISSN: 00027863 (2007).

82. Bayley, H. *et al.* Droplet interface bilayers. *Molecular BioSystems* **4,** 1191–1208. ISSN: 1742206X (Dec. 2008).

83. Krishna Kumar, R. *et al.* Droplet printing reveals the importance of micron-scale structure for bacterial ecology. *Nature Communications 2021 12:1* **12,** 1–12. ISSN: 2041-1723 (Feb. 2021).

84. Alcinesio, A. *et al.* Controlled packing and single-droplet resolution of 3D-printed functional synthetic tissues. *Nature Communications* **11,** 2105. ISSN: 2041-1723 (2020).

85. Alcinesio, A., Krishna Kumar, R. & Bayley, H. Functional Multivesicular Structures with Controlled Architecture from 3D-Printed Droplet Networks. *ChemSystemsChem* **4.** ISSN: 2570-4206 (2022).

86. Schaffter, S. W. *et al.* T7 RNA polymerase non-specifically transcribes and induces disassembly of DNA nanostructures. *Nucleic Acids Research* **46,** 5332–5343. ISSN: 13624962 (June 2018).

87. Breslauer, K. J., Frank, R., Blocker, H. & Marky, L. A. Predicting DNA duplex stability from the base sequence. *Proceedings of the National Academy of Sciences of the United States of America* **83.** ISSN: 00278424 (11 1986).

88. Woo, C. H., Jang, S., Shin, G., Jung, G. Y. & Lee, J. W. Sensitive fluorescence detection of SARS-CoV-2 RNA in clinical samples via one-pot isothermal ligation and transcription. *Nature Biomedical Engineering* **4,** 1168–1179. ISSN: 2157846X (Sept. 2020).

89. Endoh, T., Tan, J. H., Chen, S. B. & Sugimoto, N. Cladogenetic Orthogonal Light-Up Aptamers for Simultaneous Detection of Multiple Small Molecules in Cells. *Analytical Chemistry* **95,** 976–985. ISSN: 15206882 (2023).

90. Kraus, G. A. *et al.* Fluorinated analogs of malachite green: Synthesis and toxicity. *Molecules* **13,** 986–994. ISSN: 14203049 (Apr. 2008).

91. Sunbul, M. & Jäschke, A. SRB-2: A promiscuous rainbow aptamer for live-cell RNA imaging. *Nucleic Acids Research* **46,** e110–e110. ISSN: 13624962 (Oct. 2018).

92. Lu, Z. & Imlay, J. A. *When anaerobes encounter oxygen: mechanisms of oxygen toxicity, tolerance and defence* Dec. 2021.

93. Promega. *BioMatch - Tm Calculations for Oligos*

94. Paul, S., Stang, A., Lennartz, K., Tenbusch, M. & Überla, K. Selection of a T7 promoter mutant with enhanced in vitro activity by a novel multi-copy bead display approach for in vitro evolution. *Nucleic Acids Research* **41.** ISSN: 03051048 (2013).

95. Chen, Y. H. & Bogenhagen, D. F. Effects of DNA lesions on transcription elongation by T7 RNA polymerase. *Journal of Biological Chemistry* **268,** 5849–5855. ISSN: 00219258 (Mar. 1993).

96. Marimuthu, C., Tang, T. H., Tominaga, J., Tan, S. C. & Gopinath, S. C. Single-stranded DNA (ssDNA) production in DNA aptamer generation. *Analyst* **137,** 1307–1315. ISSN: 00032654 (Feb. 2012).

97. Sanchez, J. A., Pierce, K. E., Rice, J. E. & Wangh, L. J. Linear-After-The-Exponential (LATE)–PCR: An advanced method of asymmetric PCR and its uses in quantitative real-time analysis. *Proceedings of the National Academy of Sciences* **101,** 1933–1938. ISSN: 0027-8424 (Feb. 2004).

98. Tominaga, J. *et al.* Asymmetric PCR for good quality ssDNA generation towards DNA aptamer production. *Songklanakarin Journal of Science and Technology (SJST)* **34,** 125–131. ISSN: 0125-3395 (Apr. 2012).

99. Heiat, M., Ranjbar, R., Latifi, A. M., Rasaee, M. J. & Farnoosh, G. Essential strategies to optimize asymmetric PCR conditions as a reliable method to generate large amount of ssDNA aptamers. *Biotechnology and Applied Biochemistry* **64,** 541–548. ISSN: 14708744 (2017).

100. Smith, J. M., Hartmann, D. & Booth, M. J. Engineering cellular communication between light-activated synthetic cells and bacteria. *bioRxiv,* 2022.07.22.500923 (July 2022).

101. Tan, X. *et al.* Fluoromodules Consisting of a Promiscuous RNA Aptamer and Red or Blue Fluorogenic Cyanine Dyes: Selection, Characterization, and Bioimaging. *Journal of the American Chemical Society* **139,** 9001–9009. ISSN: 15205126 (2017).

102. Shelke, S. A. *et al.* Structural basis for activation of fluorogenic dyes by an RNA aptamer lacking a G-quadruplex motif. *Nature Communications* **9,** 1–10. ISSN: 20411723 (Oct. 2018).

103. Dykstra, P. B., Kaplan, M. & Smolke, C. D. *Engineering synthetic RNA devices for cell control* 2022.

104. Zhu, Y., Zhu, L., Wang, X. & Jin, H. RNA-based therapeutics: an overview and prospectus. *Cell Death and Disease 2022 13:7* **13,** 1–15. ISSN: 2041-4889 (2022).

105. England, C. G., Ehlerding, E. B. & Cai, W. *NanoLuc: A Small Luciferase Is Brightening Up the Field of Bioluminescence* 2016.

106. Romei, M. G. & Boxer, S. G. Split Green Fluorescent Proteins: Scope, Limitations, and Outlook. *Annu. Rev. Biophys. 2019* **48,** 19–44 (2019).

107. Broome, A. M., Bhavsar, N., Ramamurthy, G., Newton, G. & Basilion, J. P. Expanding the utility of β-galactosidase complementation: Piece by piece. *Molecular Pharmaceutics* **7,** 60–74. ISSN: 15438384 (2010).

108. Spitzer, S. & Eckstein, F. Inhibition of deoxyribonucleases by phosphorothioate groups in oligodeoxyribonucleotides. *Nucleic Acids Research* **16,** 11691–11704. ISSN: 03051048 (Dec. 1988).

109. Song, L. *et al.* Structure of staphylococcal α-hemolysin, a heptameric transmembrane pore. *Science* **274,** 1859–1866. ISSN: 00368075 (Dec. 1996).

110. Bayley, H. Nanopore sequencing: From imagination to reality. *Clinical Chemistry* **61,** 25–31. ISSN: 15308561 (2015).

111. Maglia, G., Restrepo, M. R., Mikhailova, E. & Bayley, H. Enhanced translocation of single DNA molecules through α-hemolysin nanopores by manipulation of internal charge. *Proceedings of the National Academy of Sciences of the United States of America* **105,** 19720–19725. ISSN: 00278424 (Dec. 2008).

112. Kasianowicz, J. J., Brandin, E., Branton, D. & Deamer, D. W. Characterization of individual polynucleotide molecules using a membrane channel. *Proceedings of the National Academy of Sciences* **93,** 13770–13773. ISSN: 14319268 (1996).

113. Lee, S. & Bayley, H. Reconstruction of the Gram-Negative Bacterial Outer-Membrane Bilayer. *Small* **18,** 2200007. ISSN: 16136829 (Apr. 2022).

114. Ayub, M. & Bayley, H. *Engineered transmembrane pores* Oct. 2016.

115. Hwang, W. L., Holden, M. A., White, S. & Bayley, H. Electrical behavior of droplet interface bilayer networks: Experimental analysis and modeling. *Journal of the American Chemical Society* **129,** 11854–11864. ISSN: 00027863 (2007).

116. Koo, S., Cheley, S. & Bayley, H. Redirecting Pore Assembly of Staphylococcal α-Hemolysin by Protein Engineering. *ACS Central Science* **5,** 629–639. ISSN: 23747951 (2019).

117. Piraner, D. I., Abedi, M. H., Moser, B. A., Lee-Gosselin, A. & Shapiro, M. G. Tunable thermal bioswitches for in vivo control of microbial therapeutics. *Food, Pharmaceutical and Bioengineering Division 2017 - Core Programming Area at the 2017 AIChE Annual Meeting* **2,** 695–702. ISSN: 15524469 (2017).

118. Xiong, L. L., Garrett, M. A., Buss, M. T., Kornfield, J. A. & Shapiro, M. G. Tunable Temperature-Sensitive Transcriptional Activation Based on Lambda Repressor. *ACS Synthetic Biology* **11,** 2518–2522. ISSN: 21615063 (2022).

119. Evans, B. C. *et al.* Ex vivo red blood cell hemolysis assay for the evaluation of pH-responsive endosomolytic agents for cytosolic delivery of biomacromolecular drugs. *Journal of visualized experiments : JoVE,* 50166. ISSN: 1940087X (2013).

120. Thiam, A. R., Bremond, N. & Bibette, J. From stability to permeability of adhesive emulsion bilayers. *Langmuir* **28,** 6291–6298. ISSN: 07437463 (Apr. 2012).

121. Donau, C. *et al.* Active coacervate droplets as a model for membraneless organelles and protocells. *Nature Communications 2020 11:1* **11,** 1–10. ISSN: 2041-1723 (Oct. 2020).

122. Yang, B. & Wyman, C. E. BSA treatment to enhance enzymatic hydrolysis of cellulose in lignin containing substrates. *Biotechnology and Bioengineering* **94,** 611–617. ISSN: 00063592 (2006).

123. Yin, I. X. *et al.* The antibacterial mechanism of silver nanoparticles and its application in dentistry. *International Journal of Nanomedicine* **15,** 2555–2562. ISSN: 11782013 (2020).

124. Ramsay, W. J. & Bayley, H. Single-Molecule Determination of the Isomers of d-Glucose and d-Fructose that Bind to Boronic Acids. *Angewandte Chemie - International Edition* **57,** 2841–2845. ISSN: 15213773 (Mar. 2018).

125. Qing, Y., Pulcu, G. S., Bell, N. A. & Bayley, H. Bioorthogonal Cycloadditions with Sub-Millisecond Intermediates. *Angewandte Chemie - International Edition* **57,** 1218–1221. ISSN: 15213773 (Jan. 2018).

126. Lee, J. & Bayley, H. Semisynthetic protein nanoreactor for single-molecule chemistry. *Proceedings of the National Academy of Sciences of the United States of America* **112,** 13768–13773. ISSN: 10916490 (Nov. 2015).

127. Lee, J. *et al.* Semisynthetic Nanoreactor for Reversible Single-Molecule Covalent Chemistry. *ACS Nano* **10,** 8843–8850. ISSN: 1936086X (Sept. 2016).

128. Choi, L. S. & Bayley, H. S-nitrosothiol chemistry at the single-molecule level. *Angewandte Chemie - International Edition* **51,** 7972–7976. ISSN: 14337851 (Aug. 2012).

129. Pulcu, G. S., Mikhailova, E., Choi, L. S. & Bayley, H. Continuous observation of the stochastic motion of an individual small-molecule walker. *Nature Nanotechnology* **10,** 76–83. ISSN: 17483395 (2015).

130. Pulcu, G. S. *et al.* Single-Molecule Kinetics of Growth and Degradation of Cell-Penetrating Poly(disulfide)s. *Journal of the American Chemical Society* **141,** 12444–12447. ISSN: 15205126 (2019).

131. Qing, Y. *Single-molecule thiol-disulfide interchange* PhD thesis (2018).

132. Stoddart, D., Heron, A. J., Mikhailova, E., Maglia, G. & Bayley, H. Single-nucleotide discrimination in immobilized DNA oligonucleotides with a biological nanopore. *Proceedings of the National Academy of Sciences of the United States of America* **106,** 7702–7707. ISSN: 00278424 (May 2009).

133. Qing, Y., Tamagaki-Asahina, H., Ionescu, S. A., Liu, M. D. & Bayley, H. Catalytic site-selective substrate processing within a tubular nanoreactor. *Nature Nanotechnology* **14,** 1135–1142. ISSN: 17483395 (Dec. 2019).

134. Baoutina, A., Bhat, S., Partis, L. & Emslie, K. R. Storage Stability of Solutions of DNA Standards. *Analytical Chemistry* **91,** 12268–12274. ISSN: 15206882 (2019).

135. Matange, K., Tuck, J. M. & Keung, A. J. DNA stability: a central design consideration for DNA data storage systems. *Nature Communications* **12,** 1–9. ISSN: 20411723 (Mar. 2021).

136. Hwang, W. L., Chen, M., Cronin, B., Holden, M. A. & Bayley, H. Asymmetric droplet interface bilayers. *Journal of the American Chemical Society* **130,** 5878–5879. ISSN: 00027863 (May 2008).

137. Khutsishvili, I., Johnson, S., Lee, H. T. & Marky, L. A. Unfolding thermodynamics of DNA intramolecular complexes involving joined triple- and double-

helical motifs. *Methods in enzymology* **466,** 477–502. ISSN: 15577988 (Jan. 2009).

138. Arnold, S. *et al.* Kinetic modeling and simulation of in vitro transcription by phage T7 RNA polymerase. *Biotechnology and Bioengineering* **72,** 548–561. ISSN: 00063592 (Jan. 2001).

139. Noble, J. E. & Bailey, M. J. Quantitation of protein. *Methods in enzymology* **463,** 73–95. ISSN: 1557-7988 (C 2009).

140. Ouldridge, T. E., Šulc, P., Romano, F., Doye, J. P. & Louis, A. A. DNA hybridization kinetics: Zippering, internal displacement and sequence dependence. *Nucleic Acids Research* **41,** 8886–8895. ISSN: 03051048 (2013).

141. Simmel, F. C., Yurke, B. & Singh, H. R. Principles and Applications of Nucleic Acid Strand Displacement Reactions. *Chemical Reviews.* ISSN: 15206890 (2019).

142. Zhang, D. Y. & Winfree, E. Control of DNA strand displacement kinetics using toehold exchange. *Journal of the American Chemical Society* **131,** 17303–17314. ISSN: 00027863 (Dec. 2009).

143. Van Sluijs, B., Maas, R. J., van der Linden, A. J., de Greef, T. F. & Huck, W. T. A microfluidic optimal experimental design platform for forward design of cell-free genetic networks. *Nature Communications* **13,** 1–11. ISSN: 20411723 (2022).

144. Mantri, S., Tanju Sapra, K., Cheley, S., Sharp, T. H. & Bayley, H. An engineered dimeric protein pore that spans adjacent lipid bilayers. *Nature Communications* **4,** 1725–1734 (2013).

145. Montal, M. & Mueller, P. Formation of bimolecular membranes from lipid monolayers and a study of their electrical properties. *Proceedings of the National Academy of Sciences of the United States of America* **69,** 3561–3566. ISSN: 00278424 (1972).

146. Qing, Y., Ionescu, S. A., Pulcu, G. S. & Bayley, H. Directional control of a processive molecular hopper. *Science* **361,** 908–912. ISSN: 10959203 (Aug. 2018).